# APPLIED COMPUTER SCIENCE

The Journal is a peer-reviewed, international, multidisciplinary journal covering a broad spectrum of topics of computer application in production engineering, technology, management and economy.

The main purpose of Applied Computer Science is to publish the results of cutting-edge research advancing the concepts, theories and implementation of novel solutions in computer technology. Papers presenting original research results related to applications of computer technology in production engineering, management, economy and technology are welcomed.

We welcome original papers written in English. The Journal also publishes technical briefs, discussions of previously published papers, book reviews, and editorials. Especially we welcome papers which deals with the problem of computer applications in such areas as:

- manufacturing,
- engineering,
- technology,
- designing,
- organization,
- management,
- economics,
- innovations,
- competitiveness,
- quality and costs.

The Journal is published quarterly and is indexed in: BazTech, Cabell's Directory, CNKI Scholar (China National Knowledge Infrastucture), ERIH PLUS, Google Scholar, Index Copernicus, J-Gate, Scopus, TEMA Technik und Management.

Letters to the Editor-in-Chief or Editorial Secretary are highly encouraged.

# CONTENTS

Applied Computer Science, vol. 17, no. 2, pp. 5–13
doi: 10.23743/acs-2021-09

Submitted: 2021-05-13 | Revised: 2021-06-14 | Accepted: 2021-06-20

*automation controller, COM object, authorization*

*Denis RATOV* [0000-0003-4326-3030]*

# INTEGRATION WITH THE SOFTWARE INTERFACE OF THE COM SERVER FOR AUTHORIZED USER

**Abstract**

*The article is devoted to the development of a software controller for automation of access to tools and object model of the multifunctional graphic editor Adobe Photoshop. The work of the graphic editor is initiated in the form of a COM object, which contains methods available to the software controller through the COM interface, which allows the software to use the functionality of the editor. To restrict unauthorized access, a software authorization control protocol is proposed, which is based on the use of binding to the computer hardware and encryption by a 128-bit MD5 public key hashing algorithm.*

## 1. INTRODUCTION

Comprehensive implementation and development of information technology (Ratov, 2020a; 2020b) has led to the need to automate processes in many software packages that are widely used. In addition, to maintain the confidentiality of data from unauthorized access for such a system requires the use of network software.

The purpose of the work is the creation of a protected from unauthorized access software controller to automate the process of document formation, which interacts with the COM interface of the multifunctional graphic editor Adobe Photoshop.

An example of a server in the form of a file that is executed and which implements the ability to create COM objects at the request of other programs are Microsoft Office applications (Artemov, 2007). COM-server, in such applications is a program registered in the operating system, which allows clients to create and use objects implemented on the server (Elmanova, Trepalin and Tentser, 2003; Identification, n.d.). Another representative of programs with the implementation of a COM server is a multifunctional graphic editor Adobe Photoshop. All the functionality used by the user using the menu, keyboard and toolbar of this editor can be performed automatically, by means of the automation controller. Photoshop gives the automation controller access to functionality through its object model, which is a hierarchy of objects that provide access to other objects.

* Volodymyr Dahl East Ukrainian University, Faculty of Information Technology and Electronics, Department of Programming and Mathematics, Severodonetsk, Ukraine, ratov@snu.edu.ua

COM (Component Object Model – model of multicomponent objects) – one of the basic technologies of the Windows operating system. Moreover, many Windows technologies (Shell, Scripting, HTML) implement their application program interfaces (API) in the form of COM interfaces (Elmanova, Trepalin and Tentser, 2003). The main purpose of COM technology is to provide the ability to export objects, the idea of which is that one module creates an object, and the other uses it by accessing methods or services. COM object is a binary code that performs the desired function and has a software interface. The COM object contains methods that are available to an external application through the COM – interface that allows you to use the COM object.

Because the object model of the Adobe Photoshop multifunctional graphics editor has a tree-like structure topped by an Application object, it can be represented as lists (collections) of objects of the same type that are accessed by index. Individual objects can contain collections, in turn, the elements of the collection are ordinary objects. Access to any object or element of the collection is possible only through the root object Application.

Photoshop gives automation controllers access to functionality through its object model. Therefore, to automate work with the editor, it is necessary to have a program class, the methods of which interact with the object model of the editor.

## 2. CREATING AN AUTOMATION CONTROLLER

The automation controller (Fig. 1, b), using the developed methods of reading data from the xml format (Fig. 1, a), must connect to the PhotoShop interface and using its API, generate files (Fig. 1, c). In the integrated software development environment Embarcadero RAD Studio on the main form of the future controller program placed the necessary components and buttons (Fig. 1, b). When you click on the buttons "PhotoShop template", "xml-files", "PhotoShop diplomas", the appropriate directories are selected and saved in the operating system registry. Setting (unchecking) the appropriate Visible flags leads to the inclusion and use of additional server functions: background mode, report processing in Excel, saving jpeg-copies.


**Fig. 1. Scheme of data flow from the automation controller to the automation server Adobe Photoshop**

Selecting the "Compression ratio" component (Fig. 1, b) causes the controller text box to display the percentage of jpeg-copy compression, which affects the quality and size of the resulting jpeg-copy file.

The TController class has been created to control the automation server (Fig. 2). In the private section of the TController class the variable docPS of type Variant is declared. Additionally, event handlers have been created that are associated with components (a reference to the ComObj and Variants modules in the uses section is required).

The TController class introduces a public-variable PhotoShop of the Variant type (Fig. 2, line 8), which is initialized by the CreateOleObject function (Fig. 2, line 11) contained in the ComObj module. When executed, the CreateOleObject function, by calling several COM API functions, will create an instance of the COM object and return its IDispatch interface inside the variant variable. This object contains the interface of the COM object (Adobe Photoshop automation server), the methods of which will be used in the controller program. Considering the implementation of the CreateOleObject function in the source text of the ComObj module, we can find that it, in turn, calls the CoCreateInstance COM API function, which is intended to create an object from an executable file or DLL, ie uses a class factory call. A variable of type Variant can contain various data (string, number, including the interface of the COM object). The Controller object is created by calling the class constructor (Fig. 2, line 10). To save the converted data from an xml file in the TController class, an associative array ArrAttribute with key attributes of xml-files is created (Fig. 2, line 4). To read the xml-file and create an associative array by file attributes, the method of the readXML class was introduced (Fig. 2, line 6). The integrated development environment allows you to access the methods and properties of objects within the variables, and the existence of these methods and properties in the General case may be unknown in advance.

```
1  TController = class()
2  private
3     docPS : Variant;
4     arrAttribute : TStrings;
5     constructor Create;
6     function readXML(fName:string; var countDoc:integer; moveNodes:boolean):TStrings;
7     function PhotoShopOpen(filePattern:string):Variant;
8  public PhotoShop : Variant;
9  end;
10 Controller := TController.Create;
11 Controller.PhotoShop := CreateOleObject('Photoshop.Application');
12 Controller.PhotoShop.visible := not(Form1.CheckBox_FoneMode.Checked);
13 Controller.readXML(FilesXML[i], colDoc, true);
14 if (Form1.CheckBox_PS.Checked AND (findRecordExcel in [NotFind, FindAndDel])) then begin
15  Controller.docPS := Controller.PhotoShopOpen(filePattern);
16  Controller.docPS.LayerSets(1).Layers(1).TextItem.Contents := Controller.arrAttribute.Values[prefics+'DocumentSeries']+
17                  ' № '+Controller.arrAttribute.Values[prefics+'DocumentNumber'];
18  Controller.docPS.LayerSets(2).Layers(1).TextItem.Contents := Controller.arrAttribute.Values[prefics+'FirstName'] +
19                        ' ' + Controller.arrAttribute.Values[prefics+'LastName'];
20  Controller.docPS.SaveAs(directory_of_result_facultet + '\' + ps_file_name);
21  Controller.docPS.Close();
22 end;
```

**Fig. 2. Initialization of the TController class and its application for connection to the PhotoShop interface when automating file generation**

When creating controllers, the compiler does not check whether an object actually stored in a variable of type Variant, but simply takes the name of the property or method as a regular character string, without analyzing its contents.

To download the document template, a method of the PhotoShopOpen class was created (Fig. 2, line 7), its activation is shown in Fig. 2, line 15. The connection to the Adobe Photoshop automation server in this project is performed dynamically by clicking on the "Perform processing" button. The button works as a switch – if there is no connection to the server, the server starts and a connection is established with it, and if there is - the connection is broken, and the server is unloaded from memory. Code required to disconnect the server: the variant variable is assigned an indefinite value (unassigned).

With this assignment, code is generated that checks what is in the variant variable, and if there is a link to the interface, then its Release method is called. Because the server is called dynamically, each method is checked before each method is called,

Access to the corresponding layers of the PhotoShop template file is due to the use of methods of the COM-server LayerSets, Layers (Fig. 2, lines 16, 18). The data to be downloaded is used from the arrAttribute associative array, which belongs to the Controller object.

At the end of the work, the processed file is saved in psd format (Fig. 2, line 20) and the COM server completes its work (Fig. 2, line 21). When the appropriate check boxes are set, the controller additionally processes the report in Excel and saves a jpeg copy of the processed file. The COM model provides the ability to create components that are reusable and their creation does not depend on the programming language. Such components are called COM servers and are program files (EXE) or dynamic boot libraries (DLLs), specially designed to allow their universal call from any program written in a programming language that supports COM (Elmanova, Trepalin and Tentser, 2003).

## 3. CONTROLLER AUTHORIZATION

In information systems, authorization (permission, authorization) is understood as granting a certain person or group of persons the right to perform certain actions, as well as the process of verification (confirmation) of these rights when trying to perform these actions (Authorization, n.d.; User authorization, n.d.).

Quite promising for program protection is the method of authorization via the Internet (Varlataya & Shakhanova, 2007), which involves the initial activation of the product on the user's computer, as well as user authorization on the developer's server each time you run the program. This method is not widespread and there are no ready-made solutions in open access (Sklyarov, 2004; Software as a service, n.d.). User authorization at each launch of the program allows the developer to monitor statistics on the use of the program, detect cases of license violations, revoke the licenses of dishonest users, as well as flexibly change the licensing policy (Service Software Activation Service, n.d.).

The article proposes a software authorization control protocol based on the use of binding to the computer hardware and encryption with a 128-bit MD5 public key hashing algorithm (Moldovyan & Moldovyan, 2005; System for software retrieval of additional information from unauthorized copies of Asprotect, n.d.; RSA class, n.d.; MD5, n.d.). The scheme of packet exchange between software with a remote server is presented in Fig. 3.

Consider the authorization algorithm of the automation controller Diplom.exe, which is installed on the user's computer User. The remote server is owned by the controller developers or their trustee.

The software authorization protocol generates a public key (key_client), which will be encrypted with a 128-bit MD5 hashing algorithm. The private key (key_server) must be stored on the http server. The first time you run Diplom.exe, you get the Identification ID from the http server, provided that the administrator has given general permission to work on the system and add new users. Whenever a user tries to perform one of the actions assigned to the developer to control (for example, launching a program, creating, opening, or saving a document), Diplom.exe with the RequestRespons.dll dynamic library connected sends a request to the server to continue by following these steps. data transfer:

1. The automation controller Diplom.exe (1) (Fig. 3) with the help of a dynamic library (2) (Fig. 3) checks the Internet connection and in its absence hides the working functionality of the program issues a message.
2. In the admin object from the classRequest class of the dll library (2) (Fig. 3) the parameter Comp – the name of the local computer and the parameter IP – the IP address of the local computer are formed.
3. In the admin object from the classRequest class of the dll library, the SerNum parameter is calculated – binding to the hardware of the computer where it is installed (4-byte serial number of the system disk C).

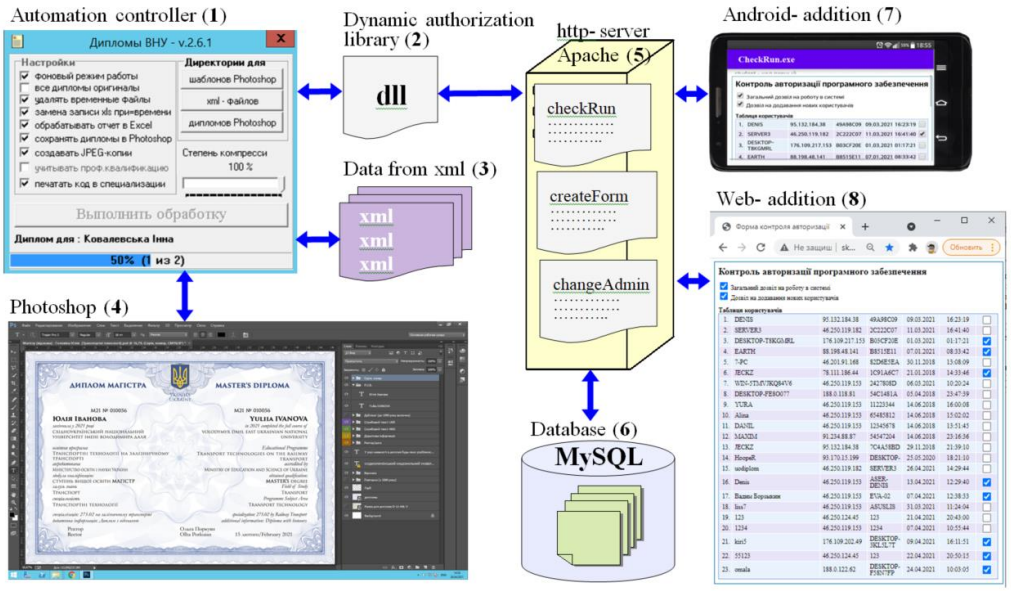


**Fig. 3. Scheme of packet exchange between software for which authorization control is organized with a remote server**

4. The controller Diplom.exe (1) (fig. 3) by means of dynamic library dll (2) transfers a packet with parameters key_client, Mode, IP, Comp, SerNum to the server (5) (fig. 3).
5. The server (5) checks the possibility of using the user program with the ID Identification, which is determined by the name of the local computer Comp, the IP address of the local computer – IP, the serial number of the system disk SerNum and compares the encrypted key key_client with the key key_server.
6. The server (5) sends a packet with the parameter f_status of the admin object from the classRequest class of the dll library associated with the Diplom.exe controller.
7. The controller (1) (Fig. 3) using a dynamic library (2) (Fig. 3) receives a packet from the server (5) (Fig. 3). If the f_status parameter confirms the ability to run, the dll library (2) (Fig. 3) activates the main form of the program (1) and displays the work panel, and if not, it issues a message and terminates the controller.

In the integrated development environment Visual Studio developed a dynamic library that integrates with the automation controller Diplom.exe and controls its authorization, while implementing early binding (early binding) of the client to the server, ie the creation and use of the controller table of virtual methods tables of virtual server methods.

The interface of the classRequest class, the methods of which implement the controller authorization protocol, is shown in Fig. 4. A 128-bit MD5 hashing algorithm was chosen as the encryption mechanism (MD5, n.d.).

The classRequest class (Fig. 4) consists of:

1. Private URL field, which specifies the address of the web-resource for pinging the presence of a connection to the global network.
2. Private structure locAnsver in which the answer from the server is formed.
3. Private Host method, in which the resource host is calculated from the resource address.
4. Class designer with pre-initialization.
5. Common methods GetPCName, GetSerialNum, which return the name and serial number of the computer.
6. The public method isInternetConected, which returns the sign of connection to the global network.
7. A public Query method that executes a GET request to a remote server.

```
namespace Control
{
    public struct AnsverServer  {...}
    public class classRequest
    {
        private string URL;
        private AnsverServer locAnsver;
        public classRequest(string url = "http://www.google.com") { this.URL = url; }
        private string Host(string URL) {...}
        public virtual AnsverServer ansver { get { return locAnsver; } }
        public virtual string GetPCName { get { return Environment.UserName; } }
        public virtual string GetSerialNum { get { return Environment.MachineName; } }
        public virtual bool isInternetConected {...}
        public virtual void Query(string addUrl) {...}
    }
}
```

**Fig. 4. ClassRequest class**

According to the developed protocol of authorization of the controller, for use of functionality of dynamic library dll in the project of the controller Diplom.exe it is necessary to change the work scenario (fig. 5). Instead of initializing the main form of the program (1), an instance of the class classRequest – admin (2) is created to ping the presence of a connection to the global network (3) and to send and receive packets from a remote server (4).

The created object allows one of three possible scenarios of the further work of the program:

1. Upon receipt of the activation permission package, the Diplom.exe controller will report the successful authorization (5) and perform the standard work of the program (Fig. 5).
2. In the absence of the Internet, the Diplom.exe controller will notify (7) and deactivate the possibility of standard operation.
3. Upon receipt of the prohibited activation package, the controller Diplom.exe will generate a message from the server (6) and deactivate the possibility of standard operation.

The server part of the software package is implemented in the PHP programming language with the ability to query the MySQL database server.

```
using System;
using System.Windows.Forms;
using Control;
namespace Check_Run
{
    static class Program
    {
        [STAThread]
        static void Main()
        {
            Application.EnableVisualStyles();
            Application.SetCompatibleTextRenderingDefault(false);
            //Application.Run(new Form1());

            classRequest admin = new classRequest();
            if (admin.isInternetConected) {
                admin.Query("http://.../server_script/checkRunProgramms.php?" +
                            "mode=checkRun" + "&comp="    + admin.GetPCName.ToString() +
                                              "&serNum=" + admin.GetSerialNum.ToString());
                if (admin.ansver.Status == 1) { Application.Run(new Form1()); }
                else { MessageBox.Show(admin.ansver.Message, "Ответ от сервера",
                                       MessageBoxButtons.OK, MessageBoxIcon.Information, 0);
                }
            }
            else {MessageBox.Show("No internet connection" + Char.ConvertFromUtf32(10) +
                                  "It is not possible to authorize", "Operation error",
                                   MessageBoxButtons.OK, MessageBoxIcon.Error, 0);
            }

        }
    }
}
```

1 2 3 4 5 6 7

**Fig. 5. Implementation of the authorization mechanism in the Diplom.exe controller project**

An embedded classRequest object can communicate with a server over the World Wide Web by its domain name or IP address.

Permission to activate the program is delegated by the remote server and can be based on the following data: the number of successful launches of the controller, the time of use of the program, the number of files created when using the controller and more.

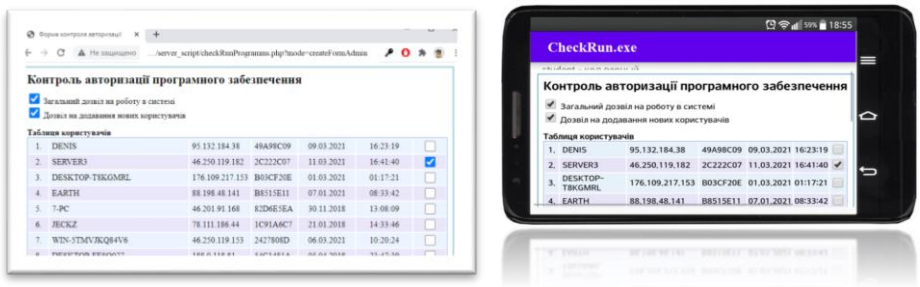


**Fig. 6. Web-form and android-application of software authorization administration**

Before the first use, the Diplom.exe controller receives an ID and, if the administrator has given general permission to work in the system and add new users, activates its functionality. Using the web-form of administration of the authorization of the controller or android-application (Fig. 6), the system administrator can control and monitor the user's

work with Diplom.exe. This process is carried out by adjusting the list of features and functionality of the controller for individual users or a general ban on activation (Fig. 6). For unique registration data for this identifier, the MySQL database stores the name of the local computer, the IP address of the local computer and the 4-byte serial number of the system disk of the computer on which the automation controller was involved.

## 4. CONCLUSIONS

As part of the study, a class was developed that provides control of the internal process automation server. This server performs its actions in the address space of the graphics editor Adobe Photoshop. This allowed to create a controller that automates the formation of image files.

Using the software authorization protocol, a dynamic library was also developed that integrates with the automation controller and monitors its authorization and functionality. For the PHP hypertext preprocessor running on the Apache http server, scripts for the interaction of the dynamic library and the MySQL database have been developed, a script for creating a web form of administration has been written, and a controller authorization administration application has been created in the Android Studio integrated development environment.

The obtained software controller and means of protection against unauthorized use and control of authorization became the basis of the software package "Diplomas SNU v.2.6.1" at the Volodymyr Dahl East Ukrainian National University. This complex is designed to create a single register of diplomas at the university, to automate the creation of files-diplomas of higher education in the multifunctional graphic editor Adobe Photoshop. All data for the analysis and formation of diplomas the controller exports from parameters of the corresponding xml-files downloaded from the uniform state base of education.

Authorization of the user at each start of a software complex allows the administrator to watch statistics of use of a complex, and also provides its protection against unauthorized use.

Scientific novelty is to obtain a class with methods that provide access to the functionality of the graphics editor using its object model and create a means of software protection against unauthorized use and control of the authorization of the software package. The practical significance lies in organization of software interaction with the COM interface of the multifunctional graphic editor Adobe Photoshop to automate the process of forming documents with restriction of unauthorized access.

### REFERENCES


Artemov, M. (2007). *Basics of COM technologies.* Voronezh. p. 84.

Authorization. (n.d.). *Wikipedia.* Retrieved May 12, 2021 from https://ru.wikipedia.org/wiki/Authorization

Elmanova, N., Trepalin, S., & Tentser, A. (2003). *Delphi and COM technology.* Petersburg. p. 698.

Identification. (n.d.). *Wikipedia.* Retrieved May 12, 2021 from https://ru.wikipedia.org/wiki/Identification

MD5. (n.d.). *Wikipedia.* Retrieved May 12, 2021 from https://ru.wikipedia.org/wiki/MD5

Moldovyan, N., & Moldovyan, A. (2005). *Introduced at the cryptosystem with an open key*. Petersburg. p. 288.

Ratov, D. (2020a). Architectural paradigm of the interactive interface module in the cloud technology model. *Applied Computer Science, 16*(4), 48–55. http://doi.org/10.23743/acs-2020-28

Ratov, D. (2020b). Model of the module for the interface of the information web-system. *Mathematical machines and systems. Kiev, 4,* 74–81.

RSA class. (n.d.). *Code.google.com.* Retrieved May 12, 2021 from http://code.google.com/p/phpjsrsa/source/browse/trunk/rsa.class.php?r=6

Service Software Activation Service. (n.d.). *Softactivation.com*. Retrieved May 12, 2021 from http://www.softactivation.com/asp/getstarted.asp

Sklyarov, D. (2004). *Mystery for the capture of evil information*. Petersburg. p. 288.

Software as a service. (n.d.). *Wikipedia*. Retrieved May 12, 2021 from http://ru.wikipedia.org/wiki/Software_as_a_service

System for software retrieval of additional information from unauthorized copies of Asprotect. (n.d.). *Jak.koshachek.com*. Retrieved May 12, 2021 from https://jak.koshachek.com/articles/asprotect-32-sistema-programnogo-zahistu-32-bitnih.html

User authorization. (n.d.). *Academic.ru.* Retrieved May 12, 2021 from https://dic.academic.ru/dic.nsf/business/17457

Varlataya, S., & Shakhanova, M. (2007). *Software and hardware protection of information.* Vladivostok. p. 318.

Applied Computer Science, vol. 17, no. 2, pp. 14–27
doi: 10.23743/acs-2021-10

Submitted: 2021-06-01 | Revised: 2021-06-20 | Accepted: 2021-06-22

AWS, IoT, MQTT

*Elizabeth PÉREZ* [0000-0002-7250-0579]*, *Juan C. ARAIZA* [0000-0002-6188-6867]*, *Dreysy POZOS* [0000-0002-7797-1230]*, *Edmundo BONILLA* [0000-0003-2062-4219]*, *José C. HERNÁNDEZ* [0000-0001-7245-9564]*, *Jesús A. CORTES***

# APPLICATION FOR FUNCTIONALITY AND REGISTRATION IN THE CLOUD OF A MICROCONTROLLER DEVELOPMENT BOARD FOR IOT IN AWS

**Abstract**

*The use of the Amazon Web Services cloud enables new functionalities that are not possible with traditional solutions: low latency, local data processing and storage, and direct connectivity to other cloud services. Reimagining the way IoT connectivity services are presented by combining AWS cloud technology with mobile connectivity offers rapid prototyping to help connect devices natively over Wi-Fi. For this, the MQTT communication protocol is used to interact with the IoT device and exchange data, which allows controlling the basic functions of a sensor node. The installation is realized through a software development kit (SDK), which allows the creation of an application for Android devices. This solution gives the option to integrate together, improving the connectivity of the IoT system. The results enable board logging and network configuration, and can also be used to control the IoT device. The embedded firmware provides the required security functions.*

## 1. INTRODUCTION

The results presented in this article are part of a development platform for Internet of Things (IoT) Solutions. But, are cloud computing technologies really necessary to create an IoT scenario?

If talk about the technical requirements, the immediate answer is no. Data processing and commands can be performed locally through an internet connection. However, there are interesting benefits for IoT applications if we are going to use the cloud. To mention some of them, there is scalability, system availability, the ability to aggregate large amounts of data, reduced infrastructure costs, etc.

*Computer Systems Department, TecNM/Campus Apizaco Tlaxcala, Mexico, m19371374@apizaco.tecnm.mx, m19371363@apizaco.tecnm.mx, m19371373@apizaco.tecnm.mx, edmundo.bh@apizaco.tecnm.mx, crispin.hh@apizaco.tecnm.mx

**Microside Technology, Software Development Department, Tlaxcala de Xicohténcatl, México, contacto@microside.com

IoT (Internet of things) is an emerging architecture based on the global Internet that facilitates the exchange of goods and services between supply chain networks and has a significant impact on the security and privacy of the actors involved(Salazar & Silvestre, n.d.). Is an extensive term that has infinite applications, however, that devices are connected or have some degree of intelligence is not new, the question is how IoT proposes to do it today, especially with the great progress it has gained with the use of mobile technology.

Amazon Web Services as a cloud computing solution became the most adopted and comprehensive platform in the world, which offers more than 200 integral services of data centers globally (AWS, n.d.).

The AWS architecture for this proposal supports devices to report their status by publishing messages using the MQTT protocol to exchange data with the cloud and the AWS mobile application (Guth et al., 2018). The message is sent to AWS IoT Device Shadow, and sends it to all users subscribed to that topic. Each device has a shadow object, or in other words a virtual representation of the device, which is used to save and retrieve information about the current state of the target in a JSON document, divided into a last reported state and a desired state (AWS Device Shadow, n.d.).

This application can send a request with the current state of the device or a change in the status of the device. When the message gets to the agent, the rules engine provides message processing and integration with other AWS services. The rest of this article presents the most significant results obtained and is organized as follows: section 2, related works and state of the problem; section 3, methodology and design procedure; section 4, results obtained; sections 5 and 6 refer to discussion and conclusion of this work.

## 2. LITERATURE REVIEW AND PROBLEM STATEMENT

The research studies consulted for this paper adopted AWS Serverless architecture as the cloud solution, focusing on a framework of mobile applications that control microcontroller devices and give way to IoT scenarios.

Wasoontarajaroen et al. (Wasoontarajaroen, Pawasan & Chamnanphrai, 2017) present an IoT device that was developed to monitor electrical energy consumption in a building. As a low cost IoT device, it consists of three modules available, including electrical power sensors, an Arduino Nano Mini microcontroller and a Wi-Fi board. The IoT device was tested by performing electrical energy measurement for a week. The test results confirmed that the device performed successfully, which could collect electrical energy data to support efficient energy management in the future.

In this paper, different techniques used for data classification in IoT devices using services provided by the AWS Kinesis platform were analyzed (Quadri & Yadav, 2018). Using Amazon Kinesis, the complete IoT architecture was analyzed in a real-world scenario, where the object of study was an agricultural station used to predict soil moisture. Subsequently, it was proposed to implement algorithms and methods such as an API for more efficient data classification and also to improve security measures, (AWS Kinesis, n.d.).

The main objective proposed by (Muñoz Carrasco & Garrido Márquez, 2018) focuses on the development of a mobile application that displays sensor data in real time and through which it is possible to act on them. All this depends on the development of two applications

for the Arduino and Raspberry boards, the last one with Android Things. A program was developed on Arduino to read analog and digital sensors, connect to Wi-Fi and both receive and send messages using MQTT.

Guha Roy et al. (Guha Roy et al., 2018) proposes a trade-off solution to explore the unusual behavior of Wireless Sensor Network gateways with theoretical expressions and apply dynamic gateway selection formulas to reduce end-to-end delay as well as increase delivery rate of packages. The project was developed using sensor devices, Arduino Uno, Raspberry Pi 3, Amazon web services, the MQTT broker, and the private cloud platform in their Mobile Cloud computer lab.

Amazon Web Services has gained popularity with IoT Core Platform, which integrates all the functions necessary to develop an IoT system. (AWS IoT Core, n.d.). The objective of (Imtiaz Jaya & Hossain, 2019) focused on exploring some of these functions and their integration into the proposed project, which consisted of the development and presentation of a prototype of an airflow control system for home automation, using AWS IoT Core and the MQTT protocol on the WebSocket server.

Kim et al. (Kim et al., 2019) proposes an MQTT as a communication protocol between Amazon Web Services and a mobile application. The problem detected in this research is the hot water wasted at sea by the electric companies. For this purpose, the hot water thermal energy management system used in an Internet of Things based fish farming system is developed. A control and monitoring system for an intelligent fish farm was proposed by building an intelligent fish that has the function of detecting and monitoring by various sensors elements such as oxygen, temperature and water level.

Villamil & Guarda (2019) focuses on the development of a mobile App with MIT app inventor, based on the analysis of an agile methodology for the development of mobile applications for the Internet of Things. In addition, it can be controlled from a LAN or WAN network by interfacing with the free hardware development boards Arduino Uno and Arduino Ethernet. The technical space is a data center in which temperature, humidity, sound recording and reproduction can be monitored by means of sensors.

The system proposed by (Mullapudi et al., 2020) is an advanced weather monitoring solution that uses AWS IoT to make real-time data easily accessible over a very wide range. The system monitors: the weather and its changes such as temperature, humidity, pressure, altitude using sensors and a Raspberry pi card as a controller. Data from these sensors is hosted in AWS Dynamo DB, which can handle more than 10 billion requests per day and can support peaks of more than 20 million requests per second (AWS DynamoDB, n.d.).

In this document (Wu et al., 2020), a new IoT fake app detection method, called MSimDroid, based on multidimensional similarities is proposed to mitigate the threat. This method focuses on application markets, and consists of complete application similarity, resource similarity, code similarity and their joint strategy. For the similarity calculation, a distinctive algorithm was designed based on the characteristic of different false patterns. Experiments showed that the accuracy of MSimDroid is over 99.31% on the ground truth dataset and 97.43% in the wild.

## 3. DESIGN PROCEDURE

### 3.1. Methodology

Three essential phases are essential in the method used for the development of the proposed model. These phases are: Design, Development and Validation, which are described below in Fig. 1.

In the Design phase, the general requirements and planning of the IoT solution are defined, wich are described in section 3.4. The design of each of the components is carried out, getting the screen design of the mobile interface, the design of the physical infrastructure and the choice of AWS cloud services. In the next phase, the development of each of the components of the system is completed, following the designs and requirements of the Design phase. The Validation phase includes a process of test protocols, which allows the verification of the correct operation of each component and then the integration of these components to build the system, validating the full compliance of the requirements stipulated in the Design phase.

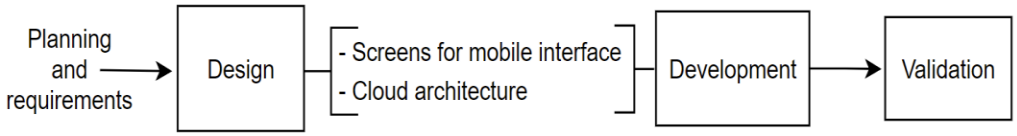


**Fig. 1. Methodology block diagram**

### 3.2. Hardware Requirements

The following hardware components are required for this work: Wi-Fi microcontroller development board, mobile device with android operating system with version 6.0 or higher and a Wi-Fi router.

#### 3.2.1. WiFi microcontroller development board

These days, there is a wide range of development boards that can be classified in several ways. According, development platforms can be classified into four groups: microcontroller-based, microprocessor-based, Field Programmable Gate Array (FPGA) and based and hybrid development platforms (Auer & Zutin, 2018).

The design of this work uses a development board includes a preloaded IEEE 802.11 b/g/n network controller for Internet of Things (IoT) applications. The main components that describe this kind of hardware are presented below in Fig.2:

- Qualified IEEE 802.11 b/g/n Network Controller Module,
- On-Board Host Microcontroller (SAML21G18B),
- CryptoAuthentication Device (ATECC608A),
- On-Board Li-Ion/Li-Po Charge Management Controller (MCP73833),
- On-Board Environment Sensor (BME280),
- Sensor de luz integrado (VEML6030).

The development board is designed to be powered by a USB interface. The central part of the board is the SAML21G18B microcontroller, which controls all the other devices that make up the board. The network controller module provides Wi-Fi capabilities. The ATECC608A handles certificate storage and authentication.

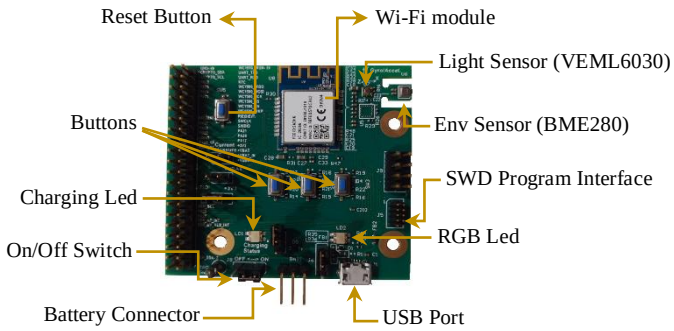


**Fig. 2. Wi-Fi microcontroller development board**

The development board is designed to be powered by a USB interface. The central part of the board is the SAML21G18B microcontroller, which controls all the other devices that make up the board. The network controller module provides Wi-Fi capabilities. The ATECC608A handles certificate storage and authentication.

### 3.3. Boot Manager Settings

A boot-loader is an application whose primary purpose is to allow a system's software to be updated without the use of specialized hardware. They can communicate over a variety of protocols such as USART, CAN, I2C, Ethernet, USB and the list goes on with all the protocols that exist. Systems with bootloaders have at least two program images coexisting on the same microcontroller and must include fork code that performs a check to see if an attempt is being made to update the software (Beningo, 2015).

For this project, the boot-loader allows programming of MCU firmware via USB port using Atmel Studio. The application firmware is used to test connection to AWS IoT. The firmware connects the board to the AWS IoT Cloud, updates the sensor data, gets the status of the leds, and publishes it to AWS Shadow. This is so that devices can communicate their status to AWS IoT and AWS IoT publishes MQTT messages to inform devices and applications of changes and events. Precisely the Message Queuing Telemetry Transport (MQTT) protocol is designed for light use of publish / subscribe messaging transport (Tsai, Hsu & Lo, 2020).

It´s important to emphasize that this service adds shadows to AWS IoT objects. Shadows can make a device's mode available for apps and other services, whether or not the device is connected to AWS IoT.

Boot-Loader mode is activated by pressing and holding the SW1 switch before turn on the board. The Samba GUI is used to load a firmware on the board using the USB port. The bootloader is saved at memory address 0x0-0x2000. The memory address for booting the firmware of an application is 0x2000.

The boot-loader can be reutilized even after modifying the application firmware and programming a new application firmware. Fig.3. shows a state machine that summarizes the bootloader process when Samba starts.

When loading the binary image into the device, only the upper part of flash starting at 0x2000 address should be programmed. Any attempt to write to the Samba Boot region using Samba GUI commands will be aborted and will return an error.

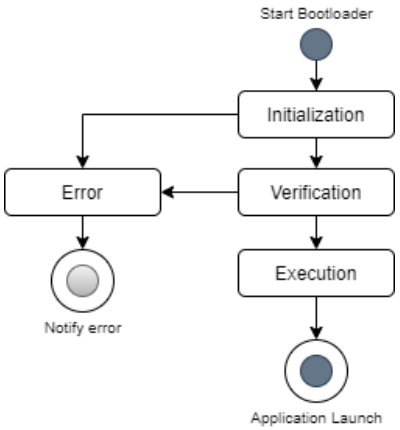


**Fig. 3. Boot-Loader process**

### 3.3.1. Firmware

The firmware of a microcontroller unit is a program consisting of a series of simple instructions intended to process data. For the most part it works like this: read input information, monitor the current state, develop a series of output instructions and send those output instructions. For this case, the option to use the MCU will be to turn on an LED when a certain condition is satisfied.

There are middleware modules between the application layer and the device driver layer. The middleware consists of different agents, such as resource manager, access controller scheduler, etc. Agents are small programs or sets of rules to execute a task. These agents depend on both the software and hardware of the connected device (Chang et al., 2020).

To develop the application, the use of middleware APIs was required to configure the device drivers. The following Tab.1. shows the middleware APIs required for this project:

**Tab. 1. Middleware APIS**

| Middleware Modules | Function |
|---|---|
| Button | Read button value. |
| Cloud Wrapper | Connect/Disconnect cloud, publish/subscribe MQTT channel. |
| Env_Sensor | Read sensor value. |
| IoT Message | Generate or parson JSON message to/from the AWS Shadow. |
| Led | Control Led LD2 color and blinking behavior. |
| Socket | Network socket API. |
| WLAN | Wlan features like app scanning, app connection, and so on. |

### 3.4. Software Requirements

The software used to successfully complete the objectives of the work are described: Samba v2.18 for programming the Application firmware of the board. Atmel Studio was used for the board firmware compilation procedure. Python scripts were used to provision the Wi-Fi board. The development of the mobile application required the official integrated development environment Android Studio. In the same way, AWS services were used for the serverless architecture of the project. Amazon Cognito was used to control users, Lambda to manage the policies that include an access token that contains the mobile application and DynamoDB to store information from the board registration process.

#### 3.4.1. Serverless architecture design with AWS

There is a way to build and deploy APIs, where there is no need to manage or maintain servers. These types of architectures are known as Serverless Architectures. Serverless computing has emerged as a new paradigm for the deployment of applications and services where the application logic is divided into functions that are executed in response to events (Parres-Peredo, Piza-Davila & Cervantes, 2019). To build our mobile back-end on AWS IoT Core, the main services for this architecture are described: Amazon Cognito, Amazon DynamoDB and AWS Lambda.

Amazon Cognito was used to provide user identity to end users of the product, including registration and login functions in the mobile application. With Amazon Cognito, the user can register and login to the account and control the development board after successful authentication. Amazon Cognito returns user group tokens to the application. For the case, tokens can be used to grant users access to their own server-side resources or the Amazon API Gateway as represented in the Fig.5.

The DynamoDB table collects the user account id, the device id and the device name. The mobile application saves this information in the DynamoDB table during the board check-in procedure.

The Lambda function browses the AWS DynamoDB table to find the element id of the device that corresponds to the account id of the application. Then, the Lambda function code updates the value to AWS IoT Shadow and gets the device's AWS IoT Shadow to control the led.

To exchange data from the device to the IoT backend, messages must be published via the MQTT protocol to the AWS IoT Core message broker, this process is shown in the description of the solution in Fig. 6.

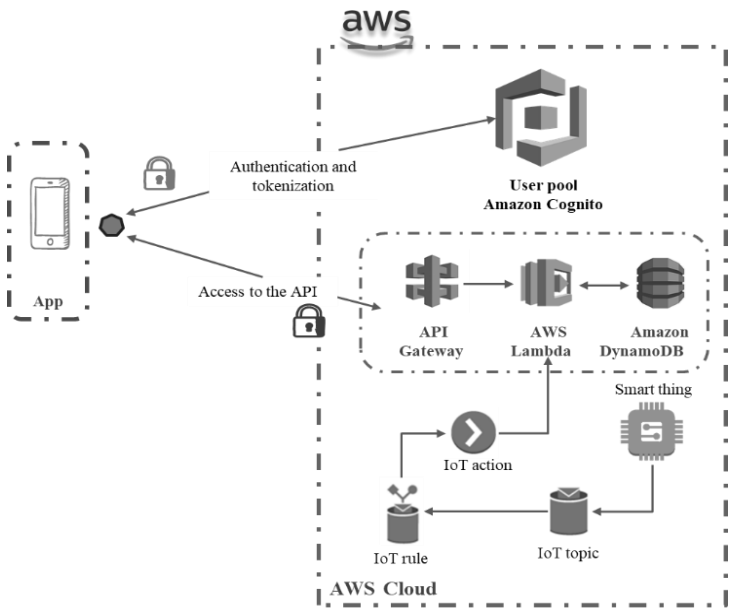


**Fig. 5. Serverless architecture in AWS**

The AWS IoT Device Shadow service collects and retrieves the current status information from the board. The board updates the sensor and LED data in AWS IoT by posting an MQTT message in Shadow MQTT and thus obtains the latest LED status from AWS IoT by subscribing to Shadow MQTT/update/delta topics. The shared message is shown in the Fig.7. This is how the mobile application controls the LED color by posting an MQTT message on Shadow.

The MCU runs AWS IoT sdk to connect the AWS IoT cloud board. AWS IoT sdk includes the cloud connection API and the MQTT signature and publishing API. The MQTT client ID is required for the connection and the subject key identifier of the device certification, which is used as the MQTT client ID. The board connects to the AWS IoT cloud with the TLS encryption suite 1. 2. The device certificate and private key are stored in the cryptographic authentication device.

The device's certificate and private key are stored in the Crypto Authentication ECC608 device. To perform authentication with the cloud, the certificate and key in ECC608 are used. After Cloud Configuration, Id's values corresponding to the identity group are collected from the Cognito console identity group, the AWS IoT Endpoint, which can be found in the AWS IoT console configuration page, to build the application apk file, as shown in Fig. 8.

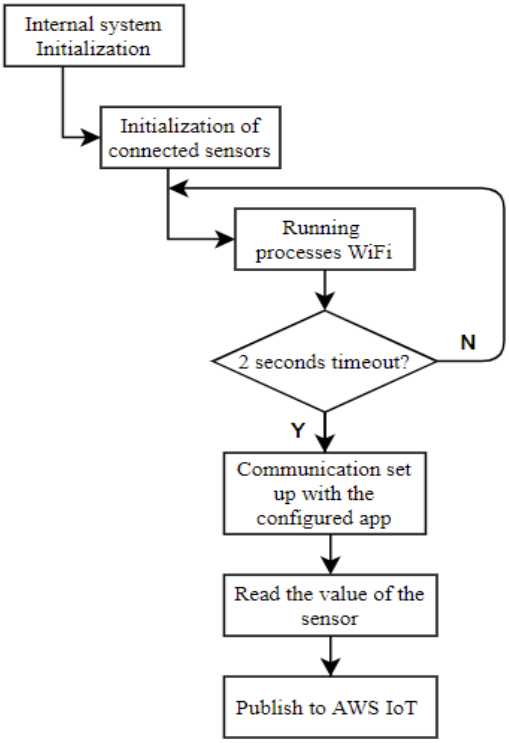


**Fig. 6. Application flowchart**


```
{
 "reported": {
   "Mac Address": f8f00570c942,
   "uv": 427000,
   "COUNT": 34,
   "hum": 48,
   "temp": 2468,
   "BUTTON_1": 1,
   "BUTTON_2": 1,
   "LED_R": 1,
   "LED_G": 0,
   "LED_B": 1,
   "LED_INTENSITY": 21,
   "Light": 1
  }
}
```


**Fig.7. Shared shadow message**

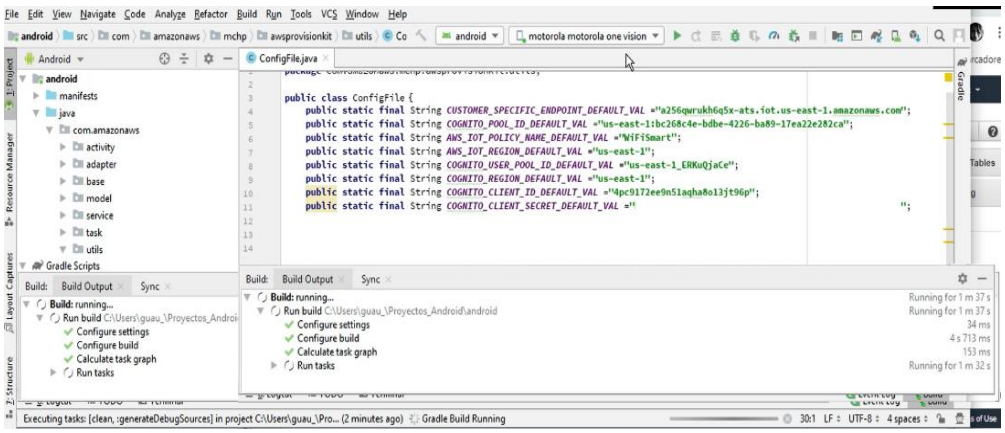


**Fig. 8. Mobile app source file**

## 4. SOLUTION DESCRIPTION AND RESULTS

When the development board is turned on, the internal MCU system and all connected sensors go through the initialization stage. After this stage, the board tries to connect to the configured app. LD2 flashes blue every 500 ms during this process. When the board successfully connects to the app and obtains the IP address, the LED flashes blue every 100 ms. Then, the board tries to connect to AWS IoT. After successful connection to the cloud, LD2 remains solid blue as shown in Fig. 11. The board tests the sensor data every two seconds.If the sensor data changes, the data is published to AWS IoT Shadow, this process is described in the flowchart Fig. 6. At this point, can control the microcontroller device with the mobile application.

Led LD2 shows the operation of the board. When the board connects to the AWS cloud, LD2 turns on and the color can be changed using the mobile app; Tab. 2 describes the behavior depending the status of LD2 led.

**Tab. 2. LD2 States**

| LD2 | Status | Description |
|---|---|---|
| Red | Blinks for every 0.5 seconds | Network provisioning mode. |
| | Blinks for every 100 milliseconds | The mobile app successfully connects to the card for Network Configuration. |
| Blue | Blinks for every 0.5 seconds | Attempts to connect to the Application. |
| | Blinks for every 100 milliseconds | It successfully connects to the Application, and attempts to connect to AWS IoT Cloud. |
| | Turn on | The Wi-Fi sensor board successfully connects to the AWS IoT cloud. |
| Green | Blinks for every 0.5 seconds | Firmware update mode. |

The following process is used to register the card and configure the network with the application: The board is connected to the network and allows control of the board using the mobile application account, for this it is necessary to register as a new user.

This record will be reflected in our User Group in the Amazon Cognito management console. For the test, have the user *testuser* item a) Fig. 13. During this process, the board must be prepared for board registration mode and network configuration. The LD2 Led flashes red.

Then, the mobile application acts as a Wi-Fi station to connect the board. A TCP tunnel is created with port 8899. The SSID of the target network and the password phrase are transferred from the mobile application to the target in this tunnel. When the board successfully obtains the SSID and password phrase, it switches to Wi-Fi station mode and connects to the target App using the Wi-Fi credential.

In this process, the Device Thing ID is also transferred from the board to the mobile application. When the mobile application obtains the Device Thing ID Fig.9, joins the Device Thing ID with the account ID of the mobile application and the name of the device on the board in an AWS DynamoDB table. Fig.12.

When the user sign in to the mobile app, the mobile app scans the table in AWS DynamoDB to display the dashboard information that corresponds to their mobile app account ID.

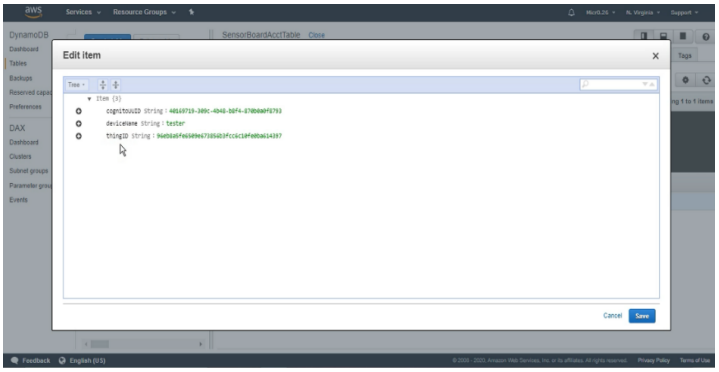


**Fig. 9. Device thing Id**

Fig. 13. show the process that the application follows to register a new device, item a) of the same figure, shows the parameters of the card, which are the color of the LED LD2, the current temperature and humidity.

**Fig. 10. Provisioning status**

**Fig. 11. Successful connection status**

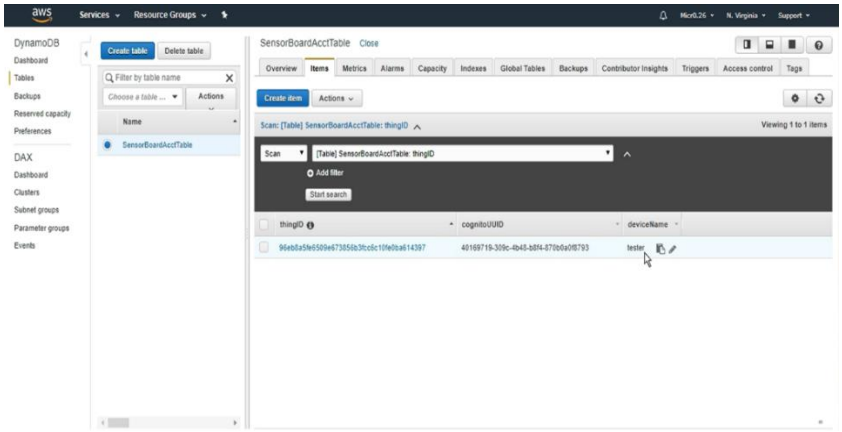


**Fig. 12. Table with thing information in DynamoDB**

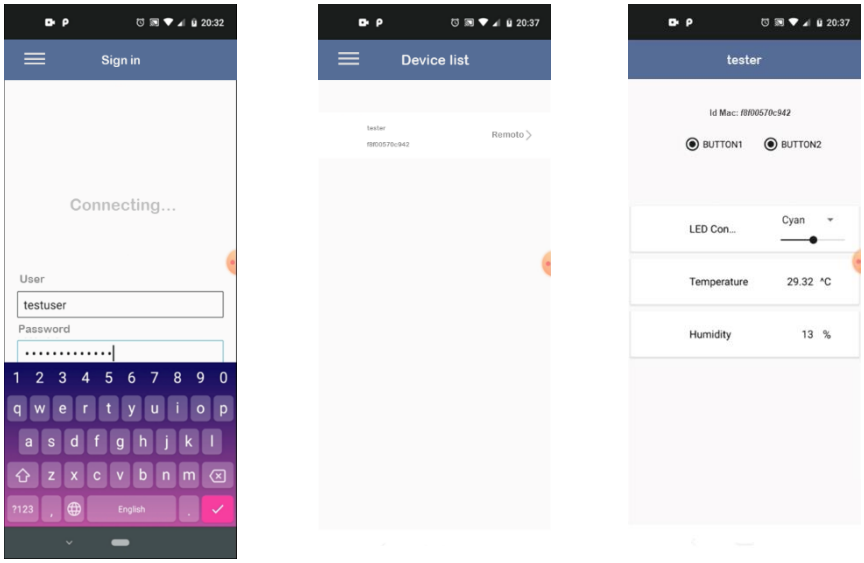


**a) Login** **b) Paired devices** **c) Device control**

**Fig. 13. App Screenshots**

## 5. DISCUSSION

The percentage of progress of the project is calculated based on (DocIRS Document Information Retrieval Systems, n.d.), and the subprojects to be completed for the second part of this project are listed in Tab.3.

It's important to emphasize that the AWS cloud registration goal is successfully completed, as well as the basic control of Led LD2, and the knowledge of the humidity and temperature of the microcontroller board. With the cloud registration of an object, is possible manage the number of connected and controlled devices and ensure a successful connection for the subsequent implementation of the Alexa voice assistant. The mobile application only

presented compatibility issues for higher versions of Android 9 (Pie), so these requests will be resolved subsequently.

$$AP = \sum_{i=1}^{n} B_i \cdot AS_i \quad (1)$$

$$AS = \frac{N° \; completed \; subproject \; processes}{N° \; total \; subproject \; processes \; completed} \cdot 100 \quad (2)$$

where: *AP* – project progress measured as a percentage,
*n* – no. of subprojects in the project,
*B* – weighting (ratio of processes in the subproject/total number of processes),
*AS* – subproject progress in percentage,
*i* – summation index, *i* = 1,2, 3…*n.*

**Tab. 3. Project progress**

| Subprojects | % state of progress |
|---|---|
| Planning<br>✓ Data collection<br>✓ Analysis<br>✓ Requirements | 100 |
| Design<br>✓ AWS Architecture<br>✓ Interface App mobile | 100 |
| Development<br>✓ Boot-Loader Firmware<br>✓ Application Firmware<br>✓ AWS Provision<br>✓ Mobile App<br>AWS Architecture<br>Alexa Skills | 66.66 |
| Testing<br>✓ System testing<br>✓ Document problems found<br>Correct issues found | 66.66 |
| *AP= 71.42%* | |

## 5. CONCLUSIONS AND FUTURE WORK

The proposed architecture in AWS to manage IoT devices had a positive effect, for the continuous registration of devices, after having tested with different certificates. This system has the ability to scale the functionality of different microcontroller development cards for Wi-Fi. As well as the technological interaction of users with connected devices. Future research areas include:

1. Incorporate the AWS Amplify framework as a user administrator resource to easily manage application content outside of the AWS console.
2. Integration of the Amazon Alexa Voice Assistant.
3. Lambda functions to process Alexa skill directives.

## REFERENCES


Auer, M.E., & Zutin, D.G. (2018). *Online Engineering & Internet of Things. Proceedings of the 14th International Conference on Remote Engineering and Virtual Instrumentation REV 2017, held 15–17 March 2017, Columbia University, New York, USA.* Springer.

AWS. (n.d.). *Amazon Web Services*. Retrieved March 18, 2021 from https://aws.amazon.com/es/what-is-aws

AWS Kinesis. (n.d.). *Amazon Web Services*. Retrieved March 18, 2021 from https://aws.amazon.com/es/kinesis

AWS Device Shadow. (n.d.). *Amazon Web Services*. Retrieved March 18, 2021 from https://docs.aws.amazon.com/es_es/iot/latest/developerguide/iot-device-shadows.html

AWS DynamoDB. (n.d.). *Amazon Web Services*. Retrieved March 18, 2021 from https://aws.amazon.com/es/dynamodb

AWS IoT Core. (n.d.). *Amazon Web Services*. Retrieved March 18, 2021 from https://aws.amazon.com/es/iot-core/

Beningo, B.J. (2015). *Bootloader design for MCUs in Embedded Systems, Rev A2*. Beningo Engineering.

Chang, K.C., Chu, K.C., Wang, H.C., Lin, Y.C., & Pan, J.S. (2020). Agent-based middleware framework using distributed CPS for improving resource utilization in smart city. *Future Generation Computer Systems*, *108*, 445–453. https://doi.org/10.1016/j.future.2020.03.006

DocIRS Document Information Retrieval Systems. (n.d.). *DocIRS Technology*. Retrieved March 18, 2021 from https://www.docirs.cl

Guha Roy, D., Mahato, B., De, D., & Buyya, R. (2018). Application-aware end-to-end delay and message loss estimation in Internet of Things (IoT) — MQTT-SN protocols. *Future Generation Computer Systems*, *89*, 300–316. https://doi.org/10.1016/j.future.2018.06.040

Guth, J., Breitenbücher, U., Falkenthal, M., Fremantle, P., Kopp, O., Leymann, F., & Reinfurt, L. (2018). *A Detailed Analysis of IoT Platform Architectures: Concepts, Similarities, and Differences*. In B. Di Martino, K.C. Li, L. Yang, A. Esposito (Eds.), *Internet of Everything. Internet of Things (Technology, Communications and Computing)* (pp. 81–101). Springer. https://doi.org/10.1007/978-981-10-5861-5_4

Imtiaz Jaya, N., & Hossain, M.F. (2019). A Prototype Air Flow Control System for Home Automation Using MQTT over Websocket in AWS IoT Core. In *Proceedings – 2018 International Conference on Cyber-Enabled Distributed Computing and Knowledge Discovery, CyberC 2018* (pp. 111–117). IEEE. https://doi.org/10.1109/CyberC.2018.00032

Kim, Y., Lee, N., Kim, B., & Shin, K. (2019). Realization of IoT based fish farm control using mobile app. In *Proceedings - 2018 International Symposium on Computer, Consumer and Control* (pp. 189–192). IEEE. https://doi.org/10.1109/IS3C.2018.00055

Mullapudi, R.K., Mallika, G., Nikitha, K., & Bhanu Sree, M. (2020). Weather Monitoring using AWS Cloud Computing. *International Journal of Advance Research and Innovation*, *8*(2), 205–208.

Muñoz Carrasco, J., & Garrido Márquez, D. (2018). *IoT home automation application using Android Things*. https://riuma.uma.es/xmlui/bitstream/handle/10630/17551/Mu%C3%B1oz%20Carrasco%2C%20Juan%20Memoria.pdf?sequence=1&isAllowed=y

Parres-Peredo, A., Piza-Davila, I., & Cervantes, F. (2019). Building and evaluating user network profiles for cybersecurity using serverless architecture. In *2019 42nd International Conference on Telecommunications and Signal Processing, TSP 2019* (pp. 164–167). IEEE. https://doi.org/10.1109/TSP.2019.8768825

Quadri, N.S., & Yadav, K. (2018). Efficient Data Classification for IoT Devices using AWS Kinesis Platform. In *21st Saudi Computer Society National Computer Conference, NCC 2018* (pp. 1–5). IEEE. https://doi.org/10.1109/NCG.2018.8593105

Salazar, J., & Silvestre, Y. S. (n.d.). *Internet de las cosas*. https://core.ac.uk/download/pdf/81581111.pdf

Tsai, M.H., Hsu, Y.C., & Lo, N.W. (2020). An Efficient Blockchain-based Firmware Update Framework for IoT Environment. In *Proceedings - 2020 15th Asia Joint Conference on Information Security, AsiaJCIS 2020* (pp. 121–127). IEEE. https://doi.org/10.1109/AsiaJCIS50894.2020.00030

Villamil, X., & Guarda, T. (2019). Mobile application developed with agile methodology for IoT controlled from a LAN / WAN network with a free hardware development board (Arduino). *Iberian Journal of Information Systems and Technologies*, *17*, 379–392.

Wasoontarajaroen, S., Pawasan, K., & Chamnanphrai, V. (2017). Development of an IoT device for monitoring electrical energy consumption. In *2017 9th International Conference on Information Technology and Electrical Engineering, ICITEE 2017* (pp. 1–4). IEEE. https://doi.org/10.1109/ICITEED.2017.8250475

Wu, P., Liu, D., Wang, J., Yuan, B., & Kuang, W. (2020). Detection of Fake IoT App Based on Multidimensional Similarity. *IEEE Internet of Things Journal*, *7*(8), 7021–7031. https://doi.org/10.1109/JIOT.2020.2981693

Applied Computer Science, vol. 17, no. 2, pp. 28–39
doi: 10.23743/acs-2021-11

Submitted: 2021-04-20 | Revised: 2021-05-15 | Accepted: 2021-06-15

*pantograph system, model reduction, PSO,G.A-PID,IMC,LQR*

*Nasir A. AL-AWAD* [0000-0003-3059-4375]*, *Izz K. ABBOUD* [0000-0002-8344-8585]*, *Muaayed F. AL-RAWI* [0000-0003-1841-1222]*

# GENETIC ALGORITHM-PID CONTROLLER FOR MODEL ORDER REDUCTION PANTOGRAPHCATENARY SYSTEM

**Abstract**

*Controlling the contact force between the pantograph and the catenary has come to be a requirement for improving the performances and affectivity of high-speed train systems Indeed, these performances can also significantly be decreased due to the fact of the catenary equal stiffness variation. In addition, the contact force can also additionally differ and ought to end up null, which may additionally purpose the loss of contact. Then, in this paper, we current an active manipulate of the minimize order model of pantograph-catenary system. The proposed manipulate approach implements an optimization technique, like particle swarm (PSO), the usage of a frequent approximation of the catenary equal stiffness. All the synthesis steps of the manipulate law are given and a formal evaluation of the closed loop stability indicates an asymptotic monitoring of a nominal steady contact force. Then, the usage of Genetic Algorithm with Proportional-Integral-derivative (G.A-PID) as proposed controller appeared optimum response where, the contacts force consequences to be virtually equal to its steady reference. Finally it seems the advantageous of suggestion approach in contrast with classical manipulate strategies like, Internal mode control(IMC) method, linear quadratic regulator (LQR).The outcomes via the use of MATLAB simulation, suggests (G.A-PID) offers better transient specifications in contrast with classical manipulate.*

## 1. INFORMATION FOR AUTHORS

Actually, the complicated conduct of the pantograph-catenary machine received the interest of many researchers many a long time ago. Almost all ancient research have pointed out that, at high speed, better performances can be completed solely if a new layout of the standard system have been carried out,which implied a giant quantity of resources and the exchange of nearly all the structures of the railway systems. As a result, the use of lively pantographs used to be recommended as an alternative of giant investments. Thus, in order to enhance the manage device performances, approximate models of the pantograph-catenary machine have been regarded. Accordingly, many researchers assumed that the complicated dynamics of the catenary may be well approximated with the aid of a linear

* Mustansiriyah University, Faculty of Engineering, Computer Engineering Department, Baghdad, Iraq, muaayed@uomustansiriyah.edu.iq

mechanical system with space-varying lumped parameters. This means that the catenary parameters may additionally be viewed time various with a charge decided by the time pace. Then, as uncertainties are existing in nearly all designed models, many researchers proposed the use of robust manage strategies (Chater et al., 2015), whilst sometimes, the problem was solved by solely tuning popular PID controllers .More recently, a second order sliding mode primarily based control scheme that avoids the measurement of the contact force used to be suggested. Other associated 2nd order sliding mode strategies to this trouble are (Bartolini et al., 2003). However, the usage of the Algebraic Observability Theory, this thinking turns out to require greater knowledge, as it requires the cost of the manipulate force utilized to the higher frame, the speed and the acceleration of the top and lower frames, which can also render the manipulate system complicated and expensive. Hence, in all following works, to operate output feedback, the contact force is evaluated by using skill of load cells whose measurements are compensated by means of accelerometers (Pisano & Usai, 2008).While some other is to take benefit of the improvement in manage theory—this is the idea of energetic manipulate of pantograph-catenary's machine in order to keep an superior contact force. Indeed this has attracted a lot interest in the study of pantograph-catenary interaction. For example, easy nation comments control approach is viewed in (Arnold & Simenon, 2000); in (Giovanelli & Farella, 2016), an LQR is designed the use of a linear pantograph-catenary model, whilst in (Liu et al., 2016) a high order sliding mode variable structure controller is built for the energetic manipulate of pantograph; an evolutionary multiobjective optimization method is utilized taking into account the perturbations brought on by means of the time-varying stiffness of catenary, differential-geometric idea is used for output-perturbation decoupling for a nonlinear pantograph-catenary model in (O'Connor et al., 1997); very recently fuzzy common sense has additionally discovered application in the active control strategies such as in (Pourzeynali, Lavasani & Modarayi, 2007). The pantograph and catenary form an oscillating gadget that is coupled by way of the contact force between the pantograph head and the contact wire. Too giant contact force variation can lead to loss of contact, arcing and wear as properly as harm to the system. The mission of regulating the contact pressure to a pre-specified steady value in the presence of model uncertain-ties and exterior disturbances is suggested.

This paper is arrangement as following: In section 2, the mathematical model of the pantograph-catenary device is represented. Section three it gives the model order reduction. In section 4, we present the controller design of classical and proposed method. Section 5 presents the discussion and evaluation of simulation results.

## 2. MATEHMATICAL MODEL OF THE SYSTEM

This section is dealing with the components of the electrical train and can be divided by sub-mechanical systems.

### 2.1. Pantograph

The purpose of pantograph device is to accumulate electrical current from the catenary cable system. In order to gather the current and no longer to interfere with the passing non-electric train below the overhead lines, the essential frame is fold-able and can vertically increase the pantograph head a full-size distance. To gain appropriate current collection,

the pantograph head is sprung and is pushed towards the overhead line. The drive, typically operated via compressed air from the brake system, is used to energy the device to raise or fall, and offers enough uplift force to preserve the contact between overhead line and pantograph head. Nowadays, there are several kinds of pantographs existing, but the standards are almost the identical (Matvejevs & Matvejevs, 2011). The pantograph consists of a part of physique that come in contact with the overhead catenary and a body that supports it. The body is divided into upper frame and lower frame. The important spring acts to lift the whole pantograph upwards as shown in Fig. 1.The pantograph doesn't control the versions of the contact force by means of itself. In order to control the contact force between the pantograph and the catenary, the active pantographs with the pneumatic actuator have been developed. It used to be found via some experiments that the frame had flexibility which may want to not be omitted to control the contact force. Some high-speed rail structures are powered with the aid of electrical energy furnished to a pantograph on the train's roof from a catenary overhead. The force applied with the aid of the pantograph to the catenary is regulated to keep away from loss of contact due to immoderate transient motion. A proposed method to adjust the force makes use of a closed-loop feedback system, whereby a force, $F_{up}$, is utilized to the bottom of the pantograph, resulting in an output force applied to the catenary at the top. The contact between the head of the pantograph and the catenary is represented with the aid of a spring. The output force is proportional to the displacement of this spring, which is the distinction between the catenary and pantograph head vertical positions.

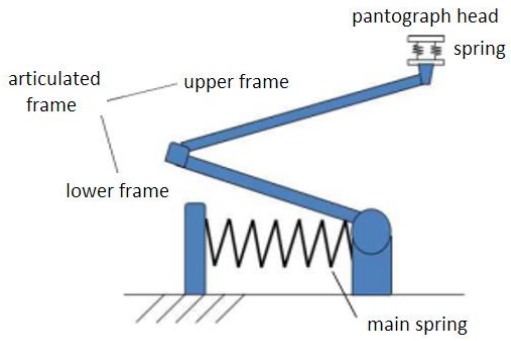


**Fig. 1. Pantograph system**

## 2.2. Catenary

The catenary usually consists of the contact wire, a continuous conduction which transfers electric powered present day to the transferring train through the pantograph, and some different supporters to aid the weight of the contact line and to keep the contact wire in a certain form at positive positions. The structure of the catenary proven in Figure 2. In general, a catenary is composed of one or two wires that make sure the strength transmission to the pantograph, and it also counts with one or two complementary wires that are charged of maintaining the horizontality of the contact wire, as found in Fig. 2.

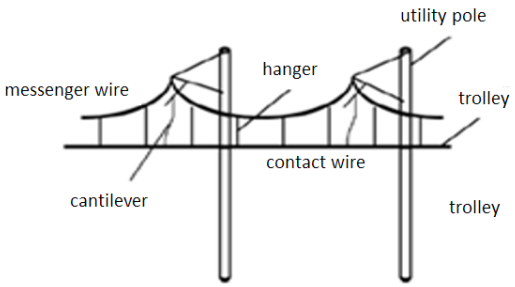


**Fig. 2. Catenary system**

The train is linked to the catenary system by way of pantograph which is set up on the roof of the train. The catenary has two wires, the contact wire which is connected to the pantograph and the messenger wire above the contact wire is linked together over the droppers. The pantograph catenary is targeted to transfer electric current to the train. As a contact pair is continually moving, it is necessary to maintain the contact between pantograph and catenary tight and stable.

Consider the train circumstance is continually moving, it is wanted to control the contact power varieties and not to get the contact misfortunes between the pantograph and catenary framework. The overhead contact wire and pantograph need to stay in touch with one another.

The proposed strategy to manage the power between the pantograph shoe and the electric contact utilizes a closed-loop framework, whereby a force is connected to the base of the pantograph, bringing about a yield power connected to the catenary at the top. Fig. 3, demonstrates the pantograph and catenary coupling.

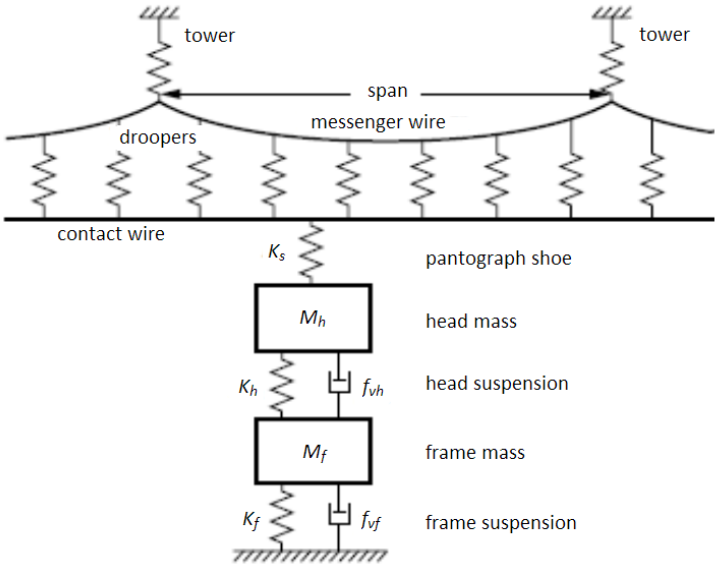


**Fig. 3. Pantograph and catenary coupling system**

Assuming that the overhead contact wire and the shoe on the pantograph head are linked all the time, the contact between the head of the pantograph and the catenary is represented with the aid of a spring. Output force is proportional to the displacement of the spring, which is the distinction between the catenary and pantograph head vertical positions. Let is static uplift force generated through the essential spring which is denoted as the actuator force and is the role at the top of catenary, so that the equations of movement are (Lin, Lin & Yang, 2007):

$$F_{up} - f_{vf}\dot{Y}_f - K_h\left(Y_f - Y_h\right) - f_{vf}\left(\dot{Y}_f - \dot{Y}_h\right) = M_f\ddot{Y}_f \tag{1}$$

$$K_h\left(Y_f - Y_h\right) - f_{vh}\left(\dot{Y}_f - \dot{Y}_h\right) - K_s(Y_h - Y_{cat}) = M_h\ddot{Y}_h \tag{2}$$

$$K_sY_h - \left(K_s + K_f\right)Y_{cat} = 0 \tag{3}$$

Where $M_f$ and $M_h$ are frame and head masses, $f_{vf}$ and $f_{vh}$ are frame and head dampers coefficients, finally$K_f$, $K_h$ and $K_s$ are frame, head and spring stiffness coefficients. Take all the physical parameters from (Shudong, Jingbo & Guosheng, 2008), and these are shown in Tab. 1:

**Tab.1. Physical parameters**

| Parameter | Value |
|---|---|
| $M_f$ | 17.2 [Kgd] |
| $M_h$ | 9.1 [Kg] |
| $f_{vf}$ | 30 [N.s/m] |
| $f_{vh}$ | 130 [N.s/m] |
| $K_f$ | $1.535{\cdot}10^6$ [N/m] |
| $K_h$ | $7{\cdot}10^3$ [N/m] |
| $K_s$ | $82.3{\cdot}10^3$ [N/m] |

By solving Eq. (1), Eq. (2) and Eq. (3), the transfer function is determined as (Shudong, Jingbo & Guosheng, 2008):

$$G(s) = \frac{Y_h(s) - Y_{cat}(s)}{F_{up(s)}} = \frac{0.7883(s+53.85)}{s^4+23.59s^3+9785s^2+81190s+3.493{\cdot}10^6} \tag{4}$$

## 3. MODEL ORDER REDUCTION

As considered from Eq. (4), the order is fourth, this gives a complicated analysis and design, so that it wishes model order reduction. There many methods for this and can be classified in classical and modern (Makino et al., 2018) but in this paper can be used particle swarm optimization (PSO) technique, Which has been proposed via (Al-Awad & Al-Seady, 2020), as a result developed in hundreds of scientific papers, and utilized to many numerous problems, for instance neural networks training, information mining, signal processing, and optimum plan of experiments. PSO is a population-based method, that is, it represents the

nation of the algorithm by using a population, which is iteratively modified until a termination criterion is satisfied. In PSO algorithms, the populace P= {p1,…,pn} of the possible options is regularly referred to as a swarm. The feasible solutions p1,…,pn are called particles. The PSO technique views the set Rd of possible options as a "space" where the particles "move". For solving practical problems, the variety of particles is usually chosen between 10 and 50. The normal aim of the particle swarm optimization (PSO) algorithm is to solve an unconstrained minimization problem. PSO would possibly sound complicated, but it is certainly a very easy algorithm. Over a range of iterations, a group of variables have their values adjusted nearer to the member whose value is closest to the goal at any given moment. Generally there are many papers about the algorithm of PSO and how can be used to solve the issues. In this paper the integral square error criteria (ISE) is used as performance index to decrease the error between the parameters of original and reduced systems. The parameters of PSO algorithm in this work are considered as follows:

1. Inertial weight: 0.9.
2. Acceleration factors (c1 and c2): are (0.12) and (1.2).
3. Population size: 200.
4. Maximum iteration: 1000.

The objective function (OF) must be a minimization problem. Let us suppose that there is a problem defined is needed to be optimized by using:

$$ISE = \int_0^{\infty} [e(t)]^2 \, dt \tag{5}$$

After using PSO MATLAB program, it is found that the reduced function is:

$$G_r(s) = \frac{9.816 \cdot 10^{-7} s + 5.881 \cdot 10^{-5}}{0.0129 s^2 + 0.1006 s + 4.843} \tag{6}$$

There are no large differences between original and reduced order systems, where both have the same overshot and settling time, Fig. 4 shows transient response of original and reduced order systems. For simplicity in design and analysis, Eq.(6) can be used instead of Eq.(4).

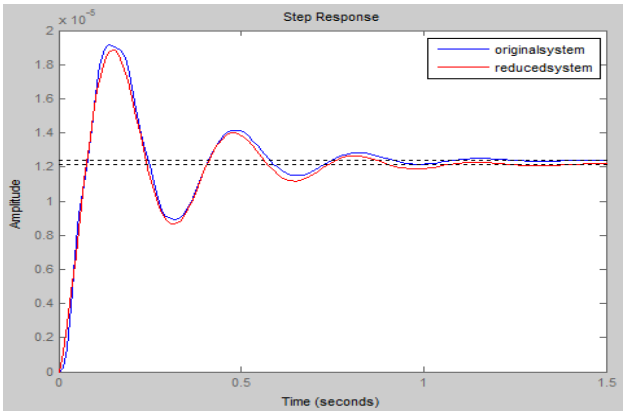


**Fig. 4. Shows step response of original and reduced order system**

As seen from Fig. 4 the transient specifications are almost identical. Tab. 2 shows comparison parameters between original and reduced system.

**Tab. 2. Transient response parameters comparison**

| System | Max. overshot Mp% | Settling time Ts (sec) | Rise time Tr (sec) | Steady-state error Ess |
|---|---|---|---|---|
| Original System | 54.8% | 0.875 | 0.0481 | 0.0000124 |
| Reduced System | 55% | 0.99 | 0.057 | 0.000012 |

## 4. CONTROLLERS DESIGN METHODS

Before starting with design methods, it is necessary, to assign the requirements design. Pantograph and catenary system must be quickly response and without overshot.

### 4.1. Internal mode control (IMC)

The improvement of IMC had begun on account that the late Nineteen Fifties in order to layout a most suitable feedback controller. The potential of IMC to meet most of the manipulate targets has led to their significant acceptance in the control industry. It is because, for practical utility is simple and strong to take care of the mannequin inaccuracies. The distinguishing characteristic of IMC shape is the incorporation of the system model which is in parallel with the proper system or the plant. Fig. 5 indicates the schematic graph for IMC process. The proposed controller works for specific values of the filter tuning parameters to achieve the preferred response As the IMC method is primarily based on pole zero cancellation, methods which incorporate IMC graph standards result in a desirable set point responses.

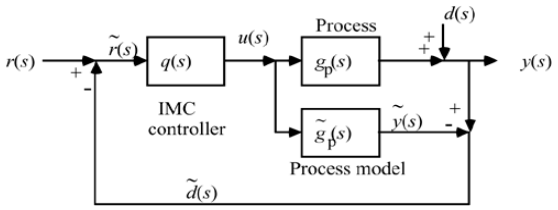


**Fig. 5. Shows IMC structure**

The IMC layout method consists of two steps: The first step will insure that q(s) is steady and causal; the second step will require q(s) to be proper. The filter transfer characteristic is to make the controller stable, causal and proper. This strong compensator (filter) performs a pivotal function in the device as it combats plant uncertainties in the system layout so that the designed manipulate system can achieve the diagram targets of strong balance and robust performance. The controller with filter is given by:

$$q(s) = \frac{{G_{p(s)}}^{-1}}{(\lambda s+1)^n} \quad (7)$$

Where $n$ is the order of the filter and $\lambda$ is the filter time constant. The order of the filter is chosen such that is appropriate to stop immoderate differential manipulate action. The filter parameter in the plan can be chosen as a rule of thumb. Considering the order of the filter same as the plant $n = 2$, and $\lambda = 0.1, 0.01$. Fig. 6. Shows step response of the system with IMC. It appears that $y1$, with $\lambda = 0.1$, there is no Mp% , but $Ts = 0.565$ sec and $Ts = 0.333$ sec, are large values. For $y2$ with $\lambda = 0.01$, there is $Mp = 5.52\%$ and short values of $Ts = 0.0466$ sec, $Tr = 0.0099$ sec, so that needs more tuning to select best value of $\lambda$.

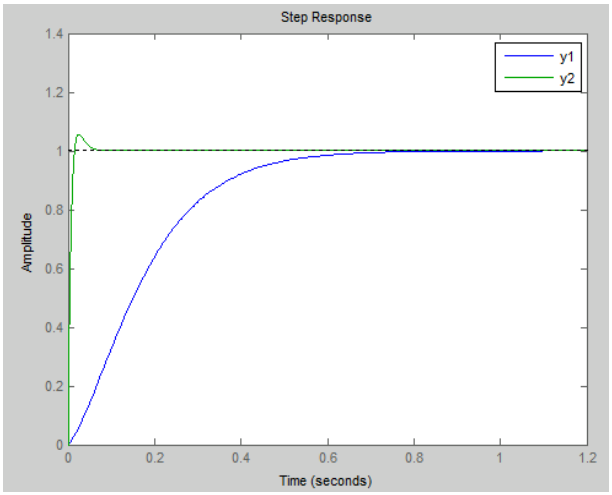


**Fig. 6. Shows step response of the system with IMC with different values of $\lambda$: $\lambda$=0.1 for $y1$ and $\lambda$ =0.01 for $y2$.**

## 4.2. Proposed G.A-PID controller

G.A-PID controller has been proposed for tuning PID boundaries for Eq.(6) utilizing a weighted mix of target work, specifically, integral absolute error (IAE). The G.A is an arbitrary pursuit technique that can be utilized to illuminate nonlinear arrangement of conditions and streamline complex issues. GA utilizes probabilistic progress administers rather than deterministic principles and handles a populace of potential arrangements known as people or chromosomes that develop interactively. Every emphasis of the calculation is named as generation. The development of arrangements is mimicked through a wellness work and hereditary administrators, for example, reproduction, crossover, and mutation (Kennedy & Eberhart, 2016). Genetic algorithm as delineated in Fig. 7. is normally instated with an irregular populace. This populace is typically spoken to by a real-valued number or a double string called a chromosome. The presentation of the individual is estimated and surveyed by the goal work, which allots every individual a comparing number called its fitness. The fitness of every chromosome is surveyed and natural selection procedure is applied. In this work, the error value is utilized to survey the fitness of every chromosome.

There are three primary activities in a Genetic algorithm, reproduction, crossover, and mutation. Crossover and mutation costs can have an effect on the convergence of GA, however nothing can evaluate to the level of manipulate carried out via manipulating of the inertial weight. The greater reduce of inertial weight the greater make bigger the swarm's convergence. This type of manipulate allows finding out the price of convergence, and the level of 'stagnation' ultimately achieved. Stagnation occurs in GA when all of the individuals have the identical genetic code. In that case the gene pool is uniform, crossover has little or no impact on population and each successive generation is surely identical as the first (Haamed & Hameed, 2020).

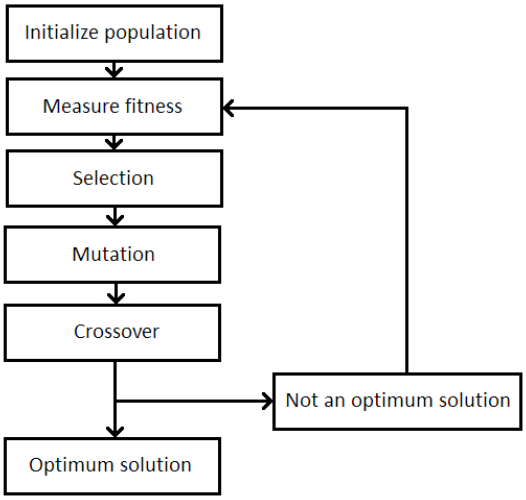


**Fig. 7. Flowchart of G.A procedure**

Genetic Algorithm Steps are:

1. Initialize the parameter with a population of random solutions, such as crossover rate, mutation rate, number of clusters, and number of generations. Determine the coding mode.
2. Compute and evaluate the value of the fitness function.
3. Proceed with crossover and mutation operation and make up the new cluster.
4. Repeat Step 2, till the best value is obtained.

In general, using the integrated absolute error (IAE), or the integral of squared error (ISE), or the integrated of time weighted squared error (ITSE), or the integral of time multiplied through absolute error (ITAE) is regularly employed in manage system due to the fact it can be evaluated analytically in frequency domain (Kłosowski, Klepka & Nowacka, 2018).

The four integral overall performance criteria have their personal advantages and disadvantages. In this paper, (IAE) can be used as:

$$IAE = \int_0^\infty |e|\, dt \tag{8}$$

G.A algorithm parameters are set based on trial and error as follows:

1. Maximum iteration: 500.
2. Population size: 100.
3. Encoding: binary.
4. Selection: uniform.
5. Crossover: single point.
6. Mutation: uniform.

Fig. 8. shows the block-diagram of G.A-PID controller, after many iterations can be estimated the optimal parameters tuning of PID controller, Kp , Ki, and Kd .

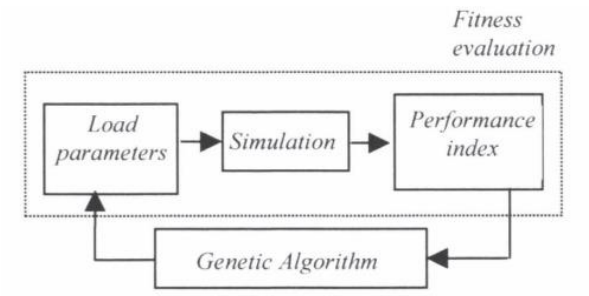


**Fig. 8. Block-diagram of G.A-PID control**

Fig. 9. shows step response of the system with G.A-PID controller, where $Mp = 0.876\%$, $Ts = 0.0673$ sec and $Tr = 0.0435$ sec, and these optimum values design requirements for pantograph-catenary System.

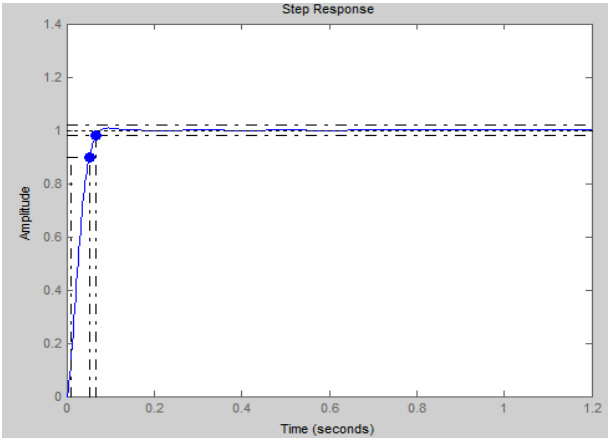


**Fig. 9. Shows step response of the system with G.A-PID controller**

## 5. RESULTS AND DISCUSSION

For the reason to assessment between the performances of all controllers and G.A-PID, it is fundamental to simulate the transient responses with recognize to settling time, maximum overshoot, rise time and steady-state error and calculate plan specifications and put it as proven in Tab. 3.

**Tab.3. Comparison between all controllers' types**

| Controller Types | Max. overshot Mp% | Settling time Ts (sec) | Rise time Tr (sec) | Steady-state error Ess |
|---|---|---|---|---|
| IMC | 0 | 0.565 | 0.333 | 0 |
| G.A-PID | 0.876 | 0.0673 | 0.0435 | 0 |

Overall results on the numerical experiment by using MATLAB had shown that the G.A-PID controller improve the effectiveness in control performance as in Fig. 9 especially on reduction of $Ts, Tr$ and very small $Mp$ of pantograph-catenary system.

Performed simulations pointed out that IMC, G.A-PID approaches lead to zero steady-state error, while LQR needs prefilter to do it and it required more tuning to meet design requirements (reduce $Mp, Ts$).

## 6. CONCLUSION

In this paper, G.A-PID controller for desired input (step) is developed based on the process model. The pantograph-catenary system is considered in the simulation study in order to demonstrate the superiority of the proposed method. A closed loop response of pantograph-catenary system tuned by the proposed method is compared with the existing conventional IMC controller. Results demonstrated that the G.A-PID has a sufficient performance to control of the system within controller design criteria. It clearly shows that G.A-PID technique gives better performances than IMC controller, when compared Figs (9,6). But G.A-PID requires 32.85 seconds computational time to reach design requirements and make performance index (IAE) with low values (approach to zero).

### REFERENCES


Al-Awad, N., & Al-Seady, A. (2020). Fuzzy Controller of Model Reduction Distillation Column with Minimal Rules. *Applied Computer Science*, *16*(2), 80–94. https://doi.org/10.23743/acs-2020-14

Arnold, M., & Simenon, B. (2000). Pantograph and catenary dynamics: a benchmark problem and its numerical solution. *Applied Numerical Mathematics*, *34*(4), 345–362. https://doi.org/10.1016/S0168-9274(99)00038-0

Bartolini, G., Pisano, A., Punta, E., & Usai, E. (2003). A survey of applications of second-order sliding mode control to mechanical systems. *International Journal of Control*, *76*(9–10), 875–892. https://doi.org/10.1080/0020717031000099010

Chater, E., Ghani, D., Giri, F., & Haloua, M. (2015). Output feedback control of pantograph–catenary system with adaptive estimation of catenary parameters. *Journal of Modern Transportation*, *23*, 252–261. https://doi.org/10.1007/s40534-015-0085-z

Giovanelli, D., & Farella, E. (2016). Force Sensing Resistor and Evaluation of Technology for Wearable Body Pressure Sensing. *Journal of Sensors*, *3*, 9391850. https://doi.org/10.1155/2016/9391850

Haamed, R., & Hameed, E. (2020). Controlling the Mean Arterial Pressure by Modified Model Reference Adaptive Controller Based on Two Optimization Algorithms. *Applied Computer Science*, *16*(2), 53–67. https://doi.org/10.23743/acs-2020-12

Kennedy, J., & Eberhart, R. (2016). Particle swarm optimization. In *IEEE International Conference on Neural Networks*, (vol. *4*, pp. 1942–1948). IEEE. https://doi.org/10.1109/ICNN.1995.488968

Kłosowski, G., Klepka, T., & Nowacka, A. (2018). Neural Controller for the Selection of Recycled Components in Polymer-Gypsy Mortars. *Applied Computer Science*, *14*(2), 48–59. https://doi.org/10.23743/acs-2018-12

Lin, Y., Lin, C., & Yang, C. (2007). Robust active vibration control for rail vehicle pantograph. *IEEE transactions on vehicular technology*, *56*(4), 1994–2004. https://doi.org/10.1109/TVT.2007.897246

Liu, R., Qian, C., Liu, S., & Jin, Y.-F. (2016). State feedback control design for Boolean networks. *BMC Systems Biology*, *10*, 70. https://doi.org/10.1186/s12918-016-0314-z

Makino, T., Yoshida, K., Seto, S., & Makino, K. (2018). Running test on current collector with contact force controller for high-speed railway. *JSME International Journal Series C*, *40*(4), 671–680. https://doi.org/10.1299/jsmec.40.671

Matvejevs, An., & Matvejevs, Al. (2011). Optimal Control of Pantograph-Catenary System Based on Parametric Identification. Scientific Journal of Riga Technical University Computer Science. *Information Technology and Management Science*, *49*.

O'Connor, D., Eppinger, S., Seering, W., & Wormley, D. (1997). Active control of a high-speed pantograph. *Journal of Dynamic Systems, Measurement and Control*, *119*(1), 1–4. https://doi.org/10.1115/1.2801209

Pisano, A., & Usai, E. (2008). Contact force regulation in wire-actuated pantographs via variable structure control and frequency-domain techniques. *International Journal of Control*, *81*(11), 1747–1762. https://doi.org/10.1080/00207170701874473

Pourzeynali, S., Lavasani, H.H., & Modarayi, A.H. (2007). Active control of high rise building structures using fuzzy logic and genetic Algorithms. *Engineering Structures*, *29*(3), 346–357. https://doi.org/10.1016/j.engstruct.2006.04.015

Shudong, W., Jingbo, G., & Guosheng, G. (2008). Research of the active control for high-speed train pantograph. In *IEEE International Conference on Cybernetics and Intelligent Systems* (pp. 749–753). IEEE. https://doi.org/10.1109/ICCIS.2008.4670754

Applied Computer Science, vol. 17, no. 2, pp. 40–55
doi: 10.23743/acs-2021-12

Submitted: 2021-05-23 | Revised: 2021-06-11 | Accepted: 2021-06-14

*Artificial Intelligence, COVID-19, diagnosis, follow-up, prognosis*

*K K Praneeth TELLAKULA* [0000-0002-3346-7251]*,
*Saravana KUMAR R* [0000-0002-8307-6208], *Sanjoy DEB* [0000-0002-0186-3938]

# A SURVEY OF AI IMAGING TECHNIQUES FOR COVID-19 DIAGNOSIS AND PROGNOSIS

**Abstract**

*The Coronavirus Disease 2019 (COVID-19) has caused massive infections and death toll. Radiological imaging in chest such as computed tomography (CT) has been instrumental in the diagnosis and evaluation of the lung infection which is the common indication in COVID-19 infected patients. The technological advances in artificial intelligence (AI) furthermore increase the performance of imaging tools and support health professionals. CT, Positron Emission Tomography – CT (PET/CT), X-ray, Magnetic Resonance Imaging (MRI), and Lung Ultrasound (LUS) are used for diagnosis, treatment of COVID-19. Applying AI on image acquisition will help automate the process of scanning and providing protection to lab technicians. AI empowered models help radiologists and health experts in making better clinical decisions. We review AI-empowered medical imaging characteristics, image acquisition, computer-aided models that help in the COVID-19 diagnosis, management, and follow-up. Much emphasis is on CT and X-ray with integrated AI, as they are first choice in many hospitals.*

## 1. INTRODUCTION

Towards the end of 2019, in early December, the outbreak of highly infectious disease is discovered. The disease named as coronavirus disease 2019 (COVID-19), is caused by the Severe Acute Respiratory Syndrome Coronavirus 2 (SARS-CoV-2). This virus has affected almost all the countries and territories, resulting in 165 million cases, over three million deaths as of 21 May 2021. This disease has given rise to unparalleled health issues in the global community. On 11 March 2020, the World Health Organization (WHO) declared it as a pandemic. The representative characteristics of COVID-19 infected cases comprise of dry cough, fever, tiredness, headache, and a decrease in lymphocyte or white blood cell count. In serious conditions, the infection may lead to difficulty in breathing or shortness of breath, chest ache, loss of speech and/or movement, pneumonia, organ failure, and death (WHO, 2020).

WHO recommends Reverse Transcription-Polymerase Chain Reaction (RT-PCR) test for recognizing COVID-19 patients. This test is a labour-intensive and has to be performed in

* Bannari Amman Institute of Technology (Anna University, Department of Electronics And Communication Engineering), Sathyamangalam, India, praneeth.tkk@gmail.com, saravanakumar@bitsathy.ac.in, sanjoydeb@bitsathy.ac.in

specialized laboratories. The RT-CPR test has low sensitivity as reported by Fang et al (Fang et al., 2009). The efficiency of the test depends on several factors, sample preparation, quality, availability, and stability of the detection kits. The RT-CPR test has low detection rates in the early stages. In many cases, the tests on alleged patients need to be repeated after some days before reaching a sanguine diagnosis. Radiological imaging is often used as an equivalent examination in COVID-19 diagnosis. The imaging analyses has played an indispensable part in the examination and treatment of corona disease and also in monitoring the development of diseases and assessing their therapeutic effectiveness (Ye, Zhang, Wang, Huang & Song, 2020), restraining the infection and combat COVID-19.

The roadmap of radiological imaging-based diagnosis includes three phases:

1. Pre-scan arrangement.
2. Image procurement.
3. Disease diagnosis.

In the first stage, the subjects are assisted by a laboratory technician to position on the table or bed of the imaging machine following the prescribed protocols. In the second stage, the radiological images are acquired. The scan ranges from top to base of the lung. From the procured data, the images are rebuilt and then transferred through Picture Archiving and Communication Systems (PACS) for eventual analysis.

Image processing techniques can be extensively administered in the medical field, for segmentation, image enhancement, and can assist in consequent diagnosis (Liu et al., 2018). Computer-Aided Diagnosis (CAD) systems are an indissoluble part of medical practice that helps radiologists diagnose efficiently. These CAD systems possess many benefits over the radiologists. These systems are adept at perceiving the elusive and fine vicissitudes that are impossible to be detected by the visual examination (Castellano, Bonilha, Li & Cendes, 2004). Radiological imaging is a significant tool that contributes to actively fight against COVID-19. AI-based procedures have been employed in innumerable situations like automated diagnoses and treatments. Several researchers are adopting AI and its subsets to find new medicines and remedies for the diseases. Multiple researchers affiliated with computer science are focusing on using medical image processing for identifying contagious patients. AI-assisted software may theoretically support less experienced practitioners triage patients by identifying vital chest regions (Wang & Wong, 2020). AI embedded with deep learning techniques of image analysis could be tailored to reinforce radiologists in analysing the data. AI solutions will analyse several cases simultaneously to detect lung anomalies in chest CT.

Because of the significance of AI in the whole spectrum of COVID-19, AI-enabled imaging-based analysis will encourage future potential uses and analytical studies. The reason for this study is to weigh the effect of the mentioned procedures and also recommend their use. This study concentrates on the advancements in artificial intelligence to tackle the coronavirus epidemic. Here we put forward radiological imaging systems for COVID-19. Finally, we provide a discussion on challenges and problems.

## 2. CONTACTLESS IMAGING PROCEDURE

SARS-CoV-2 is exceptionally infectious. This led to a precipitous rise in the percentage of affected patients. Because of the close proximity of health staff (doctors, technicians, nurses, etc.) with the patients, they are at risk of getting themselves infected. This pressurizes already overwhelmed health care institutions/systems. A world-wide deficit in Personal Protective Equipment (PPE) and various essentials is stressing the peril the health-care workers encounter as they nurse patients. There is an exigency of solutions so that hospitals and health-care systems can perform at their full efficiency.

### 2.1. Conventional imaging workflow

The traditional patient assessment involves several significant pre-scan events. These events involve physical contact between medical professionals and patients. These events involve leading the patients to the examination room, ensuring readiness for the scanning. To ensure optimal parameters for the scan, the technicians help position patients correctly.

It is necessary to exercise an automated and contactless acquisition of images to obviate perils of infection during this pandemic.

### 2.2. AI-enabled imaging procedure

Most current radiological imaging devices come furnished with cameras for patient monitoring. Throughout the COVID-19 pandemic, these devices allow patients to be screened contactless. The medical experts can now administer the scans while being physically far and safe from the chamber where the patient is contained. The patients are led to the inspection room and/or CT bed. The system ought to present visual prompts for assisting the patient and technician in appropriately preparing and positioning the patient correctly for scanning, taking images, and analysing them. Lab technicians must be personally in the operating room and use CT scanner panels for ISO-centring and orienting the patients. ISO-centring corresponds to the alignment of the subject's target body area in a way that the target body area centre overlaps with the centre of the ISO scanner for providing optimal image quality. Researchers found that the radiation amount can be whittled down with effective ISO-centring while the image retains the identical quality (Booij, Budde, Dijkshoorn & van Straten, 2019). By applying depth data to human mesh model which is premised on bodily keypoints that are detected from an RGB image, Singh et al (Singh et al., 2017) rebuilt 3D full mesh of the patients.

By acquiring the data using RGB, thermal cameras, Time-of-Flight (TOF), and pressure imaging, AI automates the process (Singh et al., 2017) of discerning the body shape and pose of the patient. By this, optimal parameters for the scan are determined.

## 3. AI-ASSISTED SEGMENTATION

Segmentation, repair, and image enhancement are essential steps in subsequent medical diagnosis (Liu et al., 2018). Segmentation facilitates the removal of irrelevant image segments which in turn aids the learning process in the detection of COVID-19. In radiological imaging, this process particularizes the Region of Interests (ROIs) like lungs, lesions,

infected regions, tumours. The partitioned regions could facilitate the extraction of self-learned or handcrafted features for use in the diagnosis or other applications. Summarization of some of the segmentation works in COVID-19 and applications are done in this subsection.

3D images of high-quality for detecting COVID-19 are obtained from CT scans. Deep learning techniques are used to segment ROI in CTs. Some of the prevalent networks for segmentation in diagnosing COVID-19 are U-Net (Qi et al., 2001; Zheng et al., 2020), VB-Net (Shan et al., 2020), U-Net++ (Chen et al., 2020; S. Jin et al., 2020), V-Net (Milletari, Navab & Ahmadi, 2016), ResNet (He, Zhang, Ren & Sun, 2006).

### 3.1. Lung lesions segmentation

Generally lung-lesion-oriented methods is used for segmentation in COVID-19 identification. The lung-lesion-oriented methods are used to isolate lesions from the (Shan, 2020; Qi et al., 2001). The detection of lesions is a strenuous responsibility as the lesions may be small in a variety of forms. Lungs and lobes in the lungs are separated from X-ray or CT images using lung-region-oriented methods (Shan, 2020; S. Jin et al., 2020; Qi et al., 2001; Zheng et al., 2020). The reason behind this is, unabridged lung lobes are needed for radiologists to evaluate and compare lesion intensity with a mean density of adjoining organs.

Transformation in lesions of lungs is akin to the development of COVID-19. This is also exhibited in lung lesions on radiological imaging within 28 hours. In CT images, U-Net and its variations are used for segmenting lungs and its lesions, whereas ResNet and its variations (2D or 3D) are for classification

### 3.2. Segmentation methods

There are myriad techniques with various purposes for segmenting lungs (Milletari, Navab & Ahmadi, 2016; Zhou, Rahman Siddiquee, Tajbakhsh & Liang, 2018). Ronneberger (Ronneberger, Fischer & Brox, 2015) proposed a CNN technique with U-shaped architecture named as U-Net. U-Net has encoding and decoding paths for segmenting lung regions and COVID-19 lesions. This network is more suitable for segmentation in medical images as it can learn better semantics and contexture.

V-Net variant with residual block and optimized network with Dice loss is put forward by Milletari et al (Milletari, Navab & Ahmadi, 2016). A three-step AI technique (S. Jin et al., 2020) for lesion segmentation and classification of the lesion is developed. In the first step, using 3D U-Net extract lung regions. In the second step, explicit lesions were segmented. In the final step, identify lesions being positive or negative using a CNN-based classifier.

U-Net++ (Zhou, Rahman Siddiquee, Tajbakhsh & Liang, 2018), based on the U-Net model, is specifically designed for the segmentation of images in biomedicine. The U-Net++ model can identify the ROIs having lesions with the bounding boxes from CT image slices. Even though the network can ameliorate the execution of segmentation, its training is onerous. With this network, lesions can be discerned in COVID-19 diagnosis (Chen et al., 2020).

Training a comprehensive network for segmentation requires adequate labelled data. The exiguous training data in COVID-19 is due to manual, labour-intensive, and time-consuming delineation of lesions. Due to exiguous training data, weakly supervised approaches of machine learning are employed. An unsupervised method for producing pseudo-segmented image masks

is proposed by Zheng et al (Zheng et al., 2020). From manually chronicled ROI, radiomic features are extracted. To diagnose the features that depict the relationship with COVID-19, Consensus clustering for unsupervised learning is used by S. Jin et al (S. Jin et al., 2020). The segmentation results of some of the best methods are shown in Fig. 1 (Q. Yan et al., 2020).

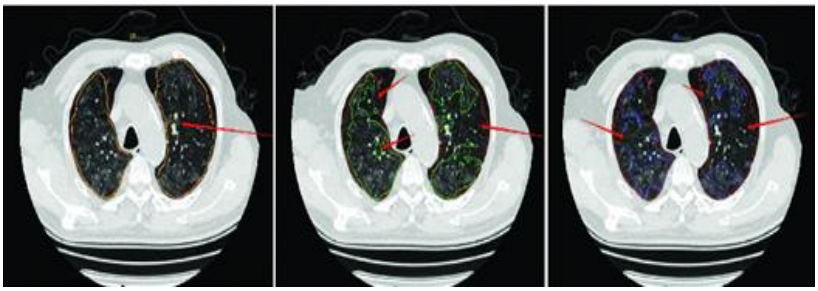

a) U-Net b) U-Net++ c) V-Net

**Fig. 1. Visual comparisons of COIVD-19 segmentation by some of the best AI methods testing data**

Semi-supervised and unsupervised techniques are much sought as there is a deficiency of annotated medical images in lung segmentation.

## 4. AI-ASSISTED DIAGNOSIS FOR COVID-19

Patients suspicious of COVID-19 greatly need a prognosis and appropriate care. CT and X-ray scans are extensively carried out to furnish radiologists with evidence. Specialists take so much time to diagnose using Chest CT as they contain hundreds of slices. AI-based diagnosis is immensely needed as COVID-19 is a newly discovered disease and radiologists need to gain experience to accomplish high performance. In Tab. 2 we list some of the applications of modern technology in COVID-19 pandemic.

Segmentation (discussed in previous section) is used to pre-process images and here we list techniques that take segmentation results into diagnosis. These techniques can escalate efficiency and ease the pressure on radiologists by identifying the positive cases of COVID-19. The Tab. 1, lists some of the AI aided analysis of COVID-19.

**Tab. 1. Summary of AI-assisted methods in Image segmentation in applications of COVID-19**

| S. No. | Literature | Procedure | AI Methods | Target Region | Application |
|---|---|---|---|---|---|
| 1. | Wang et al. (S. Wang et al., 2020) | CT | CNN | Lung | Diagnosis |
| 2. | Jin et al. (C. Jin et al., 2020) | CT | CNN | Lung Lesion | Diagnosis |
| 3. | L. Wang et al. (Wang & Wong, 2020) | X-Ray | CNN | Lung | Diagnosis |
| 4. | Narin et al. (Narin, Kaya & Pamuk, 2020) | X-Ray | ResNet50 | Lung | Diagnosis |
| 5. | Ghoshal et al. (Ghoshal & Tucker, 2020) | X-Ray | CNN | Lung | Diagnosis |
| 6. | Zhang et al. (Zhang et al., 2020) | X-Ray | ResNet5 | Lung | Diagnosis |

**Tab. 2. Modern Technology applications during the COVID-19 pandemic**

| S. No. | References | Applications | Description |
|---|---|---|---|
| 1. | L.Wang et al. (L. Wang et al., 2020), Wang et al. (S. Wang et al., 2020), Narin (Narin, Kaya & Pamuk, 2020) | diagnosis using radiological images | – Extracting radiological features using AI for accurate diagnosis of COVID-19.<br>– Usage of CNN models, 3D deep learning models with more number of images can aid in early discovery of COVID-19.<br>– COVID-Net, a variant of deep CNN system is applied on CT images and X-rays to detect COVID-19 cases.<br>– COVNet, COVID-19 detection Neural Network is used to separate COVID from other types of Pneumonia. |
| 2. | Wang et al. (Wang, Hu, Li, Zhang, Zhai & Yao, 2020) | disease tracking | – To estimate the count of infected and non-infected persons, Time-dependent susceptible-infected-recovered (SIR) model is used.<br>– Applying GRU neural network with bidirectional and Attentional mechanisms (BI-AT-GRU) to categorize substantial breathing behaviors. |
| 3. | Qi et al. (Qi et al., 2001), Yan et al. (L. Yan et al., 2020) | predicting the health status of patients | – Quantifying the risk of death using Supervised XGBoost model.<br>– Predicting the days COVID-19 patients stay in the hospital, using ML-based radiomic models (CT). |
| 4. | Richardson et al. (Richardson et al., 2020) | computational Medicines perspective | – Researchers at BenevolentAI found that blocking the way virus gets into the cell, is used to help prevent the infection. |
| 5. | He et al. (He et al., 2006), | protein structure prsedictions | – For deeper image recognition, residual learning architecture is used.<br>– To predict protein properties from its genetic sequence Critical Assessment of Techniques for Protein Structure Prediction (CASP) is used.<br>– CNN is used for dense predictions. |
| 6. | Zhavoronkov et al. (Zhavoronkov et al., 2020) | drug discovery | – To identify novel medicine compounds, AI is used. |
| 7. | Maddah and Beigzadeh (Maddah & Beigzadeh, 2020), Nemati et al. (Nemati, Rahman, Nathan, Vatanparvar & Kuang, 2019) | social control and awareness | – For measuring infected people's temperature using smartphone thermometers.<br>– By applying acoustic features to recorded audio, cough can be detected.<br>– Classify white blood cell and chest X-ray images on a mobile phone. |

## 4.1. X-ray screening for COVID-19

X-rays are the preferred way of radio imaging during the investigation of COVID-19 as it is cheap and easy compared to CT. But they are less sensitive compared to 3D CT images of the chest. Studies report that X-ray display normal in early and minimal infection (Wong et al., 2016). Abnormal chest x-rays are observed in 69% of patients at first admission and Sometime after hospitalization 80% of patients (Wong et al., 2016).

A ResNet based model to identify COVID-19 infected individuals and anomaly detection is put forward by Zhang et al (Zhang et al., 2020) and has AUC of 0.952. COVID-Net, a CNN variant to identify COVID-19 by employing X-ray images is put forward by L.Wang et al (Wang & Wong, 2020) and has obtained 83.5% test accuracy.

Several recent works use images from X-ray scan to distinguish between COVID-19 and healthy individuals and several kinds of pneumonia. These images are from online datasets with an inadequate quantity of COVID-19 images and these are inadequate to determine methodological robustness as the extent of subjects' severity is still uncertain. Future research may stress early detection of COVID-19. Comparisons of the normal person's X-ray images, with persons having COVID-19 and pneumonia in Fig. 2 (Rahimzadeh & Attar, 2020).

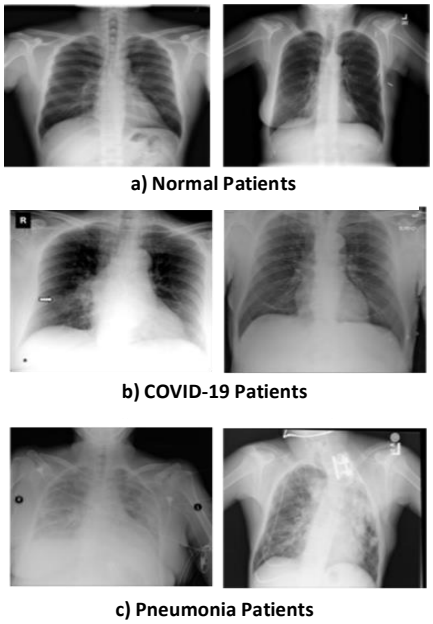


**Fig. 2. Comparisons of a normal person with patients with COVID-19 and pneumonia**

Most studies can distinguish COVID-19 from healthy patients and pneumonia subjects using X-ray images, though the severity is unknown. Future research can stress on the early detection of COVID-19.

## 4.2. COVID-19 CT screening and severity evaluation

### 4.2.1. CT characteristics of COVID-19

One salient feature to track COVID-19 is Ground-Glass Opacities (GGO). For the following characteristics (Guan et al., 2020; Bernheim et al., 2020; H. Shi et al., 2020; D. Wang et al., 2020) CT photographs of COVID-19 patients' chest may be analysed for: 1) appearance of GGO, 2) Consolidation existence, 3) lateralization of GGO and its consolidation, 4) count of impaired lobes with opacities, 5) Level of involvement of the individual lung lobes, along with the complete extent of the lung involvement is measured, 6) development of nodules, the existence of Pleural effusion, 7) detection of more than 10mm lymph nodes and airway

abnormalities, 8) axial distribution and any underlying pulmonary disease. Such radiological observations provide considerable evidence in the COVID-19 assessment.

A more detailed description of the CT phases is done by Pan (Pan et al., 2020). He has split patients into four Phases, phase-1(0-4 days), phase-2 (5-8 days), phase-3 (9-13 days), and phase-4 (≥14 days) (Figure 3). In phase-1, people have GGO, consolidation, crazy-paving pattern are also identified. In phase-2, GGO had spread to other lobes, with extended consolidation and crazy-paving pattern. In phase-3, consolidation is the primary, with shrinkage in GGO, and crazy-paving patterns. In the phase-4, partial absorption of consolidation and with none of the crazy-paving pattern. 4 stages of Lung CT of patient recovered form COVID-19 is presented in Fig. 3 (Pan et al., 2020).

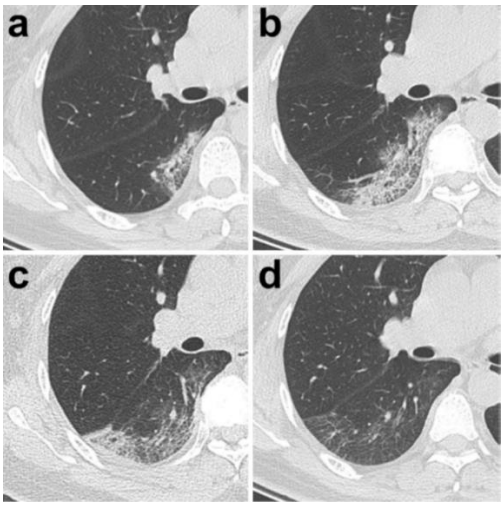


**Fig. 3. 47-year old patient's CT findings in right lung: (a) at day 3, small GGO and partial consolidation; (b) 7th day, increased GGO with crazy-paving pattern and partial consolidation; (c) at day 11, a new region of subpleural consolidation and partial GGO; (d) 20th day, parenchymal bands and slight residual GGO**

Bilateral patchy shadowing is among the most frequent radiological findings on chest CT (Guan et al., 2020). Wang *et al* (D. Wang et al., 2020) examined the proportion of bilateral engagement in COVID-19 infected patients. They found 100% involvement in people with COVID-19. Bilateral, consolidation of subsegmental areas, pulmonary fibrosis is standard discoveries in COVID-19 patients' chest CT.

Lesions with consolidation might also operate as a sign of disease advancement or disease severity (Song et al., 2020). The manifestation of multiple lesions is more likely than a single lesion in a preliminary CT scan of COVID-19.

### 4.2.2. Usage of CT features to discriminate COVID-19 against viral pneumonia

Viral pneumonia and COVID-19 have similar appearances and discerning their differences would facilitate the medical screening process. This discerning process of COVID-19 from other pneumonia using CT scans has gained attention. GGO and/or consolidation characteristics of COVID-19 and that of SARS, MERS is different from one another (Marinari, Danny & Miller, 2019). Patch and density increasing shadows are characteristics of viral pneumonia, whereas the

presence of bilaterals and mottles are typical in COVID-19 and are represented in Fig. 4 (Zhao et al., 2020). COVID-19 victims display reverse halo, vascular thickening, reticular opacity, peripheral distribution (Bai et al., 2020).

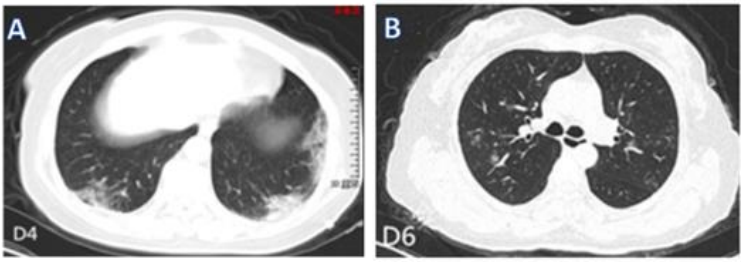


**Fig. 4. (a) Characteristics of COVID-19, multiple mottles, and GGO;**
**(b) Features of non-COVID-19 pneumonia, patchy and mottling shadows**

### 4.2.3. CT features in asymptomatic COVID-19

A significant way of regulating the transmission of COVID-19 is testing asymptomatic patients and discovering their CT characteristics. All asymptomatic patients may not exhibit standard radiographic signs. Some preliminary RT-CPR outcomes were negative, while CT included GGO and/or consolidation. Ai et al (Ai et al., 2020) found GGO, bilateral lesions, and consolidations in CT of COVID-19 suspected patients who got negative in RT-CPR testing are shown in Fig. 5.

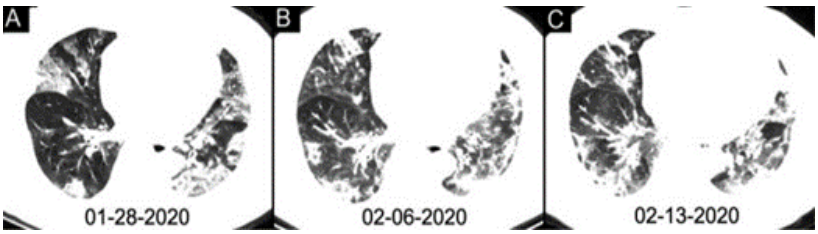


**Fig. 5. Swab samples of 63 year old woman had negative results in RT-CPR –**
**CT scans on bilateral lungs show mixed GGO and multifocal consolidation shadows over 16 days**

All asymptomatic patients may not exhibit radiographic signs. This states that Typical CT signs are not present in all asymptomatic patients. Combination of RT-CPR and chest CT can detect asymptomatic COVID-19 patients.

### 4.2.4. CT features in asymptomatic COVID-19

The severity assessment is significant for laying out plans for treatment. Shi, Xia et al (F. Shi et al., 2020) adopted VB-Net to segment lungs into sub-regions like lobes. Based on these, infection volumes and ratios are computed and train an RF model. A quantitative assessment based deep-learning technique (W. Shi et al., 2020) is used to predict COVID-19 severity. This technique calculates the Mass of Infection (MOI) and the Percentage of Infection (POI). These have higher values in a severe group of patients. Clinical characteristics including age, C-Reactive Protein (CRP), Lactate dehydrogenase (LDH), CD4+ T helper cells count, combined

with POI and MOI are fed to LASSO logistic regression model to identify the severity of patients. The prediction of COVID-19 is vitally important as it helps in treatment planning and assessment of ICU events.

### 4.3. Magnetic Resonance Imaging (MRI)

MRI is best suited for Imagining soft tissues and is also radiation free. As MRI is of excessive cost and has a long scanning period, it is not usually used for COVID-19. Diagnosis of COVID-19 in pregnant women and children can be done using MRI as it is radiation-free free (Liszewski, Görkem, Sodhi & Lee, 2017). Even though the SARS-CoV-2 is primarily spread in the lungs, the minimally invasive autopsy revealed infections in the heart, kidney, liver, and other body parts (Yao et al., 2020). SARS-CoV-2 enters lung cells via Angiotensin-Converting Enzyme 2 (ACE2) receptor and can spread to multiple organs. The patients having basic heart disease displayed a raise in ACE2 and have a greater risk of heart attacks and precarious conditions.

MRI provides excellent functional and visual information about soft organs. To understand the vulnerability of organs, the pathogenesis of COVID-19 could be understood.

### 4.4. Lung Ultrasound

Lung ultrasound (LUS) is portable, radiation-free, and non-invasive radiological imaging technique. LUS can be used for screening riskless patients, diagnosis in the emergency room, observing variations in pneumonia.

Ultrasonography of the lung does provide comparable results with that of chest CT for COVID-19-pneumonia diagnosis. Patients who are critically ill or need ventilation or admitted to ICU, LUS is an effective treatment. CT inspection is to be avoided for pregnant women suspicious of COVID-19, as radiation poses threat to the foetus. LUS (Moro et al., 2020) is recommended in these conditions and Fig. 6 displays the patterns of LUS in pregnant woman and suggestive COVID-19. LUS reduces the exposure between health care workers and patients.

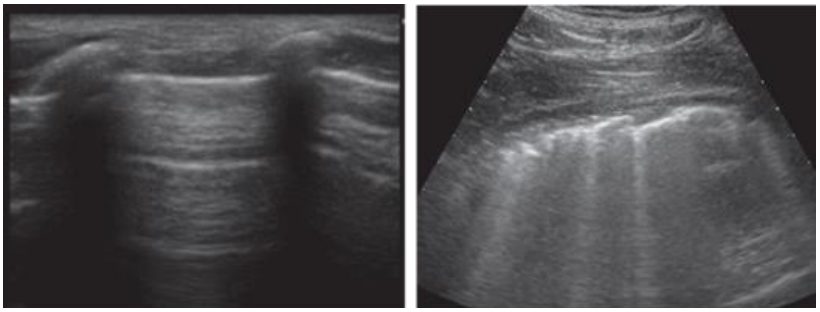

Regular A-lines and pleural lines indicate Normal Lungs

Irregular pleural line and multiple B-lines indicates COVID-19

**Fig. 6. Assessment and findings of LUS patterns in the pregnant women: (a) Regular A-lines and pleural lines indicate Normal Lungs, (b) Irregular pleural line and multiple B-lines indicates COVID-19**

### 4.5. PET/CT

For analysing pulmonary and inflammatory diseases, monitoring the progress of diseases, invasive and sensitive imaging Positron Emission Tomography (PET) plays a vital role. Qin et al (Qin, Liu, Yen & Lan, 2020) advocate that during the initial period when the diagnosis is challenging, $^{18}$F-FDG PET/CT can do supplementary diagnosis as displayed in Fig. 7. $^{18}$F-FDG PET is a sophisticated test and has a lengthy testing time which could swell the disease transmission. They suggest more research is to be done to decide if $^{18}$F-FDG PET/CT is applicable for diagnosing COVID-19.

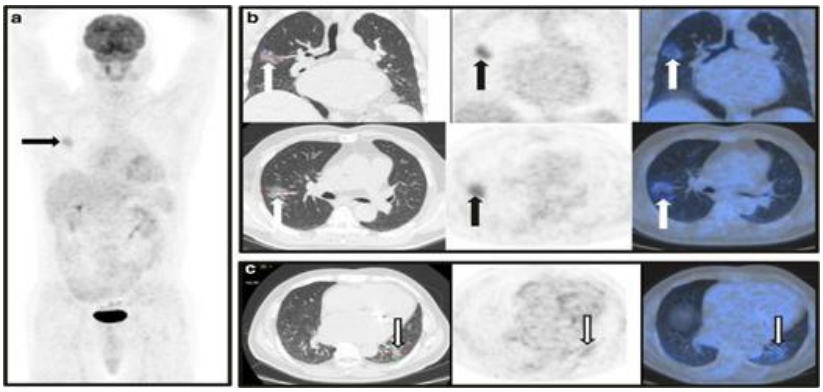


**Fig. 7. (a), (b) Peripheral GGOs identified by $^{18}$F-FDG PET/CT in the right lung and (c) Peripheral GGOs identified by $^{18}$F-FDG PET/CT in the left lung**

The ability, performance and value of X-ray, CT, MRI, LUS, PET/CT can be evaluated and compared for COVID-19 and pneumonia. Research can be done on their combinations and systematic studies of damage to the organs and mechanism of disease.

## 5. AI IN FOLLOW-UP STUDIES

The follow-ups subsequent to clinical treatment play a critical part in COVID-19 treatment. They evaluate the response and possible problems of patients after the treatment. Designing AI-empowered follow-up procedures for COVID-19 is strenuous and challenging. They are extremely limited follow-up studies for COVID-19 as current works are focused on pre-diagnosis of COVID-19. Researchers from Shanghai United Imaging Intelligence, use ML technique to determine and visualize the variations in clinical factors of patients. Clinical reports are generated automatically highlighting the changes as guidance for specialists for follow-ups. Quantification of lung infection reflects the development of COVID-19. It can be used in the follow-up research.

The research and works on the follow-up of COVID-19 are still in the initial phase. We are certain that previous work on segmentation, diagnosis, assessment can be helpful in building AI-enhanced COVID-19 follow-up studies.

## 6. DISCUSSION

The COVID-19 has emerged as a global threat and as a pandemic that affected over 48 million patients. Radiological imaging, in particular CT, have a crucial part in COVID 19 diagnosis and follow up. CT remains the key instrument for evaluating changes and the severity of lung lesions. The GGO and consolidations are the typical CT representation of COVID. A reduction in GGO and a rise in consolidation can be attributed with the progression of the disease. Variations occur in CT features including and not limited to GGO, crazy-paving, and reticular patterns. The clinical manifestations and therapeutic reaction can vary from patient to patient. Variations in lung lesions are associated with the development of COVID disease. Lung lesions are absorbed within 24–28 hours for COVID-19 patients with rapid progression, for patients with mild disease they absorbed after treatment, for critical patients the lesions may be irreversible. Additional research using larger sample sizes are required for providing further insights in evolution of GGO and lesions during and after the COVID-19 infection.

Ai et al (Ai et al., 2020), compared RT-CPR results and CT scans of 1,014 patients. CT scans have higher sensitivity than that of RT-CPR results. Chest CT results used RT-CPR results as a guideline and had 68% accuracy. Few COVID-19 patients display inflammatory changes on chest CT even though they got negative on nucleic acid tests. a lot of patients have no abnormal radiological findings (Guan et al., 2020). It is strongly recommended that the usage of chest CT, RT-PCR, and close monitoring validate and confirm the asymptomatic patients.

There's inadequate medical care in the world due to the pandemic COVID-19. Diagnosing and predicting the prognosis of individual patients is vital for managing COVID-19. AI coupled with radiological images can abet in the prognosis and diagnosis of COVID-19. Applying AI and its branches to COVID-19 research is just the prelude. More AI-enhanced technologies are expected to be incorporated into the image acquisition workflow to promote improved scanning efficiency and lower patient radiation dose. There have been studies of three forms of AI strategies. 1) Using AI to detect lesions to assist clinicians quickly screen for COVID-19, 2) use AI to diagnose CT images of whole or partial lungs, 3) Use AI to forecast other COVID-19 clinical results. Explainable Artificial Intelligence [XAI] having a finer localization map (Arrieta et al., 2020) may facilitate the use in clinical practice of diagnosis assisted with AI.

In the battle against COVID-19 deep learning has become the best strategy. Analysis of the whole lung provides comparable results that of segmented lung lesions. Datasets may be incomplete and inaccurate with a fewer number of samples and training algorithms on these datasets is a major challenge. It is costly and time-consuming to manually label the image data. Self-supervised, deep transfer learning, weakly supervised methods of deep learning can be used in these scenarios. Mobile based medical image diagnosis can be developed to identify COVID-19 in remote areas.

Follow-up studies are critical in evaluating and diagnosing COVID-19. The AI methodologies can be inspire follow-up studies. Combining data of COVID-19 patients from inside and outside the hospital for longer period of tracking the disease could benefit the follow-up procedure for COVID-19.

## 7. CONCLUSION

AI-enabled imaging techniques are very useful in COVID-19 combat. RT-CPR test is the best way for identifying the COVID-19. Imaging characteristics like GGOs, consolidations, pleural thickening, multiple mottling, and bilateral involvement in chest CT scans can help identify asymptomatic patients. X-rays and CT show the efficacy of AI-enhanced diagnostic imaging. For enhancing testing and diagnosis of COVID-19, RT-CPR, and medical imaging techniques can be combined. The usage of chest CT can counteract the low sensitivity of RT-CPR test and increases the accuracy and speed of COVID-19 diagnosis.

Follow-up reviews for COVID-19 are still inadequate and limited. Assessing the progressions of GGO, changes in lung lesions and consolidations can be observed with help of CT scans in early stages, advancement, treatment, and follow-up procedures of COVID-19. Combined usage of AI and radiological imaging can redress the drawbacks in traditional medical resources, help timely diagnosis, and COVID-19 prediction. We believe in AI for accurate and efficient diagnosis, review and follow-up of COVID-19.

### REFERENCES


Ai, T., Yang, Z., Hou, H., Zhan, C., Chen, C., Lv, W., Tao, Q., Sun, Z., & Xia, L. (2020). Correlation of Chest CT and RT-PCR Testing in Coronavirus Disease 2019 (COVID-19) in China: A Report of 1014 Cases. *Radiology*, *2019*, 200642. https://doi.org/10.1148/radiol.2020200642

Arrieta, A.B., Díaz-Rodríguez, N., Del Ser, J., Bennetot, A., Tabik, S., Barbado, A., Garcia, S., Gil-Lopez, S., Molina, D., Benjamins, R., Chatila, R., & Herrera, F. (2020). Explainable Artificial Intelligence (XAI): Concepts, Taxonomies, Opportunities and Challenges toward Responsible AI. *Information Fusion*, *58*, 82–115. https://doi.org/10.1016/j.inffus.2019.12.012

Bai, H.X., Hsieh, B., Xiong, Z., Halsey, K., Choi, J.W., Tran, T.M.L., Pan, I., Shi, L.-B., Wang, D.-C., Mei, J., Jiang, X.-L., Zeng, Q.-H., Egglin, T.K., Hu, P.-F., Agarwal, S., Xie, F.-F., Li, S., Healey, T., Atalay, M.K., & Liao, W.-H. (2020). Performance of radiologists in differentiating COVID-19 from viral pneumonia on chest CT. *Radiology*, *1*, 1–13. https://doi.org/10.1148/radiol.2020200823

Bernheim, A., Mei, X., Huang, M., Yang, Y., Fayad, Z.A., Zhang, N., Diao, K., Lin, B., Zhu, X., Li, K., Li, S., Shan, H., Jacobi, A., & Chung, M. (2020). Chest CT findings in coronavirus disease 2019 (COVID-19): Relationship to duration of infection. *Radiology*, *295*(3), 685–691. https://doi.org/10.1148/radiol.2020200463

Booij, R., Budde, R.P.J., Dijkshoorn, M.L., & van Straten, M. (2019). Accuracy of automated patient positioning in CT using a 3D camera for body contour detection. *European Radiology*, *29*(4), 2079–2088. https://doi.org/10.1007/s00330-018-5745-z

Castellano, G., Bonilha, L., Li, L.M., & Cendes, F. (2004). Texture analysis of medical images. *Clinical Radiology*, *59*(12), 1061–1069. https://doi.org/10.1016/j.crad.2004.07.008

Chen, J., Wu, L., Zhang, J., Zhang, L., Gong, D., Zhao, Y., Hu, S., Wang, Y., Hu, X., Zheng, B., Zhang, K., Wu, H., Dong, Z., Xu, Y., Zhu, Y., Chen, X., Yu, L., & Yu, H. (2020). *Deep learning-based model for detecting 2019 novel coronavirus pneumonia on high-resolution computed tomography: a prospective study*. MedRxiv. https://doi.org/10.1101/2020.02.25.20021568

Fang, Y., Zhang, H., Xie, J., Lin, M., Ying, L., Pang, P., & Ji, W. (2009). Sensitivity of Chest CT for COVID-19: Comparison to RT-PCR. *Radiology*, *296*(2), 1–30. https://doi.org/10.1148/radiol.2020200432

Ghoshal, B., & Tucker, A. (2020). *Estimating Uncertainty and Interpretability in Deep Learning for Coronavirus (COVID-19) Detection*. http://arxiv.org/abs/2003.10769

Guan, W., Ni, Z., Hu, Y., Liang, W., Ou, Ch., He, J., Liu, L., Shan, H., Lei, Ch., Hui, D.S.C., Du, B., Li, L., Zeng, G., Yuen, K.-Y., Chen, R., Tang, C., Wang, T., Chen, P., Xiang, J., Li, S., Wang, J., Liang, Z., Peng, Y., Wei, L., Liu, Y., Hu, Y., Peng, P., Wang, J., Liu, J., Chen, Z., Li, G., Zheng, Z., Qiu, S., Luo, J., Ye, Ch., Zhu, S., & Zhong, N. (2020). Clinical Characteristics of Coronavirus Disease 2019 in China. *The Journal of Emergency Medicine*, *382*, 1708-1720. https://doi.org/10.1056/NEJMoa2002032

He, K., Zhang, X., Ren, S., & Sun, J. (2006). *Deep Residual Learning for Image Recognition*. https://arxiv.org/abs/1512.03385

Jin, C., Chen, W., Cao, Y., Xu, Z., Zhang, X., Deng, L., Zheng, C., Zhou, J., Shi, H., & Feng, J. (2020). *Development and Evaluation of an AI System for COVID-19 Diagnosis*. MedRxiv. https://doi.org/10.1101/2020.03.20.20039834

Jin, S., Wang, B., Xu, H., Luo, C., Wei, L., Zhao, W., Hou, X., Ma, W., Xu, Z., Zheng, Z., Sun, W., Lan, L., Zhang, W., Mu, X., Shi, C., Wang, Z., Lee, J., Jin, Z., Lin, M., Jin, H., Zhang, L., Guo, J., Zhao, B., Ren, Z., Wang, S., You, Z., Dong, J., Wang, X., Wang, J., & Xu, W. (2020). *AI-assisted CT imaging analysis for COVID-19 screening: Building and deploying a medical AI system in four weeks*. MedRxiv. https://doi.org/10.1101/2020.03.19.20039354

Liszewski, M.C., Görkem, S., Sodhi, K.S., & Lee, E.Y. (2017). Lung magnetic resonance imaging for pneumonia in children. *Pediatric Radiology*, *47*(11), 1420–1430. https://doi.org/10.1007/s00247-017-3865-2

Liu, X., Guo, S., Yang, B., Ma, S., Zhang, H., Li, J., Sun, C., Jin, L., Li, X., Yang, Q., & Fu, Y. (2018). Automatic Organ Segmentation for CT Scans Based on Super-Pixel and Convolutional Neural Networks. *Journal of Digital Imaging*, *31*(5), 748–760. https://doi.org/10.1007/s10278-018-0052-4

Maddah, E., & Beigzadeh, B. (2020). Use of a smartphone thermometer to monitor thermal conductivity changes in diabetic foot ulcers: *A pilot study*. *Journal of Wound Care*, *29*(1), 61–66. https://doi.org/10.12968/jowc.2020.29.1.61

Marinari, L.A., Danny, M.A., & Miller, W.T. (2019). Sporadic coronavirus lower respiratory tract infection in adults: chest CT imaging features and comparison with other viruses. *European Respiratory Journal*, *54*(suppl 63), PA4547. https://doi.org/10.1183/13993003.congress-2019.PA4547

Milletari, F., Navab, N., & Ahmadi, S.A. (2016). V-Net: Fully convolutional neural networks for volumetric medical image segmentation. *Proceedings - 2016 4th International Conference on 3D Vision, 3DV 2016*, 565–571. https://doi.org/10.1109/3DV.2016.79

Moro, F., Buonsenso, D., Moruzzi, M.C., Inchingolo, R., Smargiassi, A., Demi, L., Larici, A.R., Scambia, G., Lanzone, A., & Testa, A.C. (2020). How to perform lung ultrasound in pregnant women with suspected COVID-19. *Ultrasound in Obstetrics and Gynecology*, *55*(5), 593–598. https://doi.org/10.1002/uog.22028

Narin, A., Kaya, C., & Pamuk, Z. (2020). *Automatic Detection of Coronavirus Disease (COVID-19) Using X-ray Images and Deep Convolutional Neural Networks Ali*. https://arxiv.org/abs/2003.10849

Nemati, E., Rahman, M.M., Nathan, V., Vatanparvar, K., & Kuang, J. (2019). Poster Abstract: A Comprehensive Approach for Cough Type Detection. *Proceedings - 4th IEEE/ACM Conference on Connected Health: Applications, Systems and Engineering Technologies*, CHASE 2019 (pp. 15–16). IEEE. https://doi.org/10.1109/CHASE48038.2019.00013

Pan, F., Ye, T., Sun, P., Gui, S., Liang, B., Li, L., Zheng, D., Wang, J., Hesketh, R.L., Yang, L., & Zheng, Ch. (2020). Time Course of Lung Changes On Chest CT During Recovery From 2019 Novel Coronavirus (COVID-19) Pneumonia. *Radiology*, *295*(3), 1–15. https://doi.org/https://doi.org/10.1148/radiol.2020200370

Qi, X., Jiang, Z., Yu, Q., Shao, Ch., Zhang, H., Yue, H., Ma, B., Wang, Y., Liu, Ch., Meng, X., Huang, S., Wang, J., Xu, D., Lei, J., Xie, G., Huang, H., Yang, J., Ji, J., Pan, H., Zou, S., & Ju, S. (2001). *Machine learning-based CT radiomics model for predicting hospital stay in patients with pneumonia associated with SARS-CoV-2 infection: A multicenter study*. MedRxiv. https://doi.org/10.1101/2020.02.29.20029603

Qin, C., Liu, F., Yen, T.C., & Lan, X. (2020). 18F-FDG PET/CT findings of COVID-19: a series of four highly suspected cases. *European Journal of Nuclear Medicine and Molecular Imaging*, *47*(5), 1281–1286. https://doi.org/10.1007/s00259-020-04734-w

Rahimzadeh, M., & Attar, A. (2020). A modified deep convolutional neural network for detecting COVID-19 and pneumonia from chest X-ray images based on the concatenation of Xception and ResNet50V2. *Informatics in Medicine Unlocked*, *19*, 100360. https://doi.org/10.1016/j.imu.2020.100360

Richardson, P., Griffin, I., Tucker, C., Smith, D., Oechsle, O., Phelan, A., & Stebbing, J. (2020). Baricitinib as potential treatment for 2019-nCoV acute respiratory disease. *The Lancet*, *395*(10223), e30–e31. https://doi.org/10.1016/S0140-6736(20)30304-4

Ronneberger, O., Fischer, P., & Brox, T. (2015). *U-net: Convolutional networks for biomedical image segmentation*. https://arxiv.org/abs/1505.04597

Shan, F., Gao, Y., Wang, Y., Shi, W., Shi, N., Han, M., Xue, Z., Shen, D., & Shi, Y. (2020). *Lung Infection Quantification of COVID-19 in CT Images with Deep Learning*. arXiv:2003.04655. https://doi.org/10.1002/mp.14609

Shi, F., Xia, L., Shan, F., Wu, D., Wei, Y., Yuan, H., Jiang, H., Gao, Y., Sui, H., & Shen, D. (2020). *Large-Scale Screening of COVID-19 from Community Acquired Pneumonia using Infection Size-Aware Classification*. http://arxiv.org/abs/2003.09860

Shi, H., Han, X., Jiang, N., Cao, Y., Alwalid, O., Gu, J., Fan, Y., & Zheng, C. (2020). Radiological findings from 81 patients with COVID-19 pneumonia in Wuhan, China: a descriptive study. *The Lancet Infectious Diseases*, *20*(4), 425–434. https://doi.org/10.1016/S1473-3099(20)30086-4

Shi, W., Peng, X., Liu, T., Cheng, Z., Lu, H., Yang, S., Zhang, J., Li, F., Wang, M., Zhang, X., Gao, Y., Shi, Y., Zhang, Z., & Shan, F. (2020). Deep Learning-Based Quantitative Computed Tomography Model in Predicting the Severity of COVID-19: A Retrospective Study in 196 Patients. *SSRN Electronic Journal*. https://doi.org/10.2139/ssrn.3546089

Singh, V., Ma, K., Tamersoy, B., Chang, Y.-J., Wimmer, A., O'Donnell, T., & Chen, T. (2017). DARWIN: Deformable Patient Avatar Representation With Deep Image Network. In M. Descoteaux, L. Maier-Hein, A. Franz, P. Jannin, D. Collins & S. Duchesne (Eds.), *Medical Image Computing and Computer-Assisted Intervention − MICCAI 2017. MICCAI 2017. Lecture Notes in Computer Science* (vol 10434). Springer, Cham. https://doi.org/10.1007/978-3-319-66185-8_56

Song, F., Shi, N., Shan, F., Zhang, Z., Shen, J., Lu, H., Ling, Y., Jiang, Y., & Shi, Y. (2020). Emerging 2019 novel coronavirus (2019-NCoV) pneumonia. *Radiology*, *295*(1), 210–217. https://doi.org/10.1148/radiol.2020200274

Wang, D., Hu, B., Hu, C., Zhu, F., Liu, X., Zhang, J., Wang, B., Xiang, H., Cheng, Z., Xiong, Y., Zhao, Y., Li, Y., Wang, X., & Peng, Z. (2020). Clinical Characteristics of 138 Hospitalized Patients with 2019 Novel Coronavirus-Infected Pneumonia in Wuhan, China. *JAMA - Journal of the American Medical Association*, *323*(11), 1061–1069. https://doi.org/10.1001/jama.2020.1585

Wang, L., & Wong, A. (2020). *COVID-Net: A Tailored Deep Convolutional Neural Network Design for Detection of COVID-19 Cases from Chest X-Ray Images*. http://arxiv.org/abs/2003.09871

Wang, S., Kang, B., Ma, J., Zeng, X., Xiao, M., Guo, J., Cai, M., Yang, J., Li, Y., Meng, X., & Xu, B. (2020). *A deep learning algorithm using CT images to screen for corona virus disease (COVID-19).* MedRxiv. https://doi.org/10.1101/2020.02.14.20023028

Wang, Y., Hu, M., Li, Q., Zhang, X.-P., Zhai, G., & Yao, N. (2020). *Abnormal respiratory patterns classifier may contribute to large-scale screening of people infected with COVID-19 in an accurate and unobtrusive manner*. http://arxiv.org/abs/2002.05534

WHO. (2020). *WHO Corona symptoms*. https://www.who.int/health-topics/coronavirus#tab=tab_3

Wong, H.Y.F., Lam, H.Y.S., Fong, A.H.-T., Leung, S.T., Chin, T.W.-Y., Lo, C.S.Y., Lui, M.M.-S., Lee, J.C.Y., Chiu, K.W.-H., Chung, T., Lee, E.Y.P., Wan, E.Y.F., Hung, F.N.I., Lam, T.P.W., Kuo, M., & Ng, M.-Y. (2016). Frequency and Distribution of Chest Radiographic Findings in COVID-19 Positive Patients. *Imaging*, *279*(3), 849–858. https://doi.org/10.1148/radiol.2020201160

Yan, L., Zhang, H.-T., Goncalves, J., Xiao, Y., Wang, M., Guo, Y., Sun, C., Tang, X., Jin, L., Zhang, M., Huang, X., Xiao, Y., Cao, H., Chen, Y., Ren, T., Wang, F., Xiao, Y., Huang, S., Tan, X., Huang, N., Jiao, B., Zhang, Y., Luo, A., Mombaerts, L., Jin, J., Cao, Z., Li, S., Xu, H., & Yuan, Y. (2020). *A machine learning-based model for survival prediction in patients with severe COVID-19 infection*. MedRxiv. https://doi.org/10.1101/2020.02.27.20028027

Yan, Q., Wang, B., Gong, D., Luo, C., Zhao, W., Shen, J., Shi, Q., Jin, S., Zhang, L., & You, Z. (2020). *COVID-19 Chest CT Image Segmentation – A Deep Convolutional Neural Network Solution*. http://arxiv.org/abs/2004.10987

Yao, X.H., Li, T.Y., He, Z.C., Ping, Y.F., Liu, H.W., Yu, S.C., Mou, H.M., Wang, L.H., Zhang, H.R., Fu, W.J., Luo, T., Liu, F., Guo, Q.N., Chen, C., Xiao, H.L., Guo, H.T., Lin, S., Xiang, D.F., Shi, Y., Pan, G.Q., Li, Q.R., Huang, X., Cui, Y., Liu, X.Z., Tang, W., Pan, P.F., Huang, X.Q., Ding, Y.Q., & Bian, X.W. (2020). A pathological report of three COVID-19 cases by minimal invasive autopsies. *Zhonghua bing li xue za zhi = Chinese journal of pathology*, *49*(5), 411–417. https://doi.org/10.3760/cma.j.cn112151-20200312-00193

Ye, Z., Zhang, Y., Wang, Y., Huang, Z., & Song, B. (2020). Chest CT manifestations of new coronavirus disease 2019 (COVID-19): a pictorial review. *European Radiology*, *30*(8), 4381-4389. https://doi.org/10.1007/s00330-020-06801-0

Zhang, J., Xie, Y., Liao, Z., Pang, G., Verjans, J., Li, W., Sun, Z., He, J., Li, Y., Shen, C., & Xia, Y. (2020). *COVID-19 Screening on Chest X-ray Images Using Deep Learning based Anomaly Detection*. http://arxiv.org/abs/2003.12338

Zhao, D., Yao, F., Wang, L., Zheng, L., Gao, Y., Ye, J., Guo, F., Zhao, H., & Gao, R. (2020). A Comparative Study on the Clinical Features of Coronavirus 2019 (COVID-19) Pneumonia With Other Pneumonias. *Clinical Infectious Diseases: An Official Publication of the Infectious Diseases Society of America*, *71*(15), 756–761. https://doi.org/10.1093/cid/ciaa247

Zhavoronkov, A., Aladinskiy, V., Zhebrak, A., Zagribelnyy, B., Terentiev, V., Bezrukov, D., Polykovskiy, D., Shayakhmetov, R., Filimonov, A., Orekhov, P., Yan, Y., Popova, O., Vanhaelen, Q., Aliper, A., & Ivanenkov, Y. (2020). *Potential COVID-2019 3C-like Protease Inhibitors Designed Using Generative Deep Learning Approaches*. ChemRxiv. https://doi.org/10.26434/chemrxiv.11829102.v2

Zheng, C., Deng, X., Fu, Q., Zhou, Q., Feng, J., Ma, H., Liu, W., & Wang, X. (2020). *Deep Learning-based Detection for COVID-19 from Chest CT using Weak Label*. MedRxiv. https://doi.org/10.1101/2020.03.12.20027185

Zhou, Z., Rahman Siddiquee, M.M., Tajbakhsh, N., & Liang, J. (2018). Unet++: A nested u-net architecture for medical image segmentation. In *Lecture Notes in Computer Science (Including Subseries Lecture Notes in Artificial Intelligence and Lecture Notes in Bioinformatics)* (vol. 11045 LNCS, pp. 3–11). Springer, Cham. https://doi.org/10.1007/978-3-030-00889-5_1

Applied Computer Science, vol. 17, no. 2, pp. 56–69
doi: 10.23743/acs-2021-13

Submitted: 2021-04-26 | Revised: 2021-06-01 | Accepted: 2021-06-15

*oncolytic virotherapy, feedback mechanism, crow search algorithm, Immune-LQR*

*Mohammed A. HUSSEIN*[*], *Ekhlas H. KARAM*[*], *Rokaia S. HABEEB*[*]

# CANCER GROWTH TREATMENT USING IMMUNE LINEAR QUADRATIC REGULATOR BASED ON CROW SEARCH OPTIMIZATION ALGORITHM

**Abstract**

*The rapid and uncontrollable cell division that spreads to surrounding tissues medically termed as malignant neoplasm, cancer is one of the most common diseases worldwide. The need for effective cancer treatment arises due to the increase in the number of cases and the anticipation of higher levels in the coming years. Oncolytic virotherapy is a promising technique that has shown encouraging results in several cases. Mathematical models of virotherapy have been widely developed, and one such model is the interaction between tumor cells and oncolytic virus. In this paper an artificially optimized Immune-Linear Quadratic Regulator (LQR) is introduced to improve the outcome of oncolytic virotherapy. The control strategy has been evaluated in silico on number of subjects. The crow search algorithm is used to tune immune and LQR parameters. The study is conducted on two subjects, S1 and S3, with LQR and Immune-LQR. The experimental results reveal a decrease in the number of tumor cells and remain in the treatment area from day ten onwards, this indicates the robustness of treatment strategies that can achieve tumor reduction regardless of the uncertainty in the biological parameters.*

## 1. INTORDUCTION

With more than 17 million cases registered in 2018 and reports indicating that this number will reach 23.6 million in 2030, cancer is one of the most common diseases around the world (Cancer Research UK, 2016; NIH, 2016). Cancer is the name given to a group of diseases that share a set of common characteristics, rapid uncontrollable cell division and spread into surrounding tissues (Jenner, 2020). The reason for this rapid and uncontrolled growth of cells is mutation in signaling that regulates the growth and division processes within the cells (Priya & Reyes, 2015). Conventional cancer treatment includes surgery, chemotherapy, radiotherapy, targeted therapy, immunotherapy and stem cell transfusion therapy (Cancer Research UK, 2016).

The effectiveness of cancer treatment has improved significantly in recent years, but despite this there are certain types of cancer for which treatment options are still limited,

[*] Mustansiriyah University, College of Engineering, Computer Engineering Department, Baghdad, Iraq, mohammediyad95@gmail.com, ek_karam@yahoo.com, rokaia.shalal@uomustansiriyah.edu.iq

and there are tumors that remain completely incurable, which increases the need for long-term treatment strategies (Crivelli et al., 2012).

Biotherapy is a cancer treatment that uses the ability of viruses to infect and replicate to destroy cancer cells, these viruses are often called oncolytic viruses (Arum, Handayani & Saragih, 2019). Viruses favorably act on cancer cells rather than healthy cells. There are many viruses that have proven effective against cancerous tumors, including them Adenovirus, Reovirus, Measles, Herpes Simplex, Vesicular-Stomatitis Virus (VSV) (Crivelli et al., 2012).

Oncolytic virotherapy has shown success in some patients although this is not clear how to obtain good results in all cases. It is difficult to set the injections' number, quantity and scheduling to reduce the tumor size within specified time frame (Anelone, Villa-Tamayo & Rivadeneira, 2020).

Mathematical modelling help in prediction of the system's future behavior and assess the impact of variables and parameters on the overall dynamics of a cancer. These parameters are relevant to the patient's physiology, treatment strategy and disease type. It is challenging, risky, and expensive to carry out such expectations in vivo, vitro, or clinical trials (Cancer Research UK, 2016). These models can be used to improve and optimize the impact of different factors such as changes in the virus's genetics, dosage, or injection schedule.

Optimization is the achievement of the desired goal (s) exactly or roughly by obtaining the best set of variables maybe by trial and error. Nature inspired optimization algorithms are metaheuristic algorithms developed from biological principles, swarm behavior, and chemical or physical processes (Yang, 2020). Crow search algorithm (CSA) an algorithm inspired by crow's behavior was introduced in (Askarzadeh, 2016), its main use in solving engineering problems that contain constraints.

Recently, many researches aim to apply biological information processing systems to engineering fields due to its flexibility. As these systems are more flexible than currently available systems, which makes it possible to form a system whose performance is better than the performance of conventional systems (Takahashi & Yamada, 1998). Regulation Mechanism of Bio-Inspired Systems like the immune system, is a complex system consisting of many types of immune cells and appropriate communication channels. This is an ideal control system for the human body against diseases and foreign bodies (Ding, Chen & Hao, 2018).

Interactions between virotherapy and control theory have been illustrated in many previous studies. For instance, reducing the number of cancer cells using successive state dependent algebraic Riccati equation (SDARE) have been introduced in (Arum, Handayani & Saragih, 2019). In (Saputra, Saragih & Handayani, 2019) $H_\infty$ were used to control the controller input into a system, the results showed the effectiveness of the $H_\infty$ controller in reducing the number of Human Immunodeficiency Virus (HIV) particles in the blood plasma; In (Anelone, Villa-Tamayo & Rivadeneira, 2020) impulsive controller is designed to deliver a personalized dose for each case, and feedback controller showed a tumor reduction potential better than that obtained by former protocols.

In this paper, the principle of the body's immune mechanism is presented as a controller with LQR based on CSA for parameters optimization are used to control the number of viruses given to patients. To accomplish these objectives, the result of personal protocol is investigated as a reference for comparison (Anelone, Villa-Tamayo & Rivadeneira, 2020).

The remaining sections of this paper are organized as follows, the mathematical model is discussed in the second part, the immune system is defined in the third part, and the crow

search algorithm (CSA) is demonstrated in the fourth part. The fifth section includes a definition of the proposed Immune-LQR structures controller. The simulation results and review of the proposed controllers are addressed in the sixth section, and the conclusion is presented in the final section.

## 2. MATHEMATICAL MODELLING

In the studies (Jenner et al., 2018; Kim et al., 2011), nude mice were given a genetically modified virus to reduce the number of breast cancer cells in it in just 60 days. Since these naked mice have no immune system, the tumor reduction is entirely due to the oncolytic virotherapy. Experiments began with mice containing between 90 and 300 cancer cells. All experiments follow a fixed protocol in injecting $10^{10}$ viral particles on days 0, 2, 4. The interaction between oncolytic virus and carcinoma cells shown in Fig. 1, and illustrated mathematically using (ordinary differential equations) ODEs according to work in (Jenner et al., 2018):

$$\dot{S}(\tau) = rlog\left(\frac{K}{S(\tau)}\right) - \frac{\beta V(\tau)S(\tau)}{S(\tau) + I(\tau) + \varepsilon} \tag{1}$$

$$\dot{I}(\tau) = \frac{\beta V(\tau)S(\tau)}{S(\tau) + I(\tau) + \varepsilon} - d_I I(\tau) \tag{2}$$

$$\dot{V}(\tau) = Uv(\tau) - dvV(\tau) + \alpha\, \mathrm{d}_I I(\tau) \tag{3}$$

where, $\dot{S}$ denotes the density of susceptible tumor cells ($\times 10^6$ cells), $\tau$ represents the time, $r$ is the tumor growth (day$^{-1}$), $K$ describes the caring capacity (cell x $10^6$), $\beta$ is the tumor cells rate of infection (day$^{-1}$), $\dot{I}$ refers to the density of infected tumor cells ($\times 10^6$ cells), $d_I$ is the infected tumor cells death rate (day$^{-1}$), $\dot{V}$ is the density of virus particles ($\times 10^9$ virus), $dv$ is the viral decay (day$^{-1}$) and $\alpha$ viral burst size (virus x $10^9$).

$T$=$S$+$I$ is the total number of tumor cells, $\varepsilon$ is a small value ($\varepsilon > 0$ ) set to avoid singularity occurring as ($S$+$I$) approaches zero.

The injection of virus particles is expressed by the model's input $Uv(\tau)$. While $T$ represents the model's output. The tumor volume is calculated as $T = 0.523 \times H \times B^2$, where, ($H$) is the height and ($B$) is the breadth. Both ($H$) and ($B$) are measured with a caliper (Kim et al., 2011). Then, assuming a density of $10^6$ cells per mm$^3$, $T$ is calculated (Jenner et al., 2018).

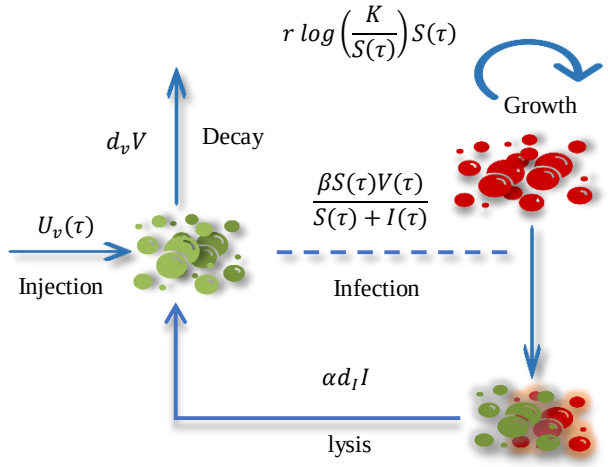


**Fig. 1. An interface between oncolytic viruses and tumor cells**

In Fig. 1, tumor cells are represented by red balls, while virus particles are represented by green balls). Table 1 summarizes the model's initial conditions and parameter values for AD- PEG-HER treatment.

**Tab. 1. Parameters and initial conditions values (Jenner et al., 2018)**

| ***Symbol*** | $S_0$ | $I_0$ | $V_0$ | $r$ | $K$ | $\beta$ | $d_I$ | $dv$ | $\alpha$ |
|---|---|---|---|---|---|---|---|---|---|
| $S_1$ | 238.3535 | 0 | 0 | 0.0378 | 8466.8 | 1.12 | 2 | 2.0872 | 2 |
| $S_2$ | 200.0340 | 0 | 0 | 0.0733 | 3179.1 | 1.4987 | 1.9995 | 3.2287 | 2.0015 |
| $S_3$ | 101.5400 | 0 | 0 | 0.0224 | 4922.4 | 0.2 | 2 | 3.5 | 2 |
| $S_4$ | 140.3436 | 0 | 0 | 0.0316 | 8317.1 | 1.2108 | 0.1 | 1.8730 | 3.7748 |
| $S_5$ | 128.1481 | 0 | 0 | 0.0603 | 936.4293 | 1.3606 | 0.1 | 1.8416 | 3.7541 |
| unit | Cells | cells | virus | day−1 | cells × $10^6$ | day−1 | day−1 | day−1 | virus × $10^9$ |

## 3. IMMUNE FEEDBACK MECHANISM

Recent immunology researches have shown that the immune system is essential in protecting the body against complex and hostile changes in the environment through the interaction between antibodies and lymphocytes. Antigens have the potential to impact the immune system's simultaneous dynamics (Rochdi, 2014). This process is known as the immune T-cell regulatory circuit because of T cells' primary function in the immune response (Takahashi & Yamada, 1998).

The main cells in this process are *Ab* antibodies, *Ag* antigens, *B* cells, suppressor *T* cells $T_s$ and *T* helper cells $T_h$. Antigen Information is passed on to *T* cells as antigens infect the body.

After receiving the message, the *T* cells activate the *B* cells, which then produce antibodies to remove the antigen. The number of $T_h$ cells in the human body increases as the number of antigens increases, and more *B* cells can be produced to protect the body (Rochdi, 2014).

*Ts* cells number in the body will increase and consequently *B* cells will decrease, in conjunction with the decrease in the antigen level. After a while the immune system begins to balance out. The immune system is able to react quickly to foreign bodies and regulate the immune system as a result of this collaboration between the feedback mechanism and the related mechanism (Rochdi, 2014). The suppression function of *B* cells will be discussed here. *B* cells are triggered and restricted by *Ts* cells in response to antigen invasion, so the *B* cells consistency of $t^{th}$ cell generation can be determined by (Rochdi, 2014):

$$B(t) = T_H(t) - T_S(t) \tag{4}$$

$$T_H(t) = K_1\alpha(t) \tag{5}$$

$$T_S(t) = K_2\{f[\Delta B(t-d)]\}\alpha(t) \tag{6}$$

where $B(t)$ represents the consistency of *B* cells, $K_1$ and $K_2$ represents the helper and suppressor genes respectively, $\alpha(t)$ refers to the $t^{th}$ generation antigen consistency, $f$ is a nonlinear function, that represents the relationship between the antigen and antibody, that elicits from the *B* cells, $d$ is the time delay of the immune response and $\Delta B$ refers to the change of consistency in the *B* cell that can be determined by:

$$\Delta B(t-d) = B(t-d) - B(t-d-1) \tag{7}$$

From equations (4–6), the relationship between the antigen and the *B*-cell's consistency, can be expressed as:

$$B(t) = K_1\{1 - \eta_0 f[\Delta B(t-d)]\}\alpha(t) \tag{8}$$

where $\boldsymbol{\eta_0}$ is the proportional coefficient between $\boldsymbol{T_H}$ and $\boldsymbol{T_S}$, $\boldsymbol{\eta_0} = \boldsymbol{K_2/K_1}$. The immune feedback mechanism performs two inconsistent processes simultaneously: it reacts quickly to foreign bodies and works to restore the immune system stability. Additionally, a high level of antibodies must be coordinated and controlled because they can be harmful to the body. Deviation must be avoided in a complex regulation control system to ensure system stability, which is consistent with the immune system's targe.

## 4. CROW SEARCH ALGORITHM

Crow search algorithm (CSA) is an optimization algorithm that mimics the crow flock behavior in storing and retrieving their surplus food (Askarzadeh, 2016).

Generally, the adjustable parameters of CSA are: population (flock) size ($N$), Flight length ($FL$), awareness probability ($AP$) and maximum number of iterations (*Maxiter*). The implementation of CSA can be done by the following steps:

1. Define the optimization problem and initialize the decision variables and any constraints needed.
2. The position and memory of each crow is initialized (each crow represents a viable solution to the optimization problem).
3. Evaluate the position of each crow using a fitness function.
4. Generate new position in the search space.
5. Determine the viability of new positions.
6. Evaluate the new position's fitness feature.
7. Update the crow memory by the new position.
8. Verify the termination criterion.

In this paper the CSA is used to tune the parameters of the Immune-LQR ($k_I$ and $\eta$, $k_1$, $k_2$, and $k_3$). The CSA can be described by the following flowchart:

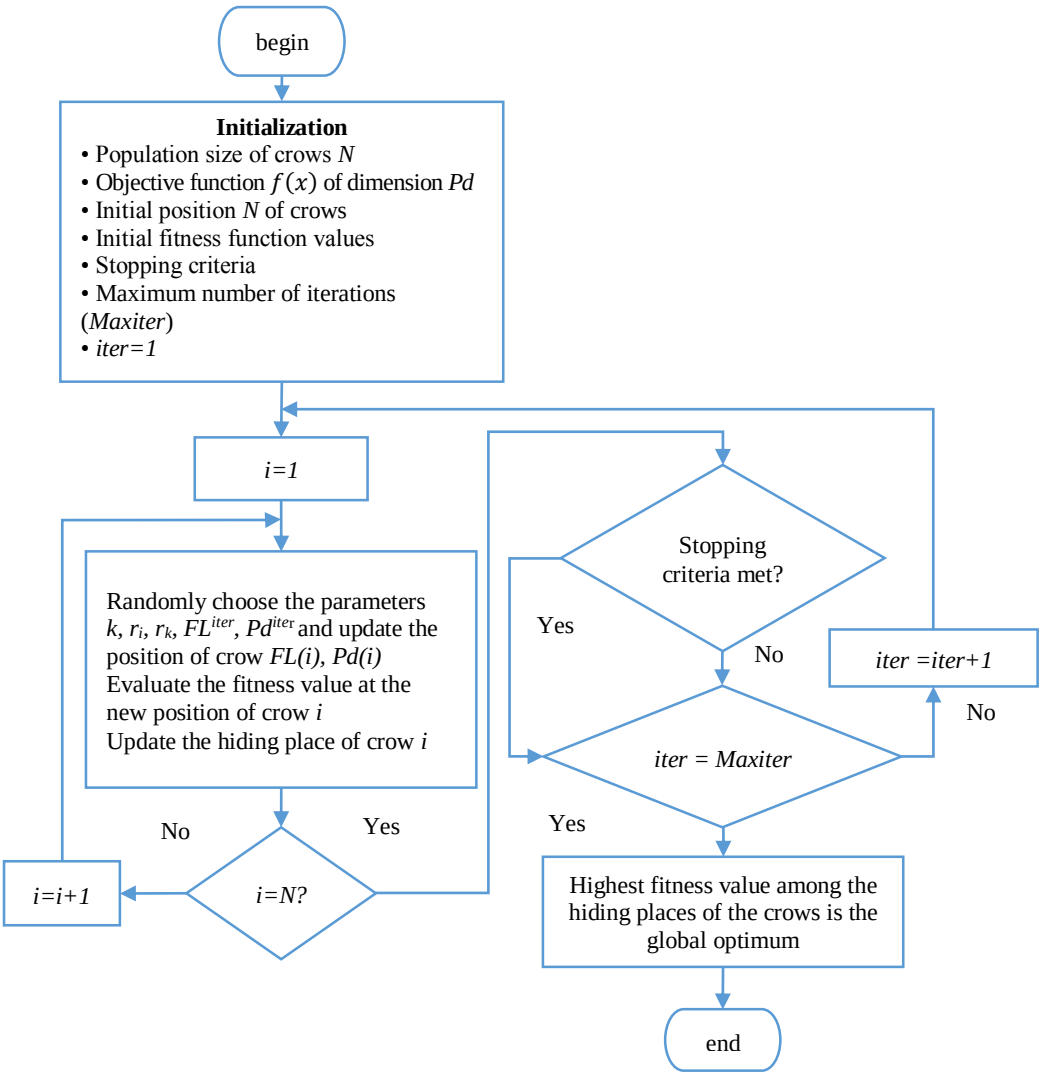


**Fig. 2. CSA Flowchart**

## 5. PROPOSED CONTROLLER

In this paper the continuous administration of viruses using an Immune-LQR controller are suggested to monitor the number viruses provided to patients. The CSA is used to tune immune and LQR parameters. The study is conducted on two subjects, S1 and S3, with LQR and Immune-LQR. The block diagram of the suggested controller is shown in Fig 3.

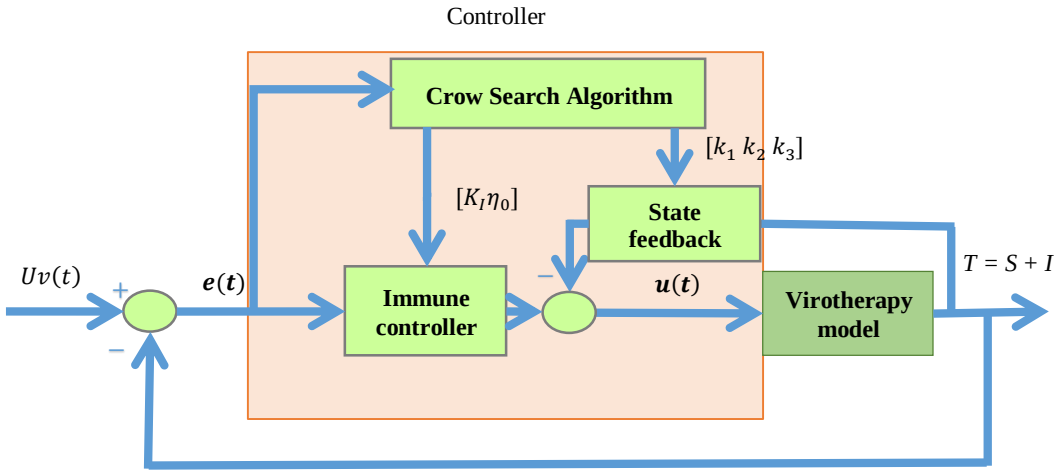


**Fig. 3. Block diagram of the suggested Immune -LQR controller based on optimization algorithm**

The error *e*(*t*) represents the amount of antigen ($\alpha(t)$ in equation 8), and the controller's input *u* (*t)* will be the total incentive that the *B* cells accept. Then the feedback control system is defined as follows:

$$u(t) = u1(t) \times u2(t) \tag{9}$$

$$u1(t) = K_1\{1 - \eta_0\, f[\Delta u(t-d)]\}\, e(t) \tag{10}$$

$$u1(t) = K_I e(t)$$

where $K_I$ is defined as the immune controller gain that is specified by the gene $\boldsymbol{\eta_0 = K_2/K_1}$. The parameter $\boldsymbol{K_1}$ controls the response speed, the parameter $\boldsymbol{\eta_0}$ controls the stabilization effect and *f* (.) denotes a nonlinear-function. This function is chosen as *T* cell's controls action-function, which is influenced by antigen consistency on antibody in immune response. The function $\boldsymbol{f(x)}$ is defined by:

$$(x) = 1.0 - exp\left(\frac{-x^2}{a}\right), \quad a > 0 \tag{11}$$

where *a* is a parameter that changes the function shape. the range of *f* (*x*) is [0,1]. The value of *a* determines the active region of *x*. The output of the immune controller can be described as:

$$u1(t) = K_1 \left\{1 - \eta_0(1.0 - exp\left(\frac{-x^2}{a}\right))\right\} e(t) \tag{12}$$

$$u1(t) = K_I e(t)$$

Since the immune controller is a nonlinear gain controller, it is not robust against noise and error induced by nonlinear disruption. To solve this problem and improve the system's efficiency, the immune controller must be combined with conventional LQR ($\boldsymbol{u2(t)}$). LQR was chosen because it can handle large disturbances while maintaining system stability without reducing working efficiency and can handle previous disturbances (Purnawan & Purwanto, 2017). When the forward gain $k_1$ of the LQR is multiplied by the immune output, the final result is $\boldsymbol{K_{I1}}$, as shown in Fig 3, and Eq. 23 shows the structure's controller output.

$$\dot{x} = Ax + Bu \tag{13}$$

$$y = Cx \tag{14}$$

$$u(t) = -kx + r \tag{15}$$

where $\dot{\boldsymbol{x}}$ denotes the state vector, $u$ is referred to the control signal, $\boldsymbol{y}$ is the output and $r$ represents the reference. The equations (1-3) can be written as a matrix as follows:

$$\begin{bmatrix} \dot{S} \\ \dot{I} \\ \dot{V} \end{bmatrix} = \begin{bmatrix} -r + r\ln\left(\frac{L}{s}\right) - \beta\frac{IV}{(I+S)^2} & \beta\frac{VS}{(I+S)^2} & -\beta\frac{S}{I+S} \\ \beta\frac{IV}{(I+S)^2} & -\beta\frac{IV}{(I+S)^2} - \mathrm{d}_I & \beta\frac{S}{I+S} \\ 0 & \alpha d_I & -\mathrm{d}_v \end{bmatrix} \begin{bmatrix} S \\ I \\ V \end{bmatrix} + \begin{bmatrix} 0 \\ 0 \\ 1 \end{bmatrix} Uv \tag{16}$$

$$y = [1\ 1\ 0] \begin{bmatrix} S \\ I \\ V \end{bmatrix} \tag{17}$$

The matrix $\boldsymbol{A}$ will differ based on the equilibrium point chosen, but the matrices $\boldsymbol{B}$ and $\boldsymbol{C}$ will remain the same (Anelone, Villa-Tamayo & Rivadeneira, 2020). Dynamic system in equations (13–15) can be written as:

$$\dot{x} = [A][x] + [B]u + [0]r \tag{19}$$

If $x(\infty)$and $u(\infty)$ reach constant value, then $y(\infty) = r$, and the system is stabilized. The state and control signal error becomes as follow:

$$x(t) - x(\infty) = x_e(t)$$

$$u(t) - u(\infty)] = u_e(t)$$

The state error equation can be written as:

$$x_e(t) = [A][x_e(t)] + [B]u_e(t) \tag{20}$$

with:

$$u_e(t) = -Kx_e(t) \tag{21}$$

$$e(t) = [x_e(t)]$$

$$u2(t) = -Kx_e(t)$$

The LQR method is used to find the value of *K*, and the LQR cost function is defined by:

$$J = 1/2 \int_0^\infty (\mathrm{e}^T Qe + u_e^T Ru_e)dt \tag{22}$$

where $Q$ is a positive-definite (or positive-semidefinite) Hermitian or real symmetric matrix, $R$ is a positive-definite Hermitian or real symmetric matrix.
and Ricarte's equation is:

$$A^T P + PA + Q - PBR^{-1}B^T P = 0 \tag{23}$$

where $P$ is a positive-definite Hermitian or real symmetric matrix, with:

$$K = -[k_1\ k_2 k_3]$$

From equation (9), (12) and (21):

$$u(t) = u1(t) \times u2(t)$$

$$u1(t) = K_I e(t)$$

$$u2(t) = -Kx_e(t)$$

The first LQR gain ($k_1$) is multiplied by immune gain ($K_I$) , then substituting equation (12) into equation (18) yields:

$$u(t) = -[K_I k_1\ \ k_2\ \ k_3\ ] \tag{24}$$

$$K_{I1} = K_I k_1$$

$$u(t) = -[K_{I1}\ \ k_2\ \ k_3]$$

where Eq. (23) represents control input.

## 6. SIMULATION RESULTS AND ANALYSIS

In this paper, toxicity and the subsequent dosages of viral injections was not considered as a limitation in the design of the controller. The toxicity tests in (Kim et al., 2011) revealed that when the oncolytic adenovirus's surface is shielded with a biocompatible polymer like polyethylene glycol (PEG), the virus therapy causes no hepatic damage and minimal liver toxicity.

For contrast, the same target in (Anelone, Villa-Tamayo & Rivadeneira, 2020) will be used, which states that the goal of the treatment is to reduce and sustain the total number of tumor cells below 50 cells in 60 days with discrete viral injections. The well-known PSO (partial swarm optimization algorithm) is used for comparison purpose with CSA. The Optimal control parameters obtained using optimization algorithms for $S_1$ and $S_3$ using LQR and Immune-LQR controller listed in Table 2 and 3 respectively (the $a, Q$ matrix, and $R$ are selected as: 0.5, $\begin{bmatrix} 0 & 0 & 0 \\ 0 & 0 & 0 \\ 0 & 0 & 1 \end{bmatrix}$, [0.1]).

**Tab. 2. Optimal parameters for LQR controller**

| *Algorithms* | $k1$ | $k2$ | $k3$ | *subjects* |
|---|---|---|---|---|
| CSA | -6.6522 | 5.1449 | 3.1093 | S1 |
| PSO | -7.1520 | 2.1023 | 2.4930 | |
| CSA | -27.9204 | 3.6500 | 6.7346 | S3 |
| PSO | -27.9640 | 0.7472 | 1.4617 | |

**Tab. 3. Optimal parameters for Immune-LQR controller**

| *Algorithms* | $k1$ | $k2$ | $k3$ | $\eta_0$ | $K_I$ | *subjects* |
|---|---|---|---|---|---|---|
| CSA | -5.9762 | 2.5627 | 6.1470 | 0.2243 | 3.7401 | S1 |
| PSO | -5.8598 | 2.4347 | 2.4930 | 0.6066 | 4.9352 | |
| CSA | -25.1379 | 2.7631 | 7.2516 | 0.5570 | 3.8160 | S3 |
| PSO | -27.9640 | 2.2416 | 1.4617 | 0 | 4 | |

The parameters used in optimization algorithms are listed in Table 4.

**Tab. 4. Optimization algorithms parameters.**

| ***Parameters*** | ***Value*** | ***Algorithms*** |
|---|---|---|
| population size($N$) | 25 | CSA, PSO |
| Max iteration ( *Maxiter* ) | 50 | |
| problem dimension ($Pd$) | 5 | CSA |
| Awareness probability ($AP$) | 1.2 | |
| Flight length ($FL$) | 0.3 | |
| Inertia weight($w_{max}$-$w_{min}$) | (0.9 – 0.4) | PSO |
| Learning rates ($c1, c2$) | 2 | |

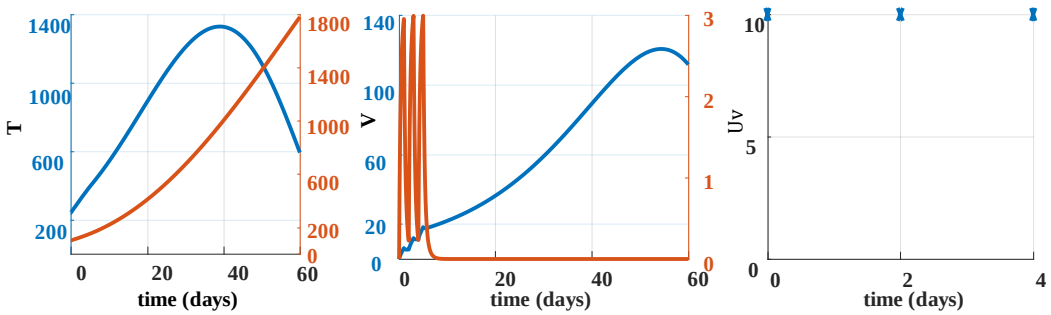


**Fig. 4. Simulation result of experimental protocol for $S_1$ (blue line) and $S_3$ (orange line)**

Fig 4. shows the experimental protocol results of S1 and S3. The left figure illustrates the total number of tumor cells over a period of 60 days. The middle figure illustrates the viral loads in vivo over the period of 60 days. The right figure illustrates the viral injections within 4 days. This is the treatment of subject S1 and S 3with the total injections of 10.

As illustrated in Fig. 4, the experimental treatment fails to reduce the size of the tumor in $S_1$ while the tumor begins to regress after an initial rise in $S_3$; traditional therapy with different subjects has various effects.

In Fig. 5, the orange dash lines and the continuous lines indicate subjects with LQR and Immune-LQR controllers respectively optimized using the PSO algorithm for number of injections determination; while the blue dash lines and the continuous lines indicate subjects with LQR and Immune-LQR units respectively optimized using the CSA algorithm for number of injections determination. The top row (a) shows the total number of tumor cells within 60 days. The middle row (b) shows the viral loads in vivo within 60 days. The bottom row (c) shows the viral injections within 30 days.

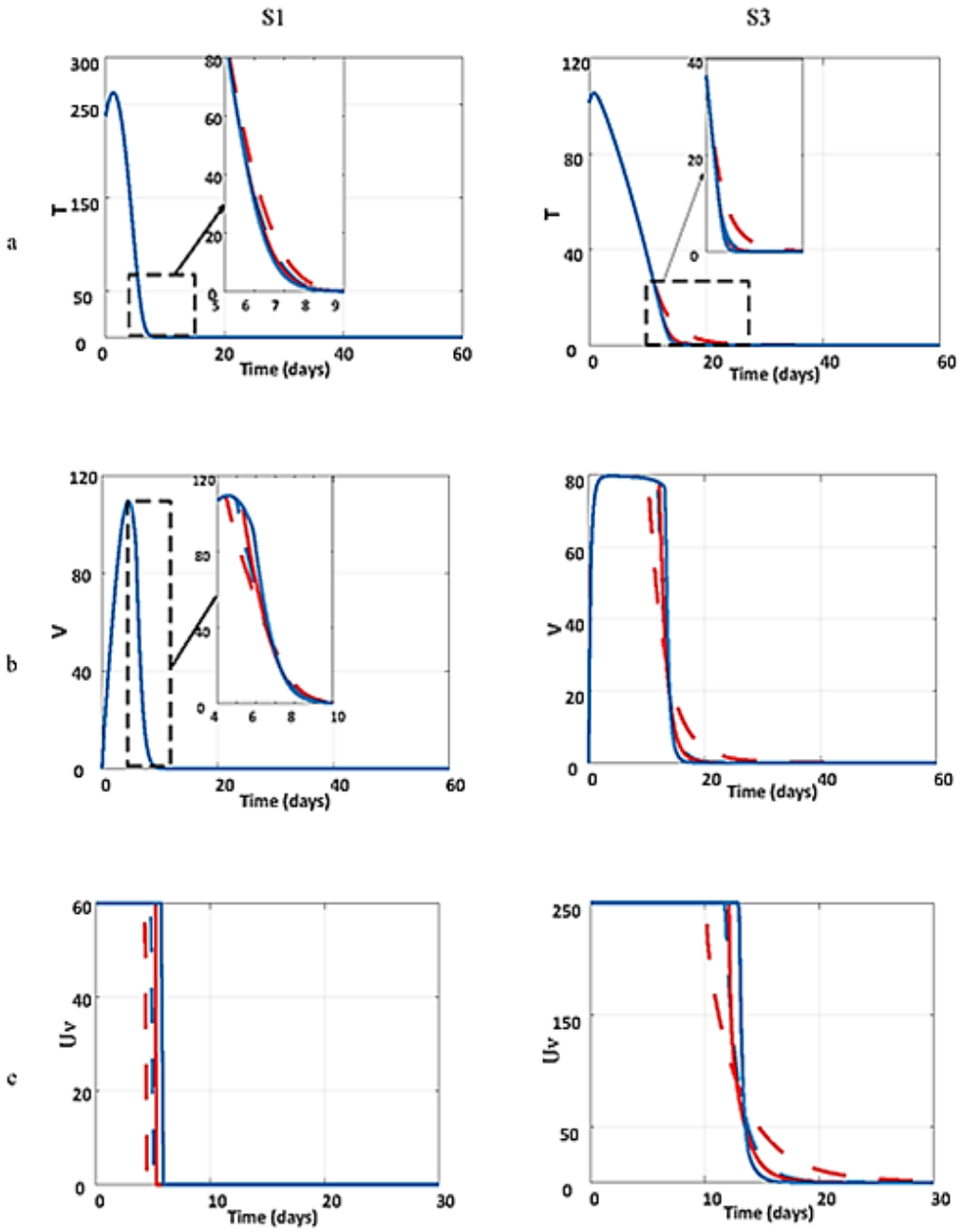


**Fig. 5. Simulation result of S1(left column) and S3(right column) using Immune-LQR control and different optimization algorithms**

The feedback control reduces the size of the tumor faster than the conventional treatment, and there are no rebounds of the tumor after the end of the treatment, as the feedback controller works to keep the tumor with therapeutic zone, i.e., less than or equal to 50 total tumour cells in all subjects, and reduce the amount of injections overtime as showing in Fig.

5(a). The personalized protocol suggested using the proposed control would give higher initial injections than the experimental treatment. Consequently, the feedback mechanism in the immune controller increases the number of injections due to an increase in the $\eta_0$, where the larger ratio indicates the increase of $T_h$ cells whose increase leads the body to form more antibodies to protect itself as shown in Fig. 5(b). As a result, the control signal is higher in treatment with feedback control than in experimental treatment during the first hours of treatment and decreases gradually as shown in Fig. 5(c). Nevertheless, the virus load tends to be lower in the feedback control compared to the experimental treatment. After the tumor has decreased in recent days, we suggest that viruses that may be toxic are quickly removed.

The results suggest applying control theory in oncolytic virotherapy has benefits by delivering an effective amount of treatment to accomplish therapeutic goals, as both LQR and Immune-LQR controllers perform this task in a relatively shorter period with superior performance Immune-LQR over LQR at S1 by 3.1807%, 1.4020% and at S3 by 2.5490%, 2.2083% using CSA and PSO respectively where the performance index used is Integral time absolute error (ITAE). Since each subject has different biological rate, they react differently across different elements. When tumor regression is as slow as in S3, the total injection will increase, implying that there is a negative relationship between the total number of injections and the tumor regression speed to overcome high starting spikes.

The results obtained are consistent with (Anelone Villa-Tamayo & Rivadeneira, 2020), as a high injection in the beginning performs well through different subjects and reduces the total number of tumor cells and total injections. When significant amounts of viral loads are injected at the start of therapy in any subject, the total number of tumor cells and the total doses are reduced. However, increased viral loads in vivo and the eventual expensive cost of viral injections pose questions about toxicity in this case. The tumor decreases and remains in the treatment area from day ten onwards; This indicates that the controller regulates the number of injections well to reduce the tumor.

## 7. CONCLUSION

In this paper, artificially tuned Immune-LQR controller is suggested to regulate the number of viral load injections that are injected in order to reduce tumor cells. The mathematical model of interaction between tumor cells and oncolytic virotherapy has been considered. In order to improve the characteristics of the proposed controllers, CSA and PSO algorithms has been applied. The simulation results show that the Immune-LQR structure outperforms the other structures. As the feedback controller acts to maintain the tumor within the therapeutic region, i.e., less than or equal to 50 total tumor cells in all subjects, and minimize the amount of injections over time, the feedback control decreases the size of the tumor faster than traditional therapy, and there are no rebounds of the tumor after the treatment ends.

To improve our understanding of the relationship between toxicity, number of viral injection doses, and viral load in vivo, further mathematical and experimental research is required. These findings may help with the development of virus therapies and control strategies to ensure tumour regression with minimal side effects.

## REFERENCES


Anelone, A.J.N., Villa-Tamayo, M.F., & Rivadeneira, P.S. (2020). Oncolytic virus therapy benefits from control theory. *Royal Society Open Science*, *7*(7), 200473. https://doi.org/10.1098/rsos.200473

Arum, A.K., Handayani, D., & Saragih, R. (2019). Robust control design for virotherapy model using successive method. *Journal of Physics: Conference Series*, *1245*(1), 12054. https://doi.org/10.1088/1742-6596/1245/1/012054

Askarzadeh, A. (2016). A novel metaheuristic method for solving constrained engineering optimization problems: crow search algorithm. *Computers & Structures*, *169*, 1–12. https://doi.org/10.1016/j.compstruc.2016.03.001

Cancer Research UK. (2016). *Worldwide cancer statistics*. *Cancer Research UK*. Cancer Research UK (pp. 1–5). https://www.cancerresearchuk.org/health-professional/cancer-statistics/worldwide-cancer

Crivelli, J.J., Földes, J., Kim, P.S., & Wares, J.R. (2012). A mathematical model for cell cycle-specific cancer virotherapy. *Journal of Biological Dynamics*, *6*(sup1), 104–120. https://doi.org/10.1080/17513758.2011.613486

Ding, Y., Chen, L., & Hao, K. (2018). *Bio-Inspired Collaborative Intelligent Control and Optimization*. Springer.

Jenner, A.L. (2020). Applications of mathematical modelling in oncolytic virotherapy and immunotherapy. *Bulletin of the Australian Mathematical Society*, *101*(3), 522–524. https://doi.org/10.1017/S0004972720000283

Jenner, A.L., Yun, C.-O., Kim, P.S., & Coster, A.C.F. (2018). Mathematical modelling of the interaction between cancer cells and an oncolytic virus: insights into the effects of treatment protocols. *Bulletin of Mathematical Biology*, *80*(6), 1615–1629. https://doi.org/10.1007/s11538-018-0424-4

Kim, P.-H., Sohn, J.-H., Choi, J.-W., Jung, Y., Kim, S.W., Haam, S., & Yun, C.-O. (2011). Active targeting and safety profile of PEG-modified adenovirus conjugated with herceptin. *Biomaterials*, *32*(9), 2314–2326. https://doi.org/10.1016/j.biomaterials.2010.10.031

NIH. (2016). *Cancer Statistics – National Cancer Institute*. NIH. https://www.cancer.gov/about-cancer/understanding/statistics

Priya, P., & Reyes, V.M. (2015). *A Cancer Biotherapy Resource*. ArXiv Preprint ArXiv:1602.08111. https://arxiv.org/abs/1602.08111

Purnawan, H., & Purwanto, E.B. (2017). Design of linear quadratic regulator (LQR) control system for flight stability of LSU-05. *Journal of Physics: Conference Series*, *890*(1), 12056.

Rochdi, B. (2014). Design and application of fuzzy immune PID control based on genetic optimization. *International Workshop on Advanced Control IWAC* (pp. 10–14).

Saputra, J., Saragih, R., & Handayani, D. (2019). Robust H∞ controller for bilinear system to minimize HIV concentration in blood plasma. *Journal of Physics: Conference Series*, *1245*(1), 12055.

Takahashi, K., & Yamada, T. (1998). Application of an immune feedback mechanism to control systems. *JSME International Journal Series C Mechanical Systems, Machine Elements and Manufacturing*, *41*(2), 184–191. https://doi.org/10.1299/jsmec.41.184

Yang, X.-S. (2020). *Nature-inspired optimization algorithms*. Academic Press.

Applied Computer Science, vol. 17, no. 2, pp. 70–89
doi: 10.23743/acs-2021-14

Submitted: 2021-05-29 | Revised: 2021-06-20 | Accepted: 2021-06-22

*assembly, production planning, support, spreadsheet, MS Excel*

*Jolanta BRZOZOWSKA* [0000-0002-4355-2847]*, *Arkadiusz GOLA* [0000-0002-2935-5003]**

# COMPUTER AIDED ASSEMBLY PLANNING USING MS EXCEL SOFTWARE – A CASE STUDY

**Abstract**

*The issue of planning assembly operations remains crucial decision-making area for many of manufacturing companies. It becomes particularly significant in case of small and medium enterprises that perform unit or small-scale production, where the option of applying specialized software is often very limited – both due to high purchase price, but also due to its applicability to single unit manufacturing, that is executed based on individual customer orders. The present article describes the possibility of applying the MS Excel spreadsheet in the planning of machine assembly processes. It emphasises, in particular, the method for using the spreadsheet in subsequent stages of the process, and the identification of possible causes that have impact on problems with the planning process. We performed our analysis on the basis of actual data from one of the machine industry enterprises that manufactures in central Poland.*

## 1. INTRODUCTION

The growing, global competition means, that apart from low-cost manufacturing of products of appropriate quality, also the ability to quickly (and most of all timely) complete production orders becomes crucial for the development options of enterprises (Wikarek, Sitek & Nielsen, 2019; Świć & Gola, 2013). Therefore, what becomes a challenge in the organization of production processes are: correct planning, supervision and introduction of required corrective actions, in case of detrimental chance factors (Paprocka, Krenczyk & Burduk, 2021; Sobaszek, Gola & Kozłowski, 2017). There are numerous IT solutions that are designed to support the production manager's work (including ERS, MES class, and other systems) available commercially, but their applicability to small and medium enterprises manufacturing according to individual or small-series orders is very limited (Danilczuk & Gola, 2020). This is often due to the very cost of purchase of this type of software, or the difficulties in current update of production data (Tarigan, Siagian & Jie, 2021).

Assembly departments are frequently the decision areas of particular importance – as there the production processes are completed, by assembly teams, in manufacturing nests – rendering the detailed planning of the process more difficult due to teamwork character of the performed operations (Gola, 2014). What is more – we should bear in mind that the unit

* International Tobacco Machinery Poland, Radom, Poland, jolantabrzozowska.89@gmail.com
** Lublin University of Technology, Faculty of Mechanical Engineering, Department of Production Computerisation and Robotisation, Lublin, Poland, a.gola@pollub.pl

or small series scale of completed production further renders detailed planning non-economical (the time for such a planning process remains disproportionately long, when compared to the assembly time). Order completion time shortening requirements exert additional pressure – thus forcing the adoption of framework approach, using cheap and generally available IT tools (Cieśla & Mleczko, 2021).

Although the problem of production and assembly planning has been known for several years it is difficult to find publications where the issue of assembly planning has been investigated efficiently. Benjaafar and ElHafsi (Benjafar & Elhafsi, 2006), and ElHafsi (ElHafsi, 2009) studied the optimal production and inventory control of and assemble-to-order system with multiple components, one end product and multiple customer classes. Pang (Pang, 2015) analysed the optimal control problem for a continuous review assemble-to-order system with multiple demand classes and backordering. Remain and Wang (Remain and Wang, 2015) made and asymptotic analysis to minimize the long-run average cost of assemble-to-order inventory systems. On the other hand, Gyulai at al. (Gyulai & Monostori, 2017; Gyulai, Kadar & Monostori, 2014) introduced a novel conceptual framework that supported the periodic revision of the capacity allocation and determined the configuration of an assembly system. Manitz (Manitz, 2008) employed queuing network to analyse an assembly lines with the asynchronous material flow and evaluate its throughput. Ju et al. (Ju & Li, 2014; Ju, Li & Deng, 2017) employed the Bernoulli model to evaluate the selective assembly system performance efficiently. Li et al. (Li, Blumenfeld, Huang & Alden, 2009) summarized studies about performance analysis of serial lines, parallel lines and assembly and disassembly systems.

As the operating practice of small and medium enterprises demonstrates it is very often so (even if they hold licences for ERP class software) that the people responsible for planning assembly resort to spreadsheet software (eg. MS Excel). Albeit commonly perceived as a non-professional software it is one of the most frequent IT solutions to support the planning process (Kamath & Sarkar, 2020). The objective of the present article is to present the course of assembly planning process in an enterprise completing one-off and small series production, with use of the MS Excel spreadsheet. We put particular emphasis on comparative evaluation of theoretical considerations with industrial practice and identification of possible causes that have impact on issues in the planning processes. We performed our analysis using actual data from one of machine building enterprises that manufactures in Poland.

## 2. THE ASSEMBLY PLANNING PROCESS IN A MACHINE INDUSTRY ENTERPRISE – A CASE STUDY

### 2.1. The Characteristics of Enterprise Subject to Our Research

We present the potential of applying a spreadsheet for the needs of planning assembly processes on the example on a machine industry enterprise that is one of the leaders in innovative technologies in tobacco industry. The business activities of the enterprise include, in particular:

- **Manufacturing filter-forming and gluing machines.** The company offers complete production lines for etery type of filters. These include manufacturing, weathering, buffering, selection and composing multi-segmented filters.

- **Manufacturing tobacco reclaiming machines.** To avoid losses of raw material the company developed machines to reclaim tobacco from cigarettes, cigars, cigarillos, and other special purpose tobacco products.
- **Logistic systems.** The company has significant experience in developing logistics systems, such as bulk belt conveyors, systems for loading and unloading, and storage systems. It developed a proprietary product transport method adhering to the FIFO principle.

Fig. 1 presents selected machines manufactured in the company subject to our analysis 1.

**Fig. 1. Selected machines manufactured as part of activities of the analyzed enterprise**

The aforelisted, three main business activities of the enterprises, reflect the three departments of the company. Each of these has different operating characteristics, due to different type of machines manufactured. The article concentrates on the logistics systems department. In this department the assembly of machines, from the delivery of parts to the plant, to the packaging of the ready machine, takes 1.5 months to 3 months.

## 2.2. Characteristics of the assembly planning process

Figure 2 presents the diagram of the entire assembly planning process of the enterprise. This diagram presents the machine assembly stages in MS Excel files, and ERP type systems, and also reporting tools, including Sharepoint. The most elaborated files are further described herein, and presented in tables. These include files, such as:

- forecast,
- master plan,
- machine plan,
- production base,
- reports.

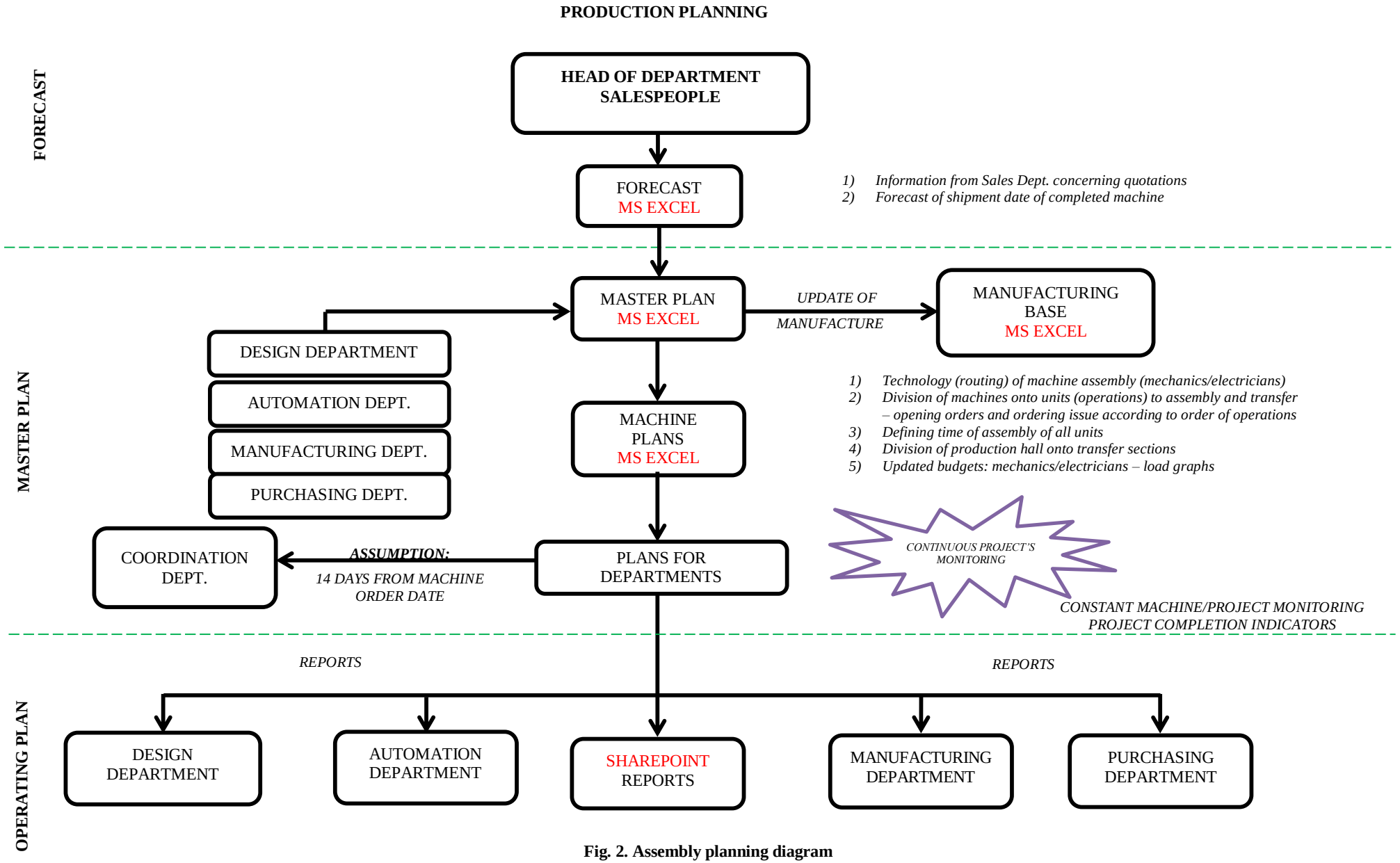


**Fig. 2. Assembly planning diagram**

The first stage of assembly planning process is the elaboration of sales forecast (table 1). The forecast is the basis for the head of the department, who receives information from sales department about orders or forecasts – quotes, which are 80-90% certain.

**Tab. 1. Forecast**

| Customer Name | Final Destination | Project Manager | New issue (1) | Machine Type | Latest issue of specification | Shipment Date | Order status |
|---|---|---|---|---|---|---|---|
| Customer A | Romania | Adam Bernat | 1 | Mach.11 | 03_2017-01-20 | 27.03.2021 | Ordered |
| Customer B | Russia | Michał Nowak | 0 | Mach.10 | 03_2016-08-30 | 27.03.2021 | Ordered |
| Customer B | Russia | Michał Nowak | 0 | Mach. 10 | 03_2016-08-30 | 27.03.2021 | Ordered |
| Customer B | Italy | Karol Kowal | 0 | Mach. 11 | 01_2016-12-02 | 03.04.2021 | Ordered |
| Customer B | Italy | Marcin Celak | 0 | Mach. 11 | 01_2020-12-09 | 05.05.2021 | Ordered |
| Customer B | Italy | Jan Drodek | 0 | Mach. 11 | 01_2020-10-10 | 26.05.2021 | Ordered |
| Customer B | Italy | Marcin Celak | 0 | Mach. 10 | 01_2020-12-09 | 26.05.2021 | Ordered |
| Customer B | Italy | Marcin Celak | 0 | Mach. 10 | 01_2020-12-09 | 26.05.2021 | Ordered |
| Customer C | Russia | Michał Nowak | 0 | Mach. 11 | 01_2021-01-18 | 01.06.2021 | Ordered |
| Customer C | Russia | Jan Drodek | 0 | Mach. 12 | - | 30.06.2021 | Not ordered |
| Customer D | Sweden | Adam Bernat | 1 | Mach. 12 | 03_2021-01-23 | 30.06.2021 | Ordered |
| Customer D | Sweden | Adam Bernat | 1 | Mach. 12 | 03_2021-01-23 | 30.06.2021 | Ordered |
| Customer D | Russia | Michał Nowak | 0 | Mach. 11 | 00_2021-01-17 | 26.07.2021 | Ordered |
| Customer A | Russia | Jan Drodek | 0 | Mach. 11 | - | 30.07.2021 | Not ordered |
| Customer A | Russia | Jan Drodek | 0 | Mach. 11 | - | 31.07.2021 | Not ordered |

The forecasts are elaborated on the basis of potential customer orders. The specifics of the production does not allow for planning based on historical data. The plants are based mainly on quotations and the knowledge of board and management. The forecast is the basis for elaboration of the master plan (table 2), which includes a 12-month machine manufacturing information. This plan is elaborated mainly on the basis of analysis of manufacturing capacities, and the capacity of Purchasing Department. The analyzed master plan is forwarded to heads of the following departments: Design, Automation, Manufacturing, Purchasing to prepare them for the tasks and to give them opportunity to include their corrections concerning the timeline for the tasks. The master plan includes the dates of shipment of machines to the customer and the dates of end of machine assembly.

**Tab. 2. Master plan**

| Customer | Country | Budget | Machine type | Change (1) | Specification rev. | Shipment | Status | End of manufacturing | Design | Automation | Manufactuirng | Purchasing |
|---|---|---|---|---|---|---|---|---|---|---|---|---|
| | | hours | | 0 / 1 | | | | | | | | |
| Customer A | Romania | 300 | Machine 11 | 1 | 03_2017-01-20 | 27.03.2021 | Ordered | 27.03.2021 | | | | |
| Customer B | Russia | 300 | Machine 10 | 1 | 03_2016-08-30 | 27.03.2021 | Ordered | 27.03.2021 | | | | |
| Customer B | Russia | 300 | Machine 10 | 1 | 03_2016-08-30 | 27.03.2021 | Ordered | 27.03.2021 | | | | |
| Customer B | Italy | 200 | Machine 11 | 1 | 01_2016-12-02 | 03.04.2021 | Ordered | 03.04.2021 | | | | |
| Customer B | Italy | 130 | Machine 11 | 1 | 01_2020-12-09 | 05.05.2021 | Ordered | 05.05.2021 | | | | |
| Customer B | Italy | 170 | Machine 11 | 1 | 01_2020-10-10 | 26.05.2021 | Ordered | 12.05.2021 | | | | |
| Customer B | Italy | 130 | Machine 11 | 1 | 01_2020-12-09 | 26.05.2021 | Ordered | 12.05.2021 | | | | |
| Customer B | Italy | 80 | Machine 11 | 0 | 01_2020-12-09 | 26.05.2021 | Ordered | 26.05.2021 | | | | |
| Customer C | Russia | 200 | Machine 12 | 0 | 01_2021-01-18 | 01.06.2021 | Ordered | 01.06.2021 | | | | |
| Customer C | Russia | 130 | Machine 12 | 0 | 01_2021-01-18 | 30.06.2021 | Ordered | 30.06.2021 | | | | |
| Customer D | Sweden | 170 | Machine 10 | 0 | 03_2021-01-23 | 30.06.2021 | Ordered | 23.06.2021 | | | | |
| Customer D | Sweden | 200 | Machine 10 | 0 | 03_2021-01-23 | 30.06.2021 | Ordered | 23.06.2021 | | | | |

The master plan of the department enables the collection, in a single location, of reliable planning information. This plan is made in an MS Excel file that can be accessed and edited simultaneously by all involved departments of the enterprise. This allows for greater elasticity and better practicality of data, without the need to wait for other departments to complete it. The data filing method was defined mainly for the purpose of specifying deadlines for each of the respective departments. Below is a schedule for data filling by all the departments and information what data will be taken into account when elaborating reports. What is of extreme importance for a new file that will be worked on by different departments is to prepare detailed file maintenance instructions (table 3):

**Tab. 3. File filling instructions**

| |
|---|
| Schedule for data filing:<br>**1)** Heads of Mechanical and Electrical Design – till 3PM on Tuesday.<br>**2)** Head of production preparation department – till 3PM on Wednesday.<br>**3)** Head of purchasing department – till 3PM on Thursday.<br>**4)** Head of automation department – confirm machine start till 2PM on Friday.<br>**5)** File supervisor – generate reports for the next week, publish the new, updated file till 10AM on Monday. |
| **PLEASE NOTE**<br>At 2PM on Fride the file editing by the department will be locked to general reports and update it. |
| Each newly introduced change will be highlighted in yellow |
| NOTES FOR SHAREPOINT REPORTS:<br>*DESIGN DEPARTMENT:*<br>**1)** Column: **Planned sending the material list**: the entered data cannot be changed<br>*ELECTRICAL DEPARTMENT:*<br>**1)** Column: **Planned sending the material list**: the entered data cannot be changed<br>*MANUFACTURING DEPARTHEMTN :*<br>**1)** Column: **Start of assembly:** the planned start assembly when all parts are available<br>**2)** Column: **End of assembly:** real date of machine's shipment date |
| **ATTENTION:**<br>Column: **Machine's shipment date** means the expected date of shipment to the customer<br>Column: **End of assembly** means the real date of shipment realized by production department |

Writing a detailed instruction is required, as the file is password-protected and connected with other file tabs, and certain file functions are automatically performed, which greatly simplifies and shortens the time of its completion, thus making it more readable for other users. Figure 3 presents a method for automatic updating and sharing a file.

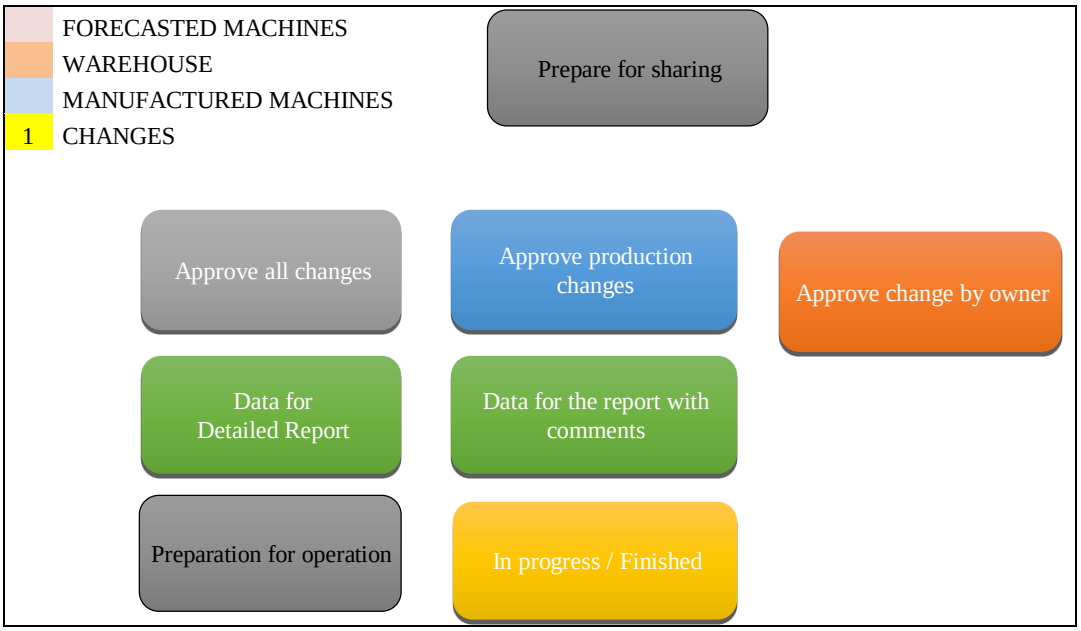


**Fig. 3. Automation of master plan file**

The master plan includes all departments that are involved and are involved in the implementation of the machine from the design phase to the shipment of the finished machine. When creating the master plan for the entire department, the data required for production planning at the tactical stage is analyzed first. The departments that significantly affect the assembly of the machine are identified and the data that will be required to create the main production planning file analyzed.

The data required for proper production planning in the Design Department (table 4) is:

- planned date for sending the mechanical Bill of Materials,
- date of sending the bill of materials (warehouse),
- date of sending the completed bill of materials.

**Tab. 4. Work schedule - Design department**

| DESIGN DEPARTMENT | | | |
|---|---|---|---|
| Planned delivery of the bill of materials (END) | Sending the bill of materials (BACKUP) | Actual Bill of Materials Sent (END) | Notes |
| (YYYY-MM-DD) | (YYYY-MM-DD) | (YYYY-MM-DD) | |
| 2019-03-31 | 2019-02-10 | 2019-05-31 | |
| 2019-03-31 | 2019-02-10 | 2019-05-31 | |
| 2019-03-31 | 2019-02-10 | 2019-05-31 | |

The data necessary for proper production planning in the Electrical Design and Automation Department (table 5) is:

- planned date for sending the electrical Bill of Materials,
- date of sending the bill of materials (warehouse),
- date of sending the completed bill of materials,
- the actual date of starting the commissioning of the machine by Automation specialists.

**Tab. 5. Work schedule – Automation Department (own elaboration)**

| AUTOMATION DEPARTMENT | | | | |
|---|---|---|---|---|
| Planned delivery of the bill of materials (END) | Sending the bill of materials (BACKUP) | Actual Bill of Materials Sent (END) | Starting the machine (START) | Notes |
| (YYYY-MM-DD) | (YYYY-MM-DD) | (YYYY-MM-DD) | (YYYY-MM-DD) | |
| 2019-04-03 | 2019-02-11 | 2019-04-17 | 2019-10-26 | |
| 2019-04-03 | 2019-02-11 | 2019-04-17 | 2019-10-13 | |
| 2019-04-03 | 2019-02-11 | 2019-04-28 | 2019-11-03 | |

The data required for proper production planning in the Production Preparation Department (table 6) is:

- the date of commencement of mechanical assembly and thus the date on which the materials are to be delivered to the production hall – the date for Supply,
- readiness of the machine to run – information for Automation Engineers,
- date of completion of production to the state of packaged machine – readiness for shipment of the machine.

**Tab. 6. Work schedule – Production Preparation Department**

| PRODUCTION PREPARATION DEPARTMENT | | | |
|---|---|---|---|
| Start of assembly | Ready to start the machine | Completion of assembly | Notes |
| (YYYY-MM-DD) | (YYYY-MM-DD) | (YYYY-MM-DD) | |
| 2019-03-03 | 2019-10-26 | 2020-01-10 | CLOSED |
| 2019-03-02 | 2019-10-13 | 2020-01-10 | CLOSED |
| 2019-03-02 | 2019-11-03 | 2020-01-10 | CLOSED |

The data required for proper production planning in the Purchasing Department (table 7) is:

- planned date of delivery of materials, parts for assembly determined by the Production Preparation Department as the date of assembly commencement,
- Actual delivery date for all parts required for assembly.

**Tab. 7. Work schedule – Purchasing Department**

| PURCHASING DEPARTMENT | | |
|---|---|---|
| Date the part was delivered (PLANNED) | Date the part was delivered (END) | Notes |
| (YYYY-MM-DD) | (YYYY-MM-DD) | |
| 2019-07-14 | 2019-07-22 | |
| 2020-01-15 | 2020-01-26 | |
| 2019-07-14 | 2019-07-14 | |

Reports created from the master plan:

1. Report for the machine/project (table 8) including stages, e.g. preparation of documentation, planned start/end of production, date of shipment of the machine confirmed to the customer, including the key (table 9).

**Tab. 9. Report key**

| KEY: | |
|---|---|
| S | SHIPPING TO CUSTOMER |
| *DESIGN DEPARTMENT* | |
| DEP | START DESIGNING |
| DEF | FINISHING THE DESIGN |
| *AUTOMATION DEPARTMENT* | |
| ATP | START DESIGNING |
| ATF | FINISHING THE DESIGN |
| ATR | STARTING |
| *PRODUCTION DEPARTMENT* | |
| PPP | PLANNED START OF ASSEMBLY |
| PPA | ACTUAL START OF ASSEMBLY |
| PPR | READY TO START |
| PPF | COMPLETION OF ASSEMBLY |
| *PURCHASING DEPARTMENT* | |
| PUR | DATE OF DELIVERY OF PARTS |

**Tab. 8. Report from the master plan of the machine/project (own elaboration)**

| | | | | 2019 | 2020 | | | | | | | | | | | | | | | | | | | | | | | |
|---|---|---|---|---|---|---|---|---|---|---|---|---|---|---|---|---|---|---|---|---|---|---|---|---|---|---|---|---|
| Machine number: 19134 | | | Month: | October | February | | March | | April | | May | | June | | August | | | September | | October | | | | | | | | |
| Project number | Project statatus | Machine type | Production stages: | 31 | 6 | 28 | 6 | 11 | 3 | 19 | 1 | 31 | 5 | 13 | 7 | 16 | 18 | 4 | 5 | 2 | 6 | 18 | 25 | | | | | |
| 19134 | CLOSED | Machine 16 | MECHANICAL LIST | DEP | | | | | | | | | | | | | | | | | | | | | | | | |
| | | | ELECTRICAL LIST | | | | | | | | | ATF | | | | | | | | | | | | | | | | |
| | | | PRODUCTION – ASSEMBLY | | | PPP | | | | PPA | | | | | | | | | | | | PPR | PPF | | | | | |
| | | | STARTING | | | | | PUR | | | | | | | | | | | | | | | | | | | | |
| | | | SHIPPING TO CUSTOMER | | | | | | | | | | | | | | | | | | | ATR | | | | | | |
| | | | MECHANICAL LIST | | | | | | | | | | | | | | | | | | S | | | | | | | |
| 005539 | CLOSED | Exit link | MECHANICAL LIST | | | | | | | | | | | | | | DEF | | | | | | | | | | | |
| | | | ELECTRICAL LIST | | | | | | | | | | | ATF | | | | | | | | | | | | | | |
| | | | PRODUCTION – ASSEMBLY | | | | | | | | | | | | | PPP | | | PPA | | | PPR | PPF | | | | | |
| | | | STARTING | | | | | | | | | | | | | | | | | | | ATR | | | | | | |
| | | | SHIPPING TO CUSTOMER | | | | | | | | | | | | | | | | | | S | | | | | | | |

2. The number of hours registered on the project, broken down by company employees and employees of external companies in relation to the allocated hourly budget (Fig. 4).

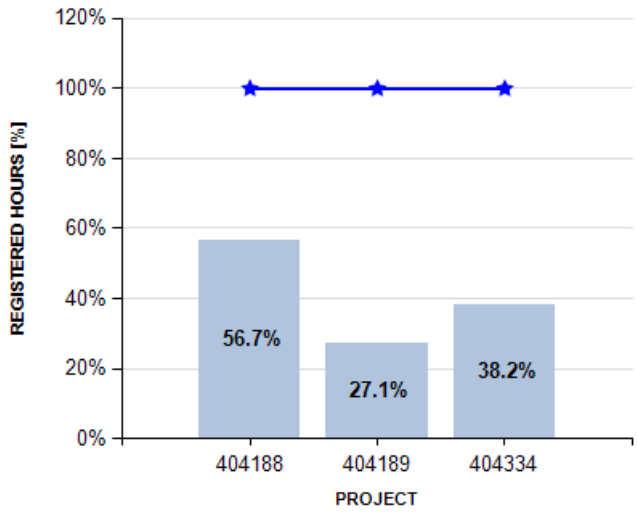


**Fig. 4. Reporting project hours**

3. The deadline for dispatch of machines by customer/coordinator shows the machines for the selected project coordinator (table 10).

**Tab. 10. Timely shipment of machines by the customer/coordinator**

| TYPE OF MACHINE | No. OF MACHINES | MACHINES ON TIME | MACHINES DELAYED |
|---|---|---|---|
| Machine 10 | 2 | 2 | 0 |

| Machine No. | Project number | Project status | Customer | Place of dispatch | Project Coordinator | Send date | Completion of assembly | DISPATCH DATE |
|---|---|---|---|---|---|---|---|---|
| 19124 | 005534 | OPEN | Customer A | USA | Jan Kowalski | 31-05-2019 | 28-05-2019 | √ |
| 19125 | 005533 | OPEN | Customer A | USA | Jan Kowalski | 31-05-2019 | 31-05-2019 | √ |

4. Machine shipment date in detail for a specific month or globally for a year – shows all machines monthly (table 11).

**Tab. 11. Timely shipment of machines in detail**

| TYPE OF MACHINE | No. OF MACHINES | MACHINES ON TIME | MACHINES DELAYED |
|---|---|---|---|
| Machine 1 | 1 | 0 | 1 |
| Machine 2 | 12 | 12 | 0 |
| Machine 4 | 13 | 13 | 0 |
| Machine 5 | 1 | 1 | 0 |
| Machine 6 | 1 | 0 | 1 |

| Machine No. | Project number | Project status | Customer | Place of dispatch | Project Coordinator | Send date | Completion of assembly | DISPATCH DATE |
|---|---|---|---|---|---|---|---|---|
| 10026 | 005569 | CLOSED | Customer B | China | Marek Nowak | 15-01-2019 | 21-11-2018 | ✓ |
| 10027 | 005548 | CLOSED | Customer B | China | Marek Nowak | 15-01-2019 | 23-11-2018 | ✓ |
| 10029 | 005650 | CLOSED | Customer B | China | Marek Nowak | 15-01-2019 | 27-11-2018 | ✓ |
| 10030 | 005751 | CLOSED | Customer B | China | Jan Kowalski | 15-01-2019 | 29-11-2018 | ✓ |
| 10038 | 005849 | CLOSED | Customer B | China | Jan Kowalski | 15-01-2019 | 03-12-2018 | ✓ |

5. Timely shipment of machines (Fig. 5).

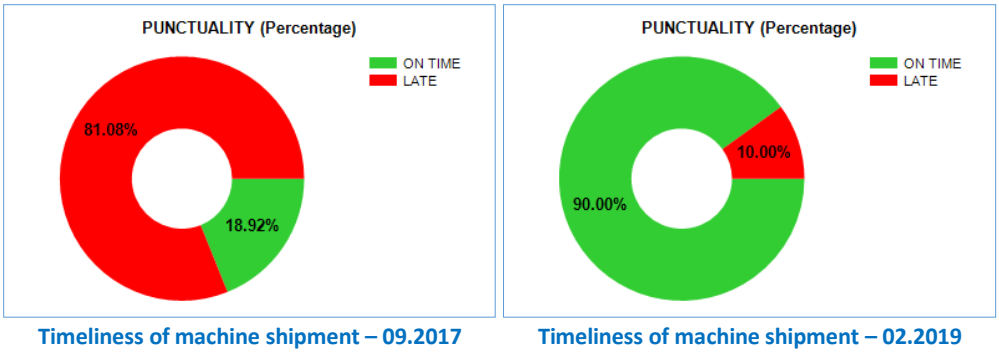


**Fig. 5. Timeliness of machines – progress**

The master production plan is broken down into operational plans – schedules (Table 12) elaborated in detail for the executive departments of the entire department.

**Tab. 12. Schedule for the machine # 1**

| 2019-01-14 | | | | | | | Foreman | Marek Nowak |
|---|---|---|---|---|---|---|---|---|
| Customer | Coordinator | Machine | Production start | Starting the machine | End of production | *Dispatch date* | Production progress | Status |
| | | | (YYYY-MM-DD) | (YYYY-MM-DD) | (YYYY-MM-DD) | (YYYY-MM-DD) | % | ORDERED/ NOT ORDERED |
| February 2019 | | | | | | | | |
| Customer A | Jan Kowalski | MACHINE 1 | 2018-12-10 | 2019-01-16 | 2019-02-08 | 2019-02-15 | 125.40% | ORDERED |
| Customer A | Jan Kowalski | MACHINE 1 | 2018-12-10 | 2019-01-25 | 2019-02-08 | 2019-02-15 | 74.90% | ORDERED |
| Customer A | Jan Kowalski | MACHINE 1 | 2018-12-17 | 2019-01-11 | 2019-02-15 | 2019-02-15 | 190.40% | ORDERED |
| Customer A | Jan Kowalski | MACHINE 1 | 2018-12-17 | 2019-02-01 | 2019-02-15 | 2019-02-15 | 75.70% | ORDERED |
| MARCH 2019 | | | | | | | | |
| CUSTOMER B | Adam Nowak | MACHINE 1 | 2018-09-20 | 2019-02-27 | 2019-03-07 | 2019-12-19 | 69.00% | ORDERED |
| CUSTOMER B | Adam Nowak | MACHINE 1 | 2019-01-16 | 2019-03-06 | 2019-03-14 | 2019-12-19 | 73.20% | ORDERED |
| CUSTOMER B | Adam Nowak | MACHINE 1 | 2019-01-23 | 2019-03-13 | 2019-03-21 | 2019-12-19 | 75.20% | ORDERED |
| APRIL 2019 | | | | | | | | |
| CUSTOMER C | Karol Boban | MACHINE 1 | 2019-01-21 | 2019-03-27 | 2019-04-04 | 2019-04-15 | 0.00% | ORDERED |
| CUSTOMER C | Karol Boban | MACHINE 1 | 2019-01-22 | 2019-03-31 | 2019-04-08 | 2019-04-15 | 0.00% | ORDERED |
| CUSTOMER C | Karol Boban | MACHINE 1 | 2019-01-23 | 2019-04-03 | 2019-04-11 | 2019-04-15 | 0.00% | ORDERED |
| CUSTOMER C | Karol Boban | MACHINE 1 | 2019-01-24 | 2019-04-07 | 2019-04-15 | 2019-04-15 | 0.00% | ORDERED |
| CUSTOMER B | Adam Nowak | MACHINE 1 | 2019-02-11 | 2019-04-08 | 2019-04-16 | 2019-04-30 | 0.00% | ORDERED |

These schedules include sub-activities performed as part of the machine assembly process, such as parts delivery date, machine commissioning, quality control, testing and packaging. These schedules are updated at least once a week. The order card usually includes a dozen or so products and each product has a separate production schedule that takes the production capacity into account. Most often, production capacity is assigned to the appropriate type of product – of course, it will vary, according to the needs. The respective stages in the entire machine assembly process are defined, i.e. start of production, and thus delivery of the material to the production hall, start-up of the machine, machine tests, quality control and packaging. At this stage, many different tools are applied for production planning, such as: ERP class system (Manufacturing module), MS Office suite (Excel, Word), data reporting program and other internal systems of the company. All these tools allow for elaboration of detailed schedules.

Schedules are frequently updated and changed due to the specifics of the company. Planning according to *Make-To-Order* and *Make-To-Stock* methods are intertwined. The *pull* system for production is often applied – "bottom-up" planning, ie. replenishment of production capacity with orders that are planned for the future to ensure continuity of production.

Machines always consist of additional input and/or output links. The technology described in this way is used to set the date of commencement of machine assembly and thus define the demand for materials. The technology is also used to create and check the load on the production hall. The technology described in this way, together with the loads, allows (already at the stage of offering the machine to the customer), determining the possible earliest date of machine manufacturing, checking the current loads of the team. An exemplary plan of one of the machines with technology is presented in table 14.

Such a description of technology allows (starting from the end date) to determine the date of commencement of the assembly of the machine and the date of the machine's readiness for start-up and testing.

The report (Figure 6) created on the basis of these files, is elaborated for the purposes of automation and quality control. It contains the list of all machines that will be assembled first. The report is prepared for approximately two months, with the subsequent two weeks planned in greater detail.

Another important stage of production planning is also the creation of the production base (Table 15). The production base was created for the needs of the production manager and foremen. This database contains detailed production orders for each machine and links, loads with division into mechanics (Table 16, Fig. 7) and electricians. The production base has tabs with loads separately for mechanics and electricians along with a diagram, making it easier to check the loads of the entire department on an ongoing basis.

Table 14. Machine 1 schedule, including technology

2019-01-14

MACHINE 1

| | Customer | Coordinator | Machine No. | 2019 | | | | | | | | | | | | |
|---|---|---|---|---|---|---|---|---|---|---|---|---|---|---|---|---|
| | | | | January | | | | | February | | | | March | | | |
| | | | | Week 1 January 2019 | Week 2 January 2019 | Week 3 January 2019 | Week 4 January 2019 | Week 5 January 2019 | Week 6 February 2019 | Week 7 February 2019 | Week 8 February 2019 | Week 9 February 2019 | Week 10 March 2019 | Week 11 March 2019 | Week 12 March 2019 | Week 13 March 2019 |
| | February 2019 | | | | | | | | | | | | | | | |
| | Customer A | Jan Kowalski | 90001 | 1M | 1M | 1M | 1M | U+Q | P | | | | | | | |
| | | | | 1L | 1L | 1L | 1L | U+Q | P | | | | | | | |
| | Customer A | Jan Kowalski | 90002 | 1M | 1M | 1M | 1M | U+Q | P | | | | | | | |
| | | | | 1L | 1L | 1L | 1L | U+Q | P | | | | | | | |
| | Customer A | Jan Kowalski | 90003 | 1M | 1M | 1M | 1M | 1M | U+Q | P | | | | | | |
| | | | | | 1L | 1L | 1L | 1L | U+Q | P | | | | | | |
| | Customer A | Jan Kowalski | 90004 | 1M | 1M | 1M | 1M | 1M | U+Q | P | | | | | | |
| | | | | | 1L | 1L | 1L | 1L | U+Q | P | | | | | | |
| | MARCH 2019 | | | | | | | | | | | | | | | |
| | CUSTOMER B | Adam Nowak | 37405 | 1M | 1M | 1M | 1M | 1M | 1M | 1M | 1M | U+Q | P | | | |
| | | | | | | | | 1L | 1L | 1L | 1L | U+Q | P | | | |
| | CUSTOMER B | Adam Nowak | 37401 | | 1M | 1M | 1M | 1M | 1M | 1M | 1M | 1M | U+Q | P | | |
| | | | | | | | | | 1L | 1L | 1L | 1L | U+Q | P | | |
| | CUSTOMER B | Adam Nowak | 37402 | | | 1M | 1M | 1M | 1M | 1M | 1M | 1M | 1M | U+Q | P | |
| | | | | | - | | | | | 1L | 1L | 1L | 1L | U+Q | P | |
| | APRIL 2019 | | | | | | | | | | | | | | | |
| | CUSTOMER C | Kamil Cebula | 37403 | | | - | | 1M | 1M | 1M | 1M | 1M | 1M | 1M | 1M | U+Q |
| | | | | | - | | | | | | | 1L | 1L | 1L | 1L | U+Q |
| | CUSTOMER C | Kamil Cebula | 37404 | | | - | | | 1M | 1M | 1M | 1M | 1M | 1M | 1M | 1M |
| | | | | | - | | | | | | | | 1L | 1L | 1L | 1L |
| | CUSTOMER C | Kamil Cebula | 37405 | | | - | | | 1M | 1M | 1M | 1M | 1M | 1M | 1M | 1M |
| | | | | | - | | | | | | | | 1L | 1L | 1L | 1L |
| | CUSTOMER C | Kamil Cebula | 37406 | | | - | | | | 1M | 1M | 1M | 1M | 1M | 1M | 1M |
| | | | | | - | | | | | | | | | 1L | 1L | 1L |
| | CUSTOMER B | Adam Nowak | 37407 | | | | | | | 1M | 1M | 1M | 1M | 1M | 1M | 1M |
| | | | | | - | | | | | | | | | 1L | 1L | 1L |

**AUTOMATION DEPARTMENT READINESS FOR START-UP**

**DECEMBER 2020**

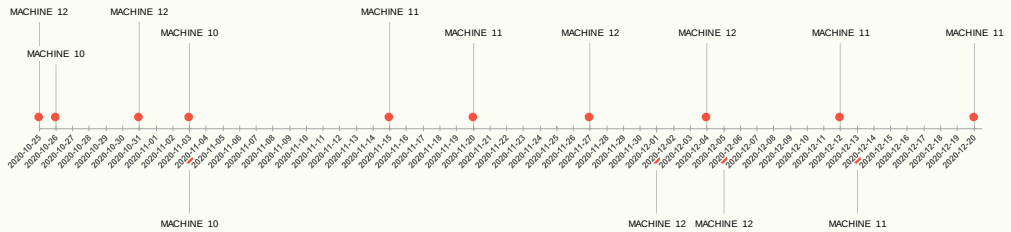


**DETAILS**

| WEEK | START UP | MACHINE TYPE | CUSTOMER | PROD. FINAL | SHIPMENT DATE | FOREMAN |
|---|---|---|---|---|---|---|
| 43 | 2020-10-25 | MACHINE 12 | China | 2020-12-13 | 2021-01-05 | Adam Nowak |
| | 2020-10-26 | MACHINE 10 | Russia | 2020-12-15 | 2021-04-14 | Jan Kowalski |
| 44 | 2020-10-31 | MACHINE 12 | China | 2020-11-29 | 2021-01-05 | Karol Boban |
| | 2020-11-03 | MACHINE 10 | Russia | 2020-12-15 | 2021-04-14 | Karol Boban |
| | 2020-11-03 | MACHINE 10 | China | 2020-11-29 | 2021-01-05 | Karol Boban |
| 46 | 2020-11-15 | MACHINE 11 | China | 2020-12-06 | 2021-01-05 | Jan Kowalski |
| 47 | 2020-11-20 | MACHINE 11 | China | 2020-12-06 | 2021-01-05 | Karol Boban |
| 48 | 2020-11-27 | MACHINE 12 | Russia | 2020-12-06 | 2021-01-10 | Adam Nowak |
| | 2020-12-01 | MACHINE 12 | China | 2020-12-13 | 2021-01-05 | Jan Kowalski |
| 49 | 2020-12-04 | MACHINE 12 | Russia | 2020-12-13 | 2020-12-13 | Adam Nowak |
| | 2020-12-05 | MACHINE 12 | USA | 2020-12-14 | 2020-12-28 | Jan Kowalski |
| 50 | 2020-12-12 | MACHINE 11 | China | 2020-12-20 | 2021-01-12 | Karol Boban |
| | 2020-12-13 | MACHINE 11 | Russia | 2020-12-22 | 2020-12-22 | Adam Nowak |
| 51 | 2020-12-20 | MACHINE 11 | China | 2021-01-10 | 2021-01-10 | Adam Nowak |

**Fig. 6. Machine commissioning report**

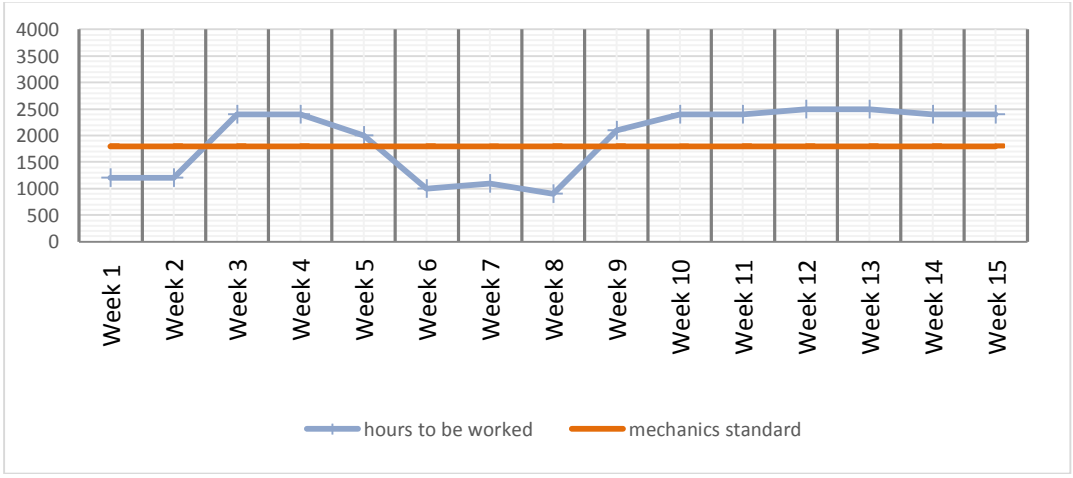


**Fig. 7. Load diagram for the mechanical department (example)**

**Tab. 15. Production base**

| Project | Order | Machine | Customer | Mach. no. | Hours limit | Total hours | % | End | Team | Status | NOTES |
|---|---|---|---|---|---|---|---|---|---|---|---|
| 4126 | 226287 | Machine 1 | Customer A | 79075 | 200 | 100.08 | 50.1% | 2021-06-30 | Kowalski | Implemented | |
| 4126 | 226288 | Packaging | Customer A | 79075 | 100 | 20.00 | 20.0% | 2021-06-30 | Nowak | Implemented | |
| 4127 | 226837 | Input link | Customer B | 79075 | 170 | 3.00 | 1.0% | 2021-06-30 | Kowalski | Implemented | |
| 4128 | 226915 | Exit link | Customer B | 79075 | 100 | 38.99 | 36.9% | 2021-06-30 | Kowalski | Implemented | |
| 4123 | 226382 | Machine 2 | Customer B | 79076 | 200 | 88.90 | 35.0% | 2021-08-15 | Kowal | Implemented | |
| 4123 | 226383 | Packaging | Customer B | 79076 | 100 | 120.00 | 60.0% | 2021-08-15 | Boban | Implemented | |
| 4124 | 227273 | Input link | Customer C | 79076 | 170 | 0.00 | 0.00% | 2021-08-15 | Boban | Planned | |
| 4125 | 227274 | Exit link | Customer C | 79076 | 100 | 0.00 | 0.00% | 2021-08-15 | Boban | Planned | |
| 4182 | 226384 | Machine 3 | Customer D | 79079 | 200 | 0.00 | 0.00% | 2021-08-15 | Nowak | Planned | |
| 4182 | 226385 | Packaging | Customer D | 79079 | 100 | 0.00 | 0.00% | 2021-08-15 | Nowak | Planned | |

**Tab. 16. Mechanical load**

| | Week 1 | Week 2 | Week 3 | Week 4 | Week 5 | Week 6 | Week 7 | Week 8 | Week 9 | Week 10 | Week 11 | Week 12 | Week 13 | Week 14 | Week 15 |
|---|---|---|---|---|---|---|---|---|---|---|---|---|---|---|---|
| hours to be worked | 1200 | 1200 | 2400 | 2400 | 2000 | 1000 | 1100 | 900 | 2100 | 2400 | 2400 | 2500 | 2500 | 2400 | 2400 |
| mechanics standard | 1800 | 1800 | 1800 | 1800 | 1800 | 1800 | 1800 | 1800 | 1800 | 1800 | 1800 | 1800 | 1800 | 1800 | 1800 |
| absent | 0 | 0 | 0 | 0 | 0 | 0 | 0 | 0 | 0 | 0 | 0 | 0 | 0 | 0 | 0 |
| | January 2021 | January 2021 | January 2021 | January 2021 | January 2021 | February 2021 | February 2021 | February 2021 | February 2021 | March 2021 | March 2021 | March 2021 | March 2021 | April 2021 | April 2021 |

The final stage of the production planning process is data analysis after the machine assembly is completed. The most important objective here, and at the same time a challenge for the company, is the timely shipment of machines to the customer. Achieving this objective largely depends on correct production planning. Therefore, on the basis of the available data, this parameter is subject to evaluation and detailed analysis.

At this stage of creating planning and production schedules, the stage of machine assembly and information flow between departments was significantly improved. We were able to respond to changes much faster and they had a smaller impact on the change of the date of shipment of the machine to the customer. Work organization in the company and employees' knowledge of production plans both improved significantly.

## 3. SUMMARY AND CONCLUSIONS

The issue of planning individual stages of the production process is one of the crucial elements in every manufacturing company – its correctness determines the possibility of timely execution of orders, as well as the optimal use of production capacity. In the case of a high degree of individualization and high variability of orders as well as high complexity of manufactured products, correct planning of assembly processes becomes a challenge – it affects both the costs of the production process and the possibility of meeting the assumed order completion date. Unfortunately, despite the numerous available methods and IT tools dedicated to the needs of production planning and management, the process of planning assembly operations poses a significant practical problem – especially for enterprises from the SME sector, for which the purchase of this type of software is associated with excessive financial expenses. Moreover, it is also problematic since there is no production planning software that does not require an individual (and often costly) configuration tailored to the specifics of a given enterprise and its production. ERP-class programs – although extremely helpful, are not adapted to every type of enterprise and require a lot of commitment on the part of the employees who operate this system.

In order to overcome these problems (as presented in this article), it is possible to use generally available IT tools (e.g. in the form of spreadsheets), the use of which provides significant support – leading to a reduction in time losses and an increase in the efficiency of the planning process. The presented case confirms that this solution is very beneficial and, despite certain limitations, allows to achieve the assumed effect. The only condition in this respect is the necessity to use network solutions – enabling simultaneous work of representatives of various departments of the enterprise.

### REFERENCES


Benjaafar, S., & El Hafsi, M. (2006). Production and inventory control of a single product assemble-to-order system with multiple customer classes. *Management Science, 52*(12), 1896–1912. https://doi.org/10.1287/mnsc.1060.0588

Ciesla, B., & Mleczko, J. (2021). Practical application of fuzzy logic in production control systems of engineer to order SMEs. *Applied Computer Science, 17*(1), 17-25. https://doi.org/10.23743/acs-2021-02

Danilczuk, W., & Gola, A. (2020). Computer-Aided Material Demand Planning Using ERP Systems and Business Intelligence Technology. *Applied Computer Science, 16*(3), 42–55. https://doi.org/10.23743/acs-2020-20

ElHafsi, M. (2009). Optimal integrated production and inventory control of an assemble-to-order system with multiple non-unitary demand classes. *European Journal of Operational Research, 194*(1), 127–142. https://doi.org/10.1016/j.ejor.2007.12.007

Gola, A. (2014). Economic Aspects of Manufacturing Systems Design. *Actual Problems of Economics, 156*(6), 205–212.

Gyulai, D., & Monostori, L. (2017). Capacity management of modular assembly systems. *Journal of Manufacturing Systems, 43*(1), 88-99. https://doi.org/10.1016/j.jmsy.2017.02.008

Gyulai, D., Kadar, B., & Monostori, L. (2014). Capacity planning and resource allocation in assembly systems consisting of dedicated and Reconfigurable lines. *Procedia CIRP, 25*, 185–191. https://doi.org/10.1016/j.procir.2014.10.028

Ju, F., & Li, J. (2014). A Bernoulli model of selective assembly systems. *IFAC Proceedings Volumes, 47*(3), 1692-1697. https://doi.org/10.3182/20140824-6-ZA-1003.00525

Ju, F., Li, J., & Deng, W. (2017). Selective assembly system with unreliable Bernoulli machines and finite buffers. *IEEE Transactions on Automation Science and Engineering, 14*(1), 171–184. https://doi.org/10.1109/TASE.2016.2604371

Kamath, R., & Sarkar, E. (2020). The Engineer… No Longer a Person, but a Number of an Excel Sheet – Enterprise Resource Planning and Commoditisation of Labour. *Global Labour Journal, 11(2)*, 103–117. https://doi.org/10.15173/glj.v11i2.4101

Li, J., Blumenfeld, D.E, Huang, N., & Alden, J.M. (2009). Throughput analysis of production systems: Recent advances and future topics. *International Journal of Production Research, 47*(14), 3823–3851. https://doi.org/10.1080/00207540701829752

Manitz, M. (2008). Queueing-model based analysis of assembly lines with finite buffers and general service times. *Computers & Operations Research, 35*(8), 2520-2536. https://doi.org/10.1016/j.cor.2006.12.016

Pang, Z. (2015). Optimal control of a single-product assemble-to-order system with multiple demand classes and backordering. *IEEE Transactions on Automatic Control, 60*(2), 480–484. https://doi.org/10.1109/TAC.2014.2328451

Paprocka, I., Krenczyk, D., & Burduk, A. (2021). The Method of Production Scheduling with Uncertaintes Using the Ants Colony Optimisation. *Applied Sciences-Basel, 11*(1), 171. https://doi.org/10.3390/app11010171

Reiman, M.I., & Wang, Q. (2015). Asymptotically optimal inventory control for assemble-to-order system with identical lead times. *Operations Research, 63*(3), 489-749. https://doi.org/10.1287/opre.2015.1372

Sobaszek, Ł., Gola, A., & Kozłowski, E. (2017), Application of survival function in robust scheduling of production jobs. In *Proceedings of the 2017 Federated Conference on Computer Science and Information Systems (FEDCSIS)* (pp. 575–578). ACSIS. https://doi.org/10.15439/2017F276

Świć, A., & Gola, A. (2013). Economic Analysis of Casing Parts Production in a Flexible Manufacturing System. *Actual Problems of Economics, 141*(3), 526–533.

Tarigan, Z.J.H., Siagian, H., & Jie, F. (2021). Impact of Enhanced Enterprise Resource Planning (ERP) on Firm Performance through Green Supply Chain Management. *Sustainability, 13(8),* 4358. https://doi.org/10.3390/su13084358

Wikarek, J., Sitek, P., & Nielsen, P. (2019). Model of decision support for the configuration of manufacturing system. *IFAC PapersOnLine, 52(13),* 826–831. https://doi.org/10.1016/j.ifacol.2019.11.232

Applied Computer Science, vol. 17, no. 2, pp. 90–99
doi: 10.23743/acs-2021-15

Submitted: 2021-05-13 | Revised: 2021-06-14 | Accepted: 2021-06-20

*Deep Convolution Network, Tamil Letter,*
*Recognition System, Font Recognition, Filtering*

*Manikandan SRIDHARAN* [0000-0002-9378-518X]*
*Delphin Carolina RANI ARULANANDAM* [0000-0002-3206-1305]**
*Rajeswari K CHINNASAMY* [0000-0003-4579-3166]***
*Suma THIMMANNA* [0000-0002-1761-7889]****
*Sivabalaselvamani DHANDAPANI* [0000-0002-3373-7610]*****

# RECOGNITION OF FONT AND TAMIL LETTER IN IMAGES USING DEEP LEARNING

**Abstract**

*This paper proposes a deep learning approach to recognize Tamil Letter from images which contains text. This is recognition process, the text in the images are divided to letter or characters. Each recognized letters are sending to recognition system and filter the text using deep learning algorithms. Our proposed algorithm is used to separate letter from the text using convolution neural network approach. The filtering system is used for identifying font based on that letters are found. The Tamil letters are test data and loaded in recognition systems. The trained data are input which contains filtered letter from image. For example, Tamil letters such as are available in test dataset. The trained data are applied into deep convolution neural network process. The two dataset are created which contains test data with Tamil letter and second one for recognized input data or trained data. 15 thousands of letters are taken and 512 X 512 X 3 size deep convolution network is created with font and letters. As the result, 85% Tamil letters are recognized and 82% are tested using font. TensorFlow is used for testing the accuracy and success rate.*

* Department of Information Technology, E. G. S. Pillay Engineering College, Nagapattinam, Tamil Nadu, India, profmaninvp@gmail.com
** Department of Computer Science and Engineering, K. Ramakrishnan College of Technology, Samayapuram, Tiruchirappalli, Tamil Nadu, India, delphinjerald29@gmail.com
*** Department of Computer Science and Engineering, Sona College of Technology, Salem, Tamil Nadu, India, rajeswarikc@sonatech.ac.in
**** Sri Venkateshwara College of Engineering, Bengaluru, Karnataka, India, tsumamurthy.cs@gmail.com
***** Department of Computer Applications, Kongu Engineering College, Perundurai, Erode, Tamil Nadu, India, sivabalaselvamani@gmail.com

## 1. INTRODUCTION

Current scenario automation is mandatory for all process including online ordering, ticketing, emailing, etc,. In Digital era intelligent applications are played vital role and different applications. Creating intelligent application means machine learning and deep learning processes are more important for data processing and analytics (Sevik, Erdogmus & Yalein, 2018). Many researchers are doing research on deep learning in different application such as medical imaging, automation, banking and IoT. Deep learning is neural network approach and follow the mechanism of decision tree approach. This is hierarchical approach to simulate input data. For example, human brain input are sensed and created deep belief representation for simulation (Manikandan & Chinnadurai, 2019).

In 2005, perception approach is suggested for analyzing neural network system in digital applications. This is a recommendation system and multiple layers are created for making effective decisions (Adomavicius & Tuzhilin, 2018). Industry 4.0 standards intelligent decision making and automated modelling are important in today's IT and ITeS (Bati, 2014).

The various studies are going for deep convolution neural network model. The given or sensed images are taken for analyzing process and set of algorithms are used to make effective decisions (Jaiem, Slimane & Kherallah, 2017). The natural language processing is important for nowadays for processing different languages. So deep learning method is very useful for finding input of various natural language data through that will take effective decisions (Eltiez, 2015).The deep learning model is very useful for finding patterns, edges, decision making, data analytics and recognizing the objects, text, characters, etc, from input images (Koyun & Afsin, 2017). It is feature extraction process so the input image data are directly taken for classification and clustering operations.

This is a process to eliminate redundant data and extract needy information. This is multilayer model and each layer is considered for evaluations in two dimensional planes (Manikandan & Chinnadurai, 2020, Manikandan et al., 2020, 2021; Tajmir & Alkasab, 2018). It has three section input, hidden and output section. The input layer is recognizing layer and getting sensed input from different environments. Hidden layer is machine learning layer for converting 0 and 1 value for data processing. Output layer is decision making layer for prediction, classification or regression (Sathiyamoorthi, 2016).

The convolution neural network is a classification process which contains set of classes and perceptions. Learning system consists of supervised and unsupervised learning methods. Supervised learning system is used for knowing input and output pairs for example clustering, decision support systems (Zhou & Tuzel, 2017). Unsupervised learning is used for unknown input and output pairs such as social media data, data logs, etc. This is fully connected layer and this method is proposed for system to recognize the Tamil letters. This papers describes various sections, section 2 explain various related works, section 3 described deep convolution process, section 4 gives experimental results and section 5 explains conclusion and future process.

## 2. RELATED WORKS

In past years, deep learning is playing important role for making effective decision making capabilities. Lot of researches are going for prediction, decision making, data analytics and recommendations using deep learning (Mainkandan & Chinnadurai, 2019). Wong et al, suggested deep learning is a subset of machine learning to predict intelligent data analytics process from set of trained data. Manikandan et al, explain TensorFlow is the simulation tool for processing deep convolution operations. Deep learning is used for predicting food ordering applications, video dataset processing, educational sciences, online learning environments and image annotation applications (Yuan, Mou & Lu, 2017).

The convolution neural network is proposed for handling big data, unsolved problems, unstructured data, ambiguous dataset, No SQL dataset and decision making applications. For handling image and video processing applications means deep learning is important for classification and prediction operations suggested by Yung et al. This is successful diagnostics method for all the data analytics processing. Aylin et al, provides deep learning method is used for recognizing letters from images using font and size. Recognition is process of extracting data from digitized input contents.

Nowadays digital information are contains images and text so extracting text from images means we need effective decision making system. Previously Rugny et al, proposed optical character recognition system is used for fining text from barcode images. Currently quick response code is used for accessing web data (Shanthi & Sabeenian, 2019). But the problem each data are structured and 20X20 pixel data. Now we are using natural language input data with unstructured dataset. So we are in need of multiple convolution neural network models for predicting characters.

Some researchers are doing research on Font recognition based on identified characters and letters. For example, Arabic, Turkish, Chinese and Korean letters are identified by using Font. Based on above related studies we are taking font and character wise recognition system for recognizing Tamil letter using TensorFlow. TensorFlow is a open source simulating tool which developed by Google for processing deep learning applications. Our proposed algorithm is tested by using TensorFlow.

## 3. RECOGNITION SYSTEM

Based on different studies and literatures, the hand written letters are analyzed and recognized in different languages. Commercially many applications are used for handling hand written input data processing. Turkish letters are identified by using deep learning process from set of images. In our proposed method we would take deep learning method to recognize font and Tamil Letter in images. Our system proposes capture the image and apply deep convolution neural network to extract letters.

In this method we took recognize Tamil letters and font based recognition system. The proposed algorithm is developed for identifying Tamil Letters. First step the pre-processing of input dataset, second step convolution process is taken and third step letters to be identified.

### 3.1. Dataset and Data Pre-processing

Here we used two dataset such as trained data as input data or recognizing data, second one is test data which is consists of pre-trained data or Tamil letters data set. The test data consists of 256 Tamil Letters and 6 Tamil fonts totally 1536 letters are pre-trained and loaded into our applications. Our system has font size minimum of 7, maximum of 72 and medium of 30 points. Input data is trained data which is applied into 512 × 512 × 3 layer deep convolution neural network process. So we can process 786432 letters can be processed and compared with 1536 test dataset. The sample image dataset are shown in below.

**Fig. 1. Tamil Letters dataset**

### 3.2. Deep Belief Network

Based on input dataset, the deep belief network is created by using TensorFlow. In TensorFlow, Alexnet model is trained to classify more than 1000 of images and obtained 25 layers learning systems. The dataset can be divided into trained data and test data. 85 percentage of images are taken from trained data after applying deep learning process. Deep learning process is consisting of two phases such as supervised and unsupervised learning. In supervised learning the data is taken and applying classification and regression for eliminating redundant data. While unsupervised learning means the supervised learning resultant data is taken and applying classification for prediction.

The 256 letters of Tamil and 6 Tamil fonts are testing dataset and created 25-layer Alexnet for pre-processing. Once pre-processing done the trained dataset is applying for learning process. The learning process scheme is shown in below.

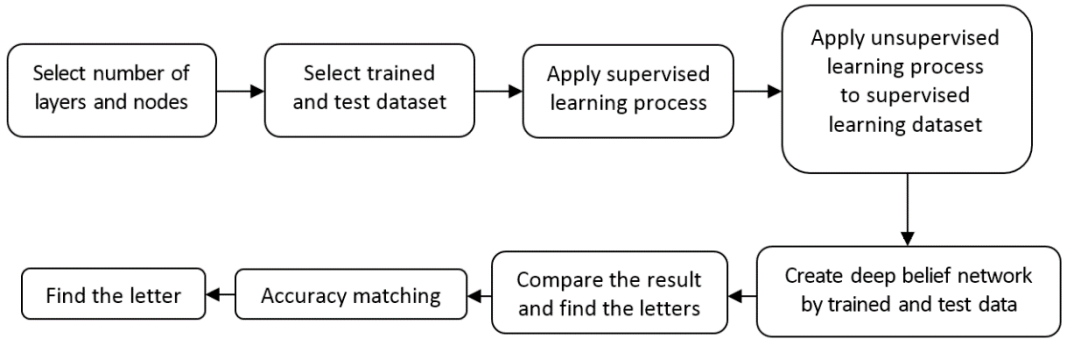


**Fig. 2. Learning Process – Deep Belief Network**

## 4. PROCESSING SYSTEM

Learning system is initiating this process, set of image(s) are taken into account and apply the following pre-processing steps

Step 1: Images are converted into grayscale format. It is called as intensity mapping to identify computer understandable or processing format

Step 2: Apply Morphological process for removing or eliminating noises, unwanted letters and characters

Step 3: Apply Matrix operation to select object location using horizontal, vertical and diagonal values

Step 4: 8 × 8 decision tree matrix is created with connected components. This stage each letter is identified and located.

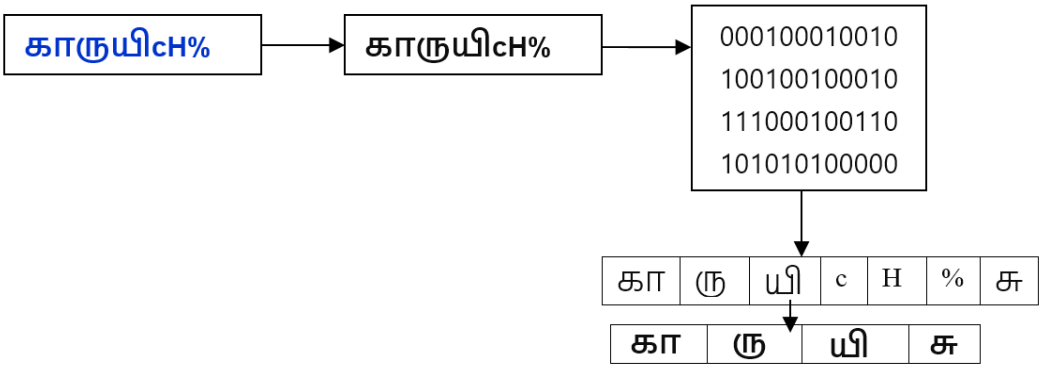


**Fig. 3. Processing and Letter Identification**

## 5. 5. DEEP LEARNING – PROCESS

After pre-processing, the letters are separated and labelling completed. The deep learning process step are:

Step 1: The label values are selected and stored in trained dataset.

Step 2: Apply proportional calculation to select labelled imaged.

Let $\{a, b\}$ set of input pair values, $N$ – Number of nodes available in matrix, $(i, j)$ – coordinate position, $l$ – labelling point, proportional point $(p)$:

$$(p) = \frac{1}{N}\sum_{i=0,j=0}^{N-1}\frac{(ai,bj)}{N} \tag{1}$$

Step 3: The letter has to be separated and labelled based on Proportional point like symbols, English and other.

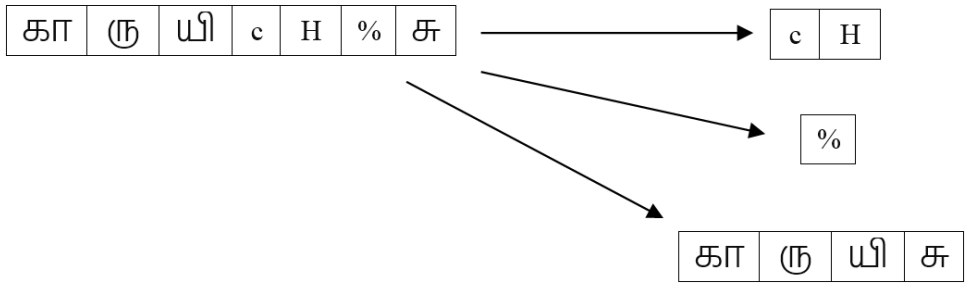


**Fig. 4. Labelling process and Elimination Selection**

Step 4: Based on this Symbol and English characters are eliminated and other dataset is stored for further process

Step 5: The stored dataset as trained dataset and created 512 × 512 × 3 size deep convolution network

Step 6: Each letter are sending to learning system and label input, output and hidden values

Step 7: The below layered process is taken for selecting each character and hidden operations – Hidden Value $(h_{(i,j)})$:

$$\left(h_{(i,j)}\right) = \begin{cases} 0, \ i = j = 0 \\ 1, \ i = j = N-1 \\ \sum_{i=0,j=0}^{N-1}\frac{(a(i),b(j)\cdot(a(j),b(i))}{N}, i = j = 1,2,\ldots,N-2 \end{cases} \tag{2}$$

Step 8: After selecting hidden values the test dataset is selected and compare the result. Each letter compared and select the Tamil letters. Same process will be continued until process will stops. The accuracy factor is obtained as accuracy rate $(A_{\%})$:

$$(A_{\%}) = \sum_{i=0,j=0}^{N-1}\frac{(a(i,j)\cdot b(i,j)}{h(i,j)^N} \tag{3}$$

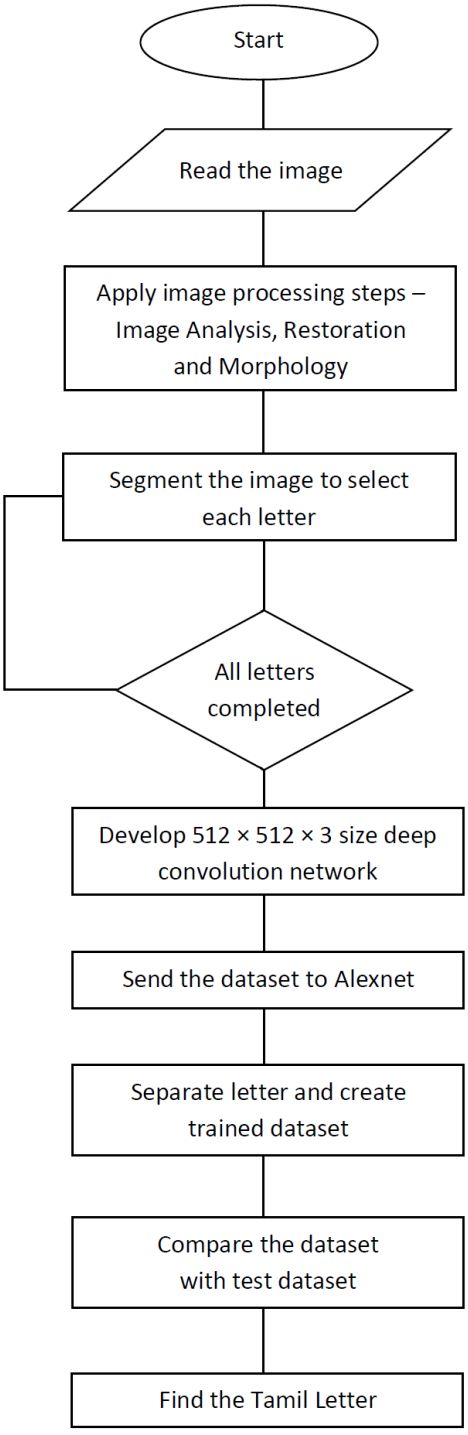


**Fig. 5. Flowchart – Deep Learning Process**

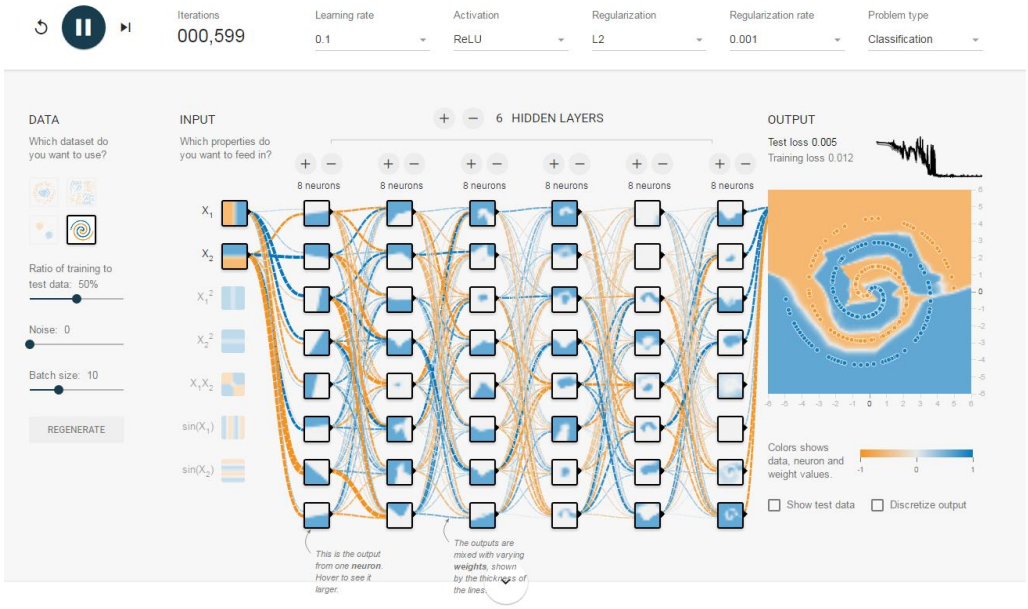


**Fig. 6. Deep Belief Network with input, output and hidden layers results from TensorFlow**

The above figure shows that generated deep belief network from TensorFlow with 512 × 512 × 3 size deep convolution network operations. Here the trained dataset are applied and compare the result with test dataset. The below table 1 shows training result and separation of letters using TensorFlow.

**Tab. 1. Learning rate result based on segmentation**

| Epoch | Iteration | Time taken (in ms) | Accuracy | Loss | Elimination factor | Proportional point (%) |
|---|---|---|---|---|---|---|
| 1 | 1 | 25 | 1.75 | 0.85 | 2.75 | 82 |
| 2 | 5 | 35 | 1.85 | 0.87 | 2.85 | 83 |
| 3 | 10 | 45 | 1.97 | 0.86 | 2.25 | 85 |
| 4 | 15 | 58 | 1.85 | 0.92 | 2.75 | 86 |
| 5 | 20 | 115 | 2.02 | 0.86 | 2.65 | 89 |
| 6 | 25 | 135 | 2.75 | 0.85 | 2.89 | 92 |
| 7 | 30 | 145 | 2.85 | 1.05 | 2.91 | 87 |
| 8 | 35 | 205 | 1.98 | 0.92 | 2.75 | 85 |
| 9 | 40 | 275 | 2.75 | 0.87 | 2.88 | 83 |
| 10 | 45 | 315 | 1.98 | 0.87 | 2.81 | 82 |

The accuracy factor is calculated based on Proportional point and learning rate.

**Tab. 2. Deep learned result – Tamil Letter Identification**

| | |
|---|---|
| **தABமி&*ழ்HJiKவாf325க்gfj919கிய() 453””ங்??/8 க76438ள்698 4^$%Q^பு&*$#*த்த*JHக(()ம்}\|??:*(ம ெ#$ன்*Uமை**)தாய்&*)சிNHGரி mnv** | தமிழ்வாக்கியங்கள்புத் தகம்மென்மைதாய்சிர ி |

**Tab. 3. Accuracy factor percentage based on learning rate and letter identification**

| Epoch | Iteration | Time taken (in ms) | Elimination factor | Proportional point (%) | Accuracy (%) |
|---|---|---|---|---|---|
| 1 | 1 | 25 | 2.75 | 82 | 87 |
| 2 | 5 | 35 | 2.85 | 83 | 88 |
| 3 | 10 | 45 | 2.25 | 85 | 85 |
| 4 | 15 | 58 | 2.75 | 86 | 84 |
| 5 | 20 | 115 | 2.65 | 89 | 86 |
| 6 | 25 | 135 | 2.89 | 92 | 87 |
| 7 | 30 | 145 | 2.91 | 87 | 92 |
| 8 | 35 | 205 | 2.75 | 85 | 88 |
| 9 | 40 | 275 | 2.88 | 83 | 91 |
| 10 | 45 | 315 | 2.81 | 82 | 87 |

**Tab. 4. Font based iteration and accuracy**

| Font Name | Iterations | Time taken (in ms) | Accuracy (%) |
|---|---|---|---|
| **Bamini** | 10 | 35 | 84 |
| | 50 | 78 | 88 |
| | 100 | 110 | 86 |
| **Kural** | 10 | 25 | 84 |
| | 50 | 65 | 92 |
| | 100 | 95 | 87 |
| **Alangaram** | 10 | 55 | 88 |
| | 50 | 92 | 84 |
| | 100 | 115 | 85 |
| **Google Tamil** | 10 | 15 | 86 |
| | 50 | 30 | 92 |
| | 100 | 50 | 91 |
| **Latha** | 10 | 65 | 87 |
| | 50 | 105 | 88 |
| | 100 | 155 | 89 |
| **Myna** | 10 | 75 | 88 |
| | 50 | 118 | 89 |
| | 100 | 185 | 92 |

## 6. CONCLUSION

In this paper, set of images are taken and apply deep learning process to found Tamil Letters and test the results using different Tamil Font also. The images are pre-trained and removed unwanted data. Creates trained and test data set. Test data consist of 256 Tamil Letters and 6 fonts. Trained data are taken from image dataset and 512 × 512 × 3 layer deep belief network is generated. We tested the result both character wise and font wise. TensorFlow tool is used for experimental setup and 85% accuracy factor is obtained to recognized Tamil letter. In future, the font based character recognition and speech input may considered for recognition.

### REFERENCES


Adomavicius, G., & Tuzhilin, A. (2018). Toward the next generation of recommender systems: a survey of the state-of-the-art and possible extensions. *IEEE Transactions on Knowledge and Data Engineering*, *17*(6), 734–749. http://dx.doi.org/10.1109/TKDE.2005.99

Bati, E. (2014). *Deep convolutional neural networks with an application towards geospatial object Recognition*. Diss. Middle East Technical University Ankara.

Elitez, E. (2015). *Handwritten digit string segmentation and recognition using deep learning*. Diss. Middle East Technical University Ankara.

Jaiem, F.K., Slimane, F., & Kherallah, M. (2017). Arabic font recognition system applied to different text entity level analysis. *2017 International Conference on Smart, Monitored and Controlled Cities (SM2C)*, 36–40. http://dx.doi.org/10.1109/SM2C.2017.8071847

Koyun, A., & Afsin, E. (2017). 2D optical character recognition based on deep learning. *Journal of Turkey Informatics Foundation of Computer Science and Engineering*, *10*(1), 11–14.

Manikandan, S., & Chinnadurai, M. (2019). Intelligent and Deep Learning Approach OT Measure E- Learning Content in Online Distance Education. *The Online Journal of Distance Education and e-Learning*, *7*(3), 199–204.

Manikandan, S., & Chinnadurai, M. (2020). Evaluation of Students' Performance in Educational Sciences and Prediction of Future Development using TensorFlow. *International Journal of Engineering Education*, *36*(6), 1783–1790.

Manikandan, S., Chinnadurai, M., Maria Manuel Vianny, D., & Sivabalaselvamani, D. (2020). Real Time Traffic Flow Prediction and Intelligent Traffic Control from Remote Location for Large-Scale Heterogeneous Networking using TensorFlow. *International Journal of Future Generation Communication and Networking*, *13*(1), 1006–1012.

Manikandan, S., Dhanalakshmi, P., Priya, S., & Mary OdilyaTeena, A. (2021). Intelligent and Deep Learning Collaborative method for E-Learning Educational Platform using TensorFlow. *Turkish Journal of Computer and Mathematics Education*, *12*(10), 2669–2676.

Sathiyamoorthi, V. (2016). A novel cache replacement policy for Web proxy caching system using Web usage mining. *International Journal of Information Technology and Web Engineering*, *11*(2), 1–13. http://dx.doi.org/10.4018/IJITWE.2016040101

Sevik, A., Erdogmus, P., & Yalein, E. (2018). Font and Turkish Letter Recognition in Images with Deep Learning. *International Congress on Big Data, Deep Learning and Fighting Cyber Terrorism* (pp. 61–64). IEEE. http://dx.doi.org/10.1109/IBIGDELFT.2018.8625333

Shanthi ,T., & Sabeenian, R.S. (2019). Modified Alexnet architecture for classification of diabetic retinopathy images. *Computers and Electrical Engineering*, *76*, 56–64. http://dx.doi.org/10.1016/j.compeleceng.2019.03.004

Tajmir, S.H., & Alkasab, T.K. (2018). Toward augmented radiologists: changes in radiology education in the era of machine learning and artificial intelligence. *Academic radiology*, *25*(6), 747–750. https://doi.org/10.1016/j.acra.2018.03.007

Yuan, Y., Mou, L., & Lu, X. (2015). Scene recognition by manifold regularized deep learning architecture. In *IEEE Transactions on Neural Networks and Learning Systems*, (vol. 26(10), pp. 2222–2233). IEEE. http://dx.doi.org/10.1109/TNNLS.2014.2359471

Zhou, Y., & Tuzel, O. (2017). *Voxelnet: End-to-end learning for point cloud based 3d object detection*. arXiv:1711.06396. https://arxiv.org/abs/1711.06396

Applied Computer Science, vol. 17, no. 2, pp. 100–126
doi: 10.23743/acs-2021-16

Submitted: 2021-05-01 | Revised: 2021-06-17 | Accepted: 2021-06-23

*Blockchain, Ethereum, Smart Contract,*
*ERC-20 Tokens, Loan Default*

*Saha RENO* [0000-0003-1897-9002]*,
*Sheikh Surfuddin Reza Ali CHOWDHURY* [0000-0001-6101-9977]**,
*Iqramuzzaman SADI* [0000-0003-1739-0896]***

# MITIGATING LOAN ASSOCIATED FINANCIAL RISK USING BLOCKCHAIN BASED LENDING SYSTEM

**Abstract**

*Lending systems in real world are not much secure and reliable as the borrower and third parties involved in this aspect may create various deceitful situations. Blockchain is a secure system where the utilization of smart contract can avoid deceptive phenomena involved in lending but the decline in exchange rate of cryptocurrency can create the opportunity to pay back less than the borrowed amount in terms of fiat money. In this paper, a blockchain and smart contract-based lending framework is designed which requires the borrower to provide Ethereum Request for Comments (ERC)-20 standard tokens as collateral to mitigate the associated risks. The smart contract feature is utilized to automate the system without any third-party management. Besides, transaction stored in the blocks creates transparency among the users of the system. To tackle the aforementioned issues, ERC-20 token value is increased periodically and the instability of the exchange rate is surveilled by the system. By the end of this paper, some test cases and charts relevant to the data set are evaluated to assess the effectiveness of the system.*

## 1. INTRODUCTION

Blockchain refers to a chain of time-stamped and immutable blocks which are linked with each other using cryptography. Each block of the chain records Bitcoin or other cyrptocurrencies related transaction data (Swan, 2015). After a block gets filled with several transactional information, another block is created and gets linked with the previous one by a cryptographic hash (Narayanan, Bonneau, Felten, Miller & Goldfeder, 2016). To alter any transaction residing in a block, more than 50% of the hashing/computational power is required which is still a hypothetical thought known as 51% Attack (Yang, Chen & Chen, 2017). That is why, once a transaction gets stored in a block, it is almost impossible to delete or modify it. This phenomenon has made the blockchain as one of the most secured and reliable technologies ever existed. There are several crypto-currency based systems which use the concept of blockchain to provide security to its users. Ethereum is an open source, decentralized

* Bangladesh Army International University of Science and Technology, Dept. of CSE, Cumilla, Bangladesh, reno.saha39@gmail.com, me@sheikhsurfuddin.com, sadivictorian@gmail.com

blockchain based platform which has several benefits over other cryptocurrency based public ledgers. What makes this Ethereum so special is one of its unique features called Smart Contract (Buterin, 2014). Smart Contract is a piece of code which manages the overall functionality of a system and can be thought of as the back-end of any Ethereum based decentralized application (Mohanta, Panda & Jena, 2018).

Blockchain can be used to implement a digital collateral-based lending system which can remove all the shortcomings of the classical loan providing systems (Firdaus & Nugraha, 2019). Instead of any third-party managing the loan, a decentralized platform can be developed using Ethereum where smart contract is a computer code running on top of Ethereum network, which is intended to preserve all the rules and regulations of a platform. If an Ethereum based collateral loan system is developed, the smart contract feature will play the role of the manager for the supervision of the whole system and will make sure of the fact that both the borrower and lender utilize the system as per the rules (Okoye & Clark, 2018). As there will be no intervention of any human managing the system and only a piece of computer code will be given the responsibility, all the terms and conditions will be maintained precisely. Moreover, smart contracts involved in this system will ensure that the money borrowed from the lender must be repaid in time and if the debtor fails to repay the borrowed amount, smart contract will make lender the owner of the collateral. As a result, the collateral provided at the time of receiving the loans will permanently be seized by the lender. Each and every transaction regarding loans will be stored in the blocks and in no means these transactions can be altered or omitted. Moreover, if the value of collateral can be increased periodically by a certain amount, more people will be interested to join the system and lend money as it will economically benefit them. Keeping the financial benefit of the lenders in mind, all the calculations will be based on paper-money and not on the cryptocurrency used by the system. This is because, the exchange rate of the cryptocurrency fluctuates over time. If the exchange rate decreases in a certain time, then the lender will actually receive less amount of paper money at the time of repaying the loan. If all the accounting cost are calculated on the verge of fiat currency, then decrement in exchange rate will result in getting more cryptocurrency and the original amount can be retrieved. Reasonable mortgage cost, increment of collateral's pricing and generating loan interest will create keenness in people to join the system for buying tokens and providing loans as the system serves both as an income source and feasible lending system.

In this paper, we have proposed a smart contract based secure lending system by implementing the above-mentioned techniques. The system mitigates the financial risk by removing the deficiencies of the classical lending system of the real world and guarantees that the lenders is benefited economically each time he/she lends money to a borrower.

## 2. PRELIMINARIES

### 2.1. Blockchain

Blockchain refers to a chain of blocks which stores transactional information in such a way that the digital data inside the blocks are immutable (Narayanan, Bonneau, Felten, Miller & Goldfeder, 2016). It can be thought of as a public ledger which is distributed and decentralized. These blocks have their own unique hash which distinguishes them from each other (Yuan & Wang, 2016). Using a mechanism named 'Consensus', blockchain ensures that no fraud transactions can occur or the transactions inside these blocks cannot be omitted or changed (Singh & Singh, 2016; Heilman, Alshenibr, Baldimtsi, Scafuro & Goldberg, 2017). Proof of Work is one of the many Consensus mechanisms; in which a miner mines a block by making sure that no fraud transactions are being stored in the blocks or no intruder can modify the information residing in the blockchain (Yang, Chen & Chen, 2017). To temper a blockchain, 51% attack must occur, which refers to an attack made by a large number of miners or just by one single block validator taking over 51% of the system's computing power, which is still hypothetical and almost impossible (Cao, Husbands, Zhang, Binns, Kassam & Lan, 2018). This decentralized ledger is also destitute of double spending and thus making it a robust and trustworthy protocol (Watanabe, Fujimura, Nakadaira, Miyazaki, Akutsu & Kishigami, 2015; Christidis & Devetsikiotis, 2016).

### 2.2. Ethereum

Ethereum is an open source, decentralized blockchain based system which has a unique functionality named Smart Contract (Buterin, 2014). Developers can use this platform to build decentralized applications and what makes this system distinguishable from other blockchains is that it is programmable (Heilman, Alshenibr, Baldimtsi, Scafuro & Goldberg, 2017; Cao, Husbands, Zhang, Binns, Kassam & Lan, 2018; Ali, Nelson, Shea & Freedman, 2016). Ethereum supports many standard tokens which are not crypto-currencies but essential for Initial Coin Offerings (ICO) to raise fund from public for a future project or new cryptocurrencies to be developed by Li et al. (Li, Fung, Tang & Song, 2018). Moreover, there are various test networks for Ethereum besides the main network, all of which can be used to test a newly developed decentralized application whether it has any kinds of flaw and working according to the desired functionality (Li, Fung, Tang & Song, 2018).

### 2.3. Smart Contract

Smart Contract is a piece of code which controls the whole decentralized app built by a developer (Mohanta, Panda & Jena, 2018). It manages all the transactions being executed without third parties. Smart contract is described as an autonomous agent residing in blockchain by Luu et al. (Luu, Chu, Olickel, Saxena & Hobor, 2016). This contract includes the terms and conditions of the agreement between buyer and seller; necessary for a transaction to be executed, which are written into lines of code (Swan, 2015). Like each of the blocks in a blockchain, smart contract also has its own address so that the contract can easily be traced (Luu, Chu, Olickel, Saxena & Hobor, 2016). After writing the smart contract, it needs to be deployed to Ethereum's main network or test network (Buterin, 2014). Jeuls, Kosba and Shi stated that smart contract has several advantages over the traditional cryptocurrencies (Juels, Kosba & Shi, 2016).

### 2.4. Initial Coin Offering

Initial Coin Offering is a process to launch one's own cryptocurrency in the market by raising fund from the people who are interested in buying the newly arrived digital currency (Burns & Moro, 2018). To raise a fund, a person needs to create a document which essentially explains the system where this cryptocurrency can be used to pay for the desired services and also the benefits of using this new currency (Hrga, Benčić & Žarko, 2019). Anyone can set their own standards to create these tokens but ERC-20 Standard is by far the most popular and widely used standard in Ethereum Blockchain platform among others (Fenu, Marchesi, Marchesi & Tonelli, 2018). Though the creation and distribution of tokens are widely accessible to everyone, many legal considerations must be taken into account before holding an ICO (Zetzsche, Buckley, Arner & Föhr, 2017). Platforms which support the smart contract feature like Ethereum and Neo allow the developers to develop their own decentralized applications in which the smart contact facility governs the trading of ICO tokens (Rosic, 2017).

### 2.5. ERC-20 Standard

ERC-20 is a technical standard, widely utilized for specifying certain standards and rules for issuing tokens on Ethereum based systems. The figure 20 is used to assign this particular standard a unique identification number, which distinguishes this protocol from other variants of ERC standard tokens (Fröwis, Fuchs & Böhme, 2019). Prior to the arrival of ERC-20, if anyone wanted their token to be available on an exchange, they had to write custom code to allow others to trade and make the exchange possible (Somin, Gordon, Pentland, Shmueli & Altshuler, 2020). ERC-20 standard brings the uniformity among various Ethereum based tokens, reduces the complexity of understanding different types of token implementation and enhances the liquidity of the tokens (Victor & Lüders, 2019). Also, risk of breaking the token contract is minimized.

## 3. LITERATURE REVIEW

### 3.1. PTPTN Study Loan using Blockchain

National Higher Education Fund Corporation (PTPTN) is an organization managed by Malaysian Government which provides study loans for their citizen but is accused of poor management the filing system is not satisfactory. Moreover, 1.25 million students failed to payback their debts and thus people are taking this PTPTN loans as granted. Failure to repay the educational loans is drastically affecting the PTPTN as providing funds to the new students are becoming much more difficult. To eliminate these problems, a blockchain and smart contract based solution is proposed to allow the PTPTN and other agencies to monitor the current status of the borrowers. The loan adjustment among the system actors are maintained by three types of smart contracts: (i) Registrar Contract (RC) which assigns an Ethereum address or a public key to the individual taking loan to track his/her status, (ii) Customer-Provider Relationship (CPR) stores and manages all the records of education loan, (iii) Summary Contract (SC) is used to store borrower's transaction history in the system. Though the system is re-invented using blockchain, it is not fully decentralized as PTPTN and other government agencies are the centralized actors in charge of issuing the loans. Moreover, as this loan is for educational purpose and is refrained to the citizens and students of that country, only Malaysian students are able to be benefited from this system (Gazali, Hassan, Nor & Rahman, 2017).

### 3.2. Poverty Alleviation Loan Management using Smart Contract

To mollify the poverty in China, Poverty Alleviation Loan is introduced to the impoverished citizens of that country. As the current system is managed by a single service node, transparency and tractability are difficult to maintain. As a result, implementing this poverty loan management system using blockchain and smart contract is proposed. In this model, digital signature and oracle are used to ensure the data privacy. Transactions of this proposed system relies on: (i) Chaincode, which is a smart contract specifying all the terms and condition which must be met to execute certain operations and (ii) Unlocking Code, which is a piece of code used to satisfy the conditions mentioned in chaincode so that any specific transaction is allowed to be executed. Only needful citizens of China are given the permission to become a user of this system and are allowed to receive this poverty alleviation loan (Guo, Ma, Wang, Cheng & Wang, 2018).

### 3.3. Dharma

Founded by Nathan Hollander, Dharma is a popular platform which allows two individuals to get engaged in lending purpose. To mitigate the risk, a trusted third-party named Underwriter investigates on whether a borrower is faithful or not. This underwriter calculates the probability that a borrower will completely repay his loan by investigating the past transactions made by the borrower. But this mechanism surely does not lessen the risk to a great extent. Later, Dharma launched collateralized loans where the borrower must provide 1.5 times the money, he/she wants to borrow as collateral to ensure the payback of the borrowed amount along with the 8% interest (14% if the amount is in DAI) if the borrower fails to repay. This is certainly not feasible for the borrowers and as a result, people are being attracted to use the system as a lender and not as a borrower (Hollander, 2017).

### 3.4. Impact of BI Rate, Exchange Rate, Inflation, Third Party Fund (DFK) on Credit Distribution and Non-Performing Loan (NPL)

A quantitative research was conducted about the effect of BI Rate, Exchange Rate, Inflation, and Third-Party Fund (DFK) on Credit Distribution and Non-Performing Loan (NPL) where the researchers used the data of Bank in Indonesia. They have found that the BI Rate along with Exchange Rate and DFK of a loan is proportional with Credit Distribution. On the other hand, BI Rate has a negative impact on NPL resulting in lesser NPL cases. Also, Credit may create a negative and small impact on NPL which is also similar to research by Al-Wesabi (2020), which stated that NPL shows a positive and negligible impact on credit (Sinaga, Muda & Silalahi, 2020).

### 3.5. VaR Assessment and Selecting Portfolio for Western Balkan Countries

Llesh and Alban analyzed the stock quotations for five Western Balkan countries on a daily basis. Their analysis was based on capital distribution return and risk level was also considered. VaR and CVaR estimators were utilized for determining loss or profit intervals. Lagrange multipliers and interpolation were used for the methodological aspect. The evaluation showed that the Western Balkans Region's stock exchange indexes are not profitable. These indexes lack economic efficiency and simultaneous investing in the indexes of every exchange market turned out to be risky for investors. This research also found that the investing strategy in passive way is a better option for financial investment than the active strategy (Lleshaj & Korbi, 2020).

## 4. PROPOSED ARCHITECTURE OF LOAN DEFAULT PREVENTION PROTOCOL

Our proposed Ethereum based lending framework is defined using several procedures intended to issue, administrate, trade and fund cryptocurrency as loan; which is managed by the system's smart contracts, structured interfaces and ERC-20 tokens being utilized as collaterals. Our protocol is based on EVM based blockchain, but can be further extended to support permissioned and private blockchain like Hyperledger using chaincode functionality. Role of the participants and smart contracts, loan issuance and repayment process along with the system's terms and conditions are described in the following subsections:

### 4.1. Participants

The end-users of the system are defined as active participants of our framework -- clients willing to lend money to the debtor or, requesting loan from the creditor. Therefore, these participants fall under two categories:

1. **Borrower**
   The party who requests loan from the system and as requirement provides some tokens as collateral. They owe the lender some agreed upon amount. The debt order from a borrower must satisfy all terms and conditions of the proposed system. The credit score determined by risk assessment indicates a debtor's trustworthiness.

2. **Lender**
   The party which lends cryptocurrency as a loan asset to the borrower and takes tokens from them as collateral. Loan requests are passed to the lenders from the relayer's side. Lenders can accept or reject a debt request according to their preferences. Upon agreement, the requested amount is transferred from lender's wallet to the borrower's one. Lenders can also issue a loan as borrower and the same is applicable for the debtors.

   The interaction among the participant and system keepers (described in the succeeding subsection) is graphically represented using Fig. 1.

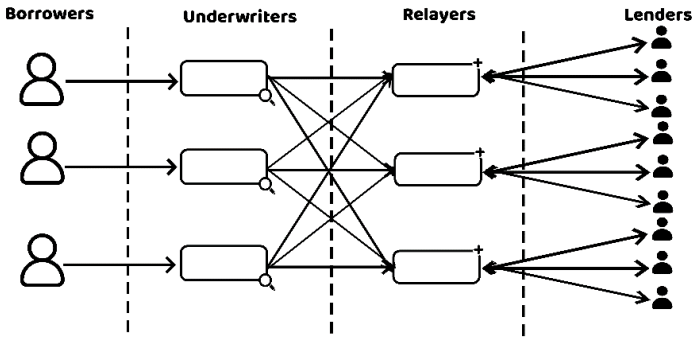


**Fig. 1. Interaction Among Different Participant Types**

### 4.2. System Keepers

We define system keepers as the managers of the overall architecture of our protocol. Keepers ensure the proper maintenance and accurate transitions of messages and information all over the system:

1. **Underwriter**
   Underwriter is one of the smart contracts of our system, certifying valid loan requests from the borrowers. It checks whether the loan request complies with the system's terms and conditions and forward the request to the relayer. The functions performed by the underwriter are as follows:
   a. Generating a loan request message to be passed from the borrower.
   b. Negotiating the debt to check the validity of the loan request.
   c. Ensuring in-time repayment in accordance with the terms agreed upon.
   d. Collecting collaterals from the borrowers and passing it to the relayer to inhibit loan defaulting.

2. **Relayer**
   Relayer receives valid loan requests from the underwriter and stores them in the memory of EVM named loan records. Relayer broadcasts these loan requests to the lenders and maps a lender to a specific loan request. Like underwriter, relayer is also a piece of smart contract where necessary instructions are provided for smooth maintenance of every loan case. Other duties of relayer includes:
   a. Keeping track of the deadlines mentioned by the borrowers.
   b. Incrementing the price of the tokens provided as collateral and make it stop after the compensation amount is reached.
   c. If the borrower fails to repay the loan, relayer takes the collaterals from the underwriter, updates its value as per the calculations and transfers them to the lender's account.
   d. Compute the risk factor for a particular end-user of the system by evaluating the transaction records and loan histories.

### 4.3. Loan Issuance Process

The order in which a loan gets issued is described as follows:

1. Borrower requests a loan by filling up necessary and required information. This information include: loan amount, deadline to repay the loan, the agreement on terms and conditions of the protocol etc.
2. The request is passed to the underwriter. Underwriter sends the requestor's user ID to the relayer to fetch the credit score for checking the eligibility of taking loans. Also, the underwriter checks whether the borrower has enough ERC-20 tokens in their wallet. It also verifies if the requested amount surpasses the maximum limit a debtor can borrow money as per his/her credit score. If the deadline mentioned by the borrower does not comply with the system's stipulation, the underwriter declines the loan request. If the request follows all the system's rules and regulations, it is forwarded to the relayer.

3. Relayer broadcasts the loan request to a number of lenders. The lender willing to provide the solicited amount forwards the acceptance message to the relayer. Relayer then records all of the relevant information about that particular loan in EVM's memory. This relevant message includes Ether's exchange rate on loan receiving date.
4. Relayer also warns the creditor if the requestor is having a bad credit score. It provides suggestions about whether lending money to that particular borrower is considered risky or not.
5. Relayer informs the underwriter about the successful issuance of loan and requests it to fetch the required number of tokens from the borrower's account.
6. After successful retrieval of the required amount of collateral, relayer starts the countdown and also starts calculating the interest. The price of the collateral taken from the debtor gets incremented on a daily basis, until the loan is repaid or the threshold value is reached.
7. While the borrower is willing to repay the loan, the relayer checks the current exchange rate of Ether and calculates how much extra cryptocurrency the borrower needs to add to the repayment if the market price of Ether decreases.
8. If the borrower fails to repay the loan by the deadline, the relayer marks it as a failed repayment, updates the borrower's credit score and transfers the tokens to the lender's account after updating its price.
9. If the exchange rate of Ether increases, the debtors are not allowed to pay less cryptocurrency than the amount he/she borrowed. Instead, the full amount must be repaid.
10. On the other hand, if the debtor successfully repays the loan in time, the increments get cancelled and the tokens are returned back to the borrower's account.
11. The details of a specific loan issuance in EVM memory gets updated by relayer after the successful repayment/failure to payback. This information is required for the purpose of risk assessment.
12. All the transaction details of our proposed system are immutable in nature, meaning that they cannot be updated, altered or deleted by any means. Thus, transparency is maintained.

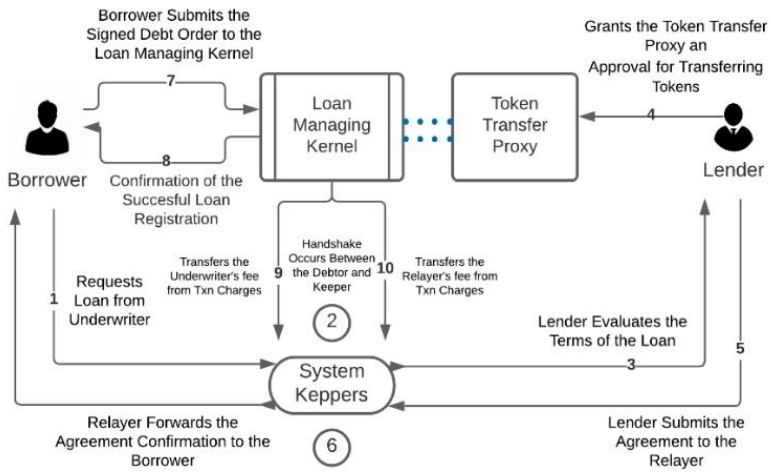


**Fig. 2. Issuance Process for Ordering a Loan**

The overall loan issuance is depicted using Fig. 2.

### 4.4. Terms and Conditions of the Protocol

To prevent loan defaulting and restrain lender's economical loss from debtor's failure to payback, the borrower must acknowledge and agree to the following terms and conditions of the proposed lending protocol:

1. Borrower must provide ERC-20 tokens worth 90% of the loan amount to request for loan issuance.
2. 2% daily interest is applicable on the lent amount. This rate can be changed and the periodical pattern can be switched from daily basis to monthly using the system's smart contract.
3. The escalation in collateral price also gets increased by 2% on a daily basis. Also, this rate and pattern of increment are adjustable.
4. The repayment deadline cannot exceed 90 days.

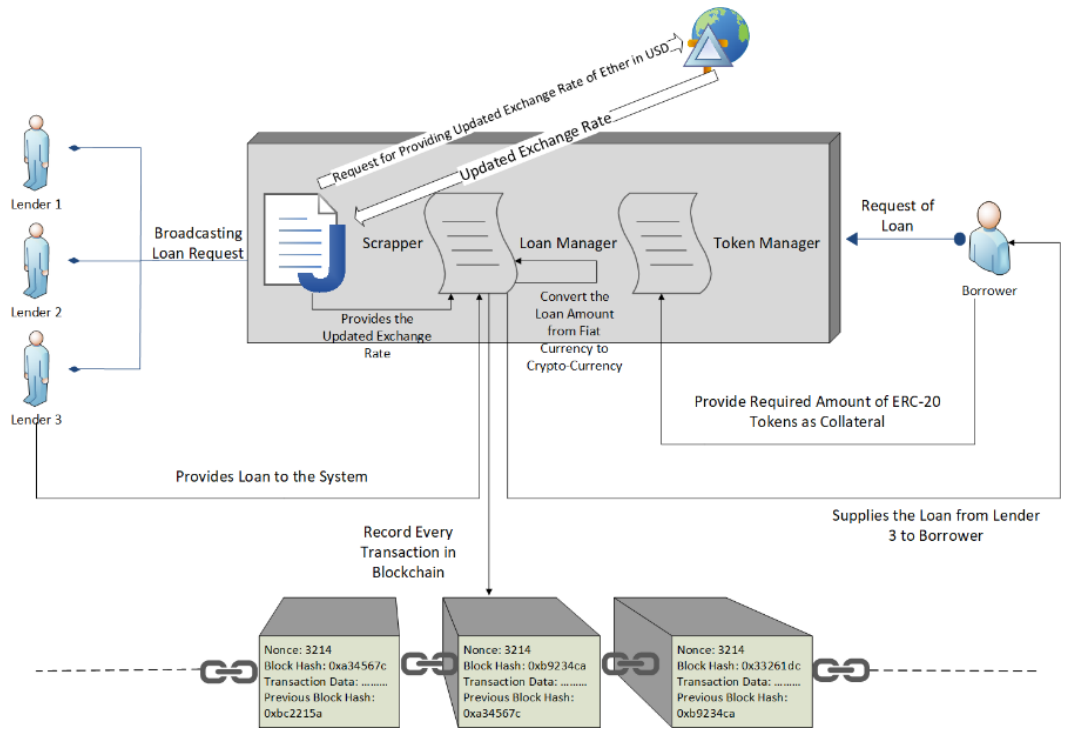


**Fig. 3. Overview of the Lending Management System**

## 5. METHODOLOGY

Although every financial transaction of the system utilizes cryptocurrency to be executed, all kinds of calculations are performed on the basis of fiat money to avoid the unwanted circumstances caused by the increase or decrease in the exchange rate of Ether. The system has its own modified ERC-20 standard tokens which are used as collateral for lending

purpose. Users can buy these tokens from the system and can sell these either to the system or other users. Two smart contracts are in charge of managing the system. One of the smart contracts creates the tokens and governs the trading of these tokens among the users. The second one administrates the lending and borrowing aspects, along with generating interest, elevating the collateral price and liquidating the lender. Fig. 3 demonstrates the basic concepts of the proposed system and the working principle and basic operations of the system can be sectioned as follows:

### 5.1. Fixing the Price of Tokens in Fiat Currency

The price of these tokens is fixed in fiat currency and not in Ether, as fluctuations in exchange rate of cryptocurrencies create different pricing of these tokens at different times and decrement in Ether's exchange rate will bring financial loss to the holder of the tokens while selling them or using them to take loans. The system keeps checking the current exchange rate of Ether and updating the price of tokens continuously. For this purpose, two JavaScript modules 'cheerio' and 'request' are used to scrap necessary data from (CoinGecko, 2021). 'request' sends a request to (CoinGecko, 2021) for fetching the current exchange rate of Ether in USD. After the request is granted, 'cheerio' fetches the equivalent USD of 1 Ether from the aforementioned website. After fetching the equivalent USD of per Ether using 'cheerio', this value is stored inside the smart contract and then converted to Wei (1 Ether = $10^{18}$ Wei). CoinGecko does not directly provide how much Ether is achievable from 1 USD, so this value is inversed to get the amount of Ether receivable per dollar, which keeps getting updated due to the fluctuating price of cryptocurrencies. This amount is then multiplied by the price of per token (in USD), which gets us each token price in Wei.

**Setting Token Price in USD**

```
INITIALIZE VARIABLE onUpdateTokenPrice =
ARROW FUNCTION : async
    SET VARIABLE const cheerio TO GET MODULE 'cheerio'
    SET VARIABLE const request TO GET MODULE 'request'
    SET tokenPriceInUSD TO 1

    MAKE HTTP REQUEST:
        METHOD: GET
        URL: https://www.coingecko.com/en/price_charts/ethereum/usd
        RECEIVE RESPONSE: err, res, body
        ARROW FUNCTION(err, res, body):
                IF err:
                    THEN RETURN console.error(er)
                END IF
                INITIALIZE VARIABLE let $ TO cheerio.load(body)
                INITIALIZE VARIABLE valueInFloat
                PARSE $('.no-wrap').text() INTO FLOAT AND STORE INTO valueInFloat
                valueInFloat = (valueInFloat/10000000000000000).toFixed(20)
                CALL FUNCTION this.setState AND PASS JSON ARGUMENT: {dollarPriceInWei:(1/
valueInFloat).toString()}
                INITIALIZE VARIABLE tokenPriceInWei
                DIVIDE tokenPriceInUSD BY valueInFloat, ROUND QOUTIENT AND STORE INTO tokenPrice
InWei
                INITIALIZE VARIABLE tokenPriceInWeiValueInString
                PARSE tokenPriceInWei INTO STRING AND STORE INTO tokenPriceInWeiValueInString
                CALL FUNCTION this.setState AND PASS JSON ARGUMENT: {tokenPriceInWeiValue : toke
nPriceInWeiValueInString}
                INITIALIZE VARIABLE d TO new Date()
        END
    END HTTP REQUEST
END
```

**Fig. 4. Setting Token Price in Fiat Money Using React.js**

As the equivalent Wei of per USD gets updated periodically inside the smart contract, the variable nature of exchange rate is thus tackled by requiring extra or less Ether from the client to buy a token from the system or its owner, ensuring that the price of the tokens does not deteriorate with the downfall of Ether's exchange rate. The code snippet to fix the price of ERC-20 tokens in fiat currency is demonstrated using Fig. 4.

## 5.2. Buying and Selling Tokens

Tokens can be purchased both from the system and other users. To buy tokens from the system, users simply need to mention the number of tokens they are willing to buy and provide the required amount of Ether to the system. Also, the users can sell their tokens to other interested users.

**Buying and Selling Tokens**

```
FUNCTION buyTokens(address _seller,unit256 _numberOfTokens,  unit256 _tokenPrice)
: public payable
    IF seller IS admin:
        THEN _tokenPrice = _tokenPrice - (_tokenPrice * .10)
    END IF
    GET 'value' FROM MODULE 'msg' AND CHECK IF  MULTIPLICATION of _tokenPrice AND
 _numberOfTokens ARE EQUAL TO 'value'
    GET 'balanceOf' _seller's _tokenPrice FROM MODULE 'tokenContract' AND CHECK I
F 'tokenContract' IS GREATER THAN OR EQUAL TO _numberOfTokens
    CALL FUNCTION _seller.send AND PASS ARGUMENT msg.sender.value
    CALL FUNCTION transfer FROM tokenContract AND PASS ARGUMENTS: _seller, msg.se
nder,_tokenPrice,_numberOfTokens
    IF _seller IS admin:
        INCREMET tokenSold BY _numberOfTokens
    END IF
    CALL FUNCTION Sell AND PASS ARGUMENTS: msg.sender, _numberOfTokens
END



FUNCTION transfer(address _from, address _to, unit256 price, unit256 _amount): BO
OLEAN success
    GET 'balanceOf[_from][price]' FROM MODULE tokenContract AND CHECK IF 'balance
Of[_from][price]' IS GREATER THAN OR EQUAL TO _amount
    DECREMENT tokenContract.balanceOf[_from][price] BY _amount
    INCREMET balanceOf[_to][price] BY _value
    CALL FUNCTION Transfer AND PASS ARGUMENTS: _from, _to, _amount
    RETURN True
END
```

**Fig. 5. Smart Contract Segment for Buying and Selling Tokens as Collateral**

To handle the trading of tokens, the smart contract is utilized to take the Ethereum wallet address of the buyer and transfer the tokens into that address. Two conditional statements ensure that (i) the buyer is providing enough Ether and (ii) the seller has enough Tokens in his/her wallet. Upon fulfilling the conditions, the Ether provided by the buyer are transferred to the seller's account. After that, the tokens are transferred from seller's wallet to the buyer's one.

As the price of some tokens which were seized as collateral during the period of a loan gets incremented, the system as well as token holders will carry tokens of different costs. As a result, there will exist both the tokens of regular price and the tokens of higher price than the original cost. To maintain tokens of different pricing (several price variations and the number of tokens under a specific price), mapping data structure from Solidity language is used, which takes the user/contract address and price variations as arguments. After providing an Ethereum address and a specific price variation, this mapping structure returns how much tokens the address currently holds for that specific price. It is up to the buyer which price-variant tokens he/she will buy from the user or from the smart contract itself (the system). System may or may not allow the smart contract to buy tokens from the users, depending on the availability of the fund raised by selling its tokens. To maintain the fund, system provides 10% less Ether than the actual price to its users in case of buying tokens from them. A conditional statement is evaluated to check whether the seller is the contract itself or not, and if the seller is the token selling contract, then the price of token is reduced to 10%. Smart contract pseudo code for buying and selling tokens is stated in Fig. 5 while Fig. 6 illuminates the basic token trading concept of the proposed lending system.

### 5.1. Lending Money to the Borrower

Before broadcasting a request of loan, with the help of the smart contact which manages the trading of tokens, the loan managing contract verifies whether the requester can provide required number of tokens as collateral. According to the current management, ERC-20 standard tokens of various price will exist in the system as the price of the tokens which are seized as collateral get increased by a certain percentage to mitigate the risk of lending money, which is described elaborately in the next subsection. As a result, tokens of different price variations can be noticed in the system. How many price-variant tokens a user owns in his wallet can be checked from the system. While requesting a loan or selling tokens to other users, a chart is shown to the users where the number of different priced tokens along with their rates can be examined. To borrow money from the creditor, the debtor must hold a certain number of tokens in his wallet, the price of which must be equal to 90% of the borrowed amount.

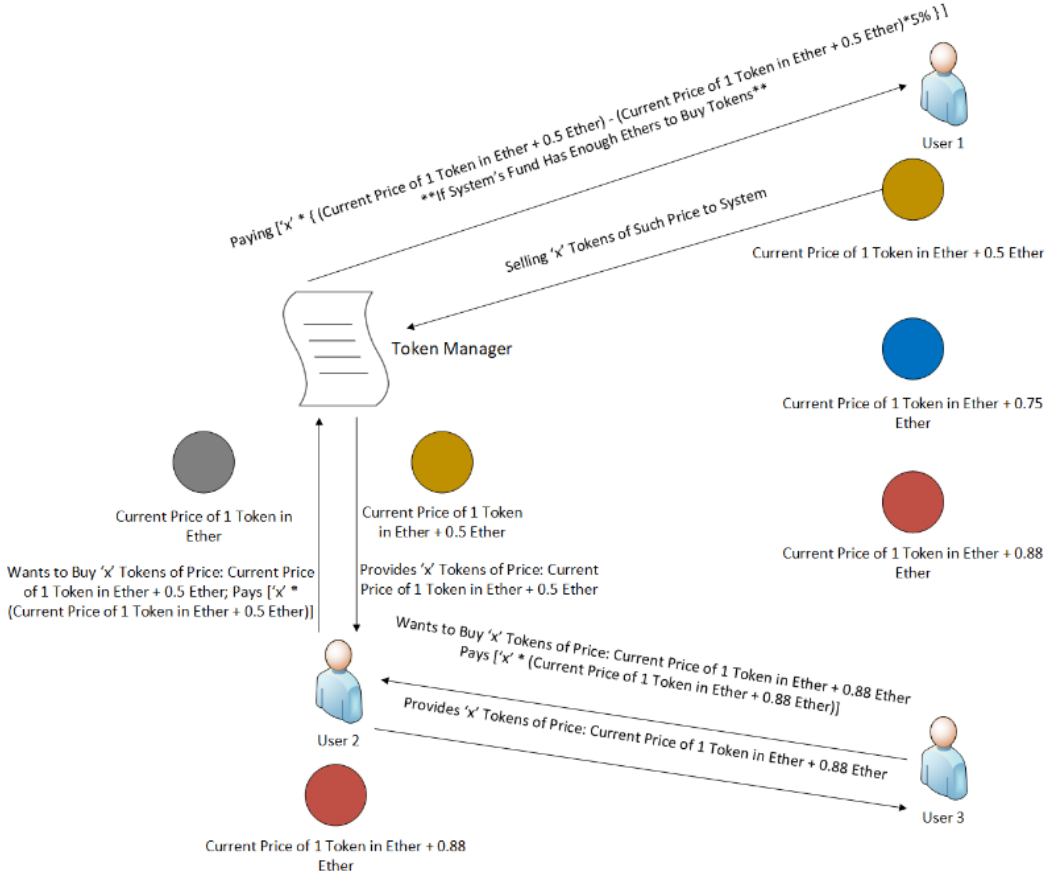


**Fig. 6. Trading of Different Price Variant Tokens Among Users and System**

Among tokens of various pricing, the borrower must select a proper combination of tokens which must satisfy the following condition:

$$\sum_{i=1}^{n}(\mathrm{TN_i} \times \mathrm{P_i}) \geq 0.9E \quad (1)$$

Where, TN refers to the number of tokens, P refers to the price of tokens and ***i*** denotes how many variants of token a user has and $E$ denotes to the amount of Ethers borrowed. In short, the borrower must provide a certain amount of collateral and the price of which must be greater than/equal to the 90% of the requested amount to be borrowed.

If the borrower is able to provide the required number of tokens as collateral, then the system marks the request as valid and broadcasts it to the lenders. After a lender accepts a request, the system collects the tokens and transfers these tokens to the smart contract serving as the back-end. The lender's money is then sent to the borrower's account. It is important to note that, to restrain the overflow of token variants caused by different pricing, the system may limit the users to hold a certain amount of price variant tokens. For example, a user cannot carry more than 10 different price variant tokens in his wallet. All of the aforementioned techniques managed by the loan managing contract is elaborately described below:

**Requesting and Providing Loans**

```
FUNCTION requestLoan(unit256 dollarBrwd, unit256 amntBrwd, unit256[] priceVariants, un
it256 rtrnMneyTmeInDys): public
    FOR EACH priceVariants: PRICE_VARIANT AS INDEX
        GET 'balanceOf[msg.sender][PRICE_VARIANT]' FROM MODULE 'tokenContract' AND CHE
CK IF balanceOf[msg.sender][PRICE_VARIANT] IS GREATER THAN OR EQUAL TO amountStarted[P
RICE_VARIANT]
        INCREMET flag
    END FOR

    GET flag FROM MODULE AND CHECK IF flag IS EQUAL TO COUNT OF priceVariants

    FOR EACH priceVariants: PRICE_VARIANT AS INDEX
        INCREMET totalTokenPrice by MULTIPLICATION OF tokenContract.balanceOf[msg.send
er][PRICE_VARIANT] AND PRICE_VARIANT
    END FOR

    IF totalTokenPrice IS GREATER THAN OR EQUAL TO amntBrwd * .90:
        THEN:
            INCREMET loanID
            STORE msg.sender INTO borrowers[loanID]
            STORE amntBrwd INTO amountBorrowed[loanID]
            STORE dollarBrwd INTO dollarBorrowed[loanID]
            STORE rtrnMneyTmeInDys INTO returnModeyTimeInDays[loanID]
            CALL transfer FUNCTION AND PASS ARGUMENTS: msg.sender, this, priceVariants
    END IF
END

FUNCTION provideLoan(unit256 loanID, address _borrower): public payable
    STORE msg.sender INTO lenders[loanID]
    CALL send FUNCTION ON borrowers[loanID] PASS ARGUMENT: msg.value
    INCREMET totalLoans[_borrower]
    STORE True INTO statusOfLoan[loanID]
END
```

**Fig. 7. Solidity Methods for Management of Requesting and Providing Loans**

The smart contract handles all the requests from the borrowers to check their eligibility of taking loans. To perform this operation, 4 parameters are required, among which the 'Amount of dollar borrowed' is required to record the requested amount in terms of USD, so that when the borrower is repaying the lender, the system can check how much extra Ether the borrower needs to pay if the exchange rate decreases. Another parameter contains the number of tokens the borrower is willing to provide against each price variants. At first, the contract determines whether the borrower's wallet actually contains the number of tokens he/she stated to be provided as collateral. A flag is used to check that the borrower's collateral combination is legit. If the combination of the total amount of different price variant tokens turns out to be valid, then the

overall price of the borrower's collateral value is to be calculated as total token price. After calculation, the price of all the tokens is compared against (Borrowed Amount X 0.9). If the total price of these tokens is enough to grant the borrower the loan he/she requested, a loan ID will be generated to track all the loans managed by the system. The smart contract algorithm for providing loan is stated in Fig. 7.

Borrower's address, the amount of loan in both Ether and USD and payback time are also recorded as the required loan information to be handled by the system later. Smart contract then locks all the collateral provided by the borrower in its own wallet. The lender then invokes the smart contract to provide the requested amount. The lender's address is recorded against the particular loan ID and smart contract transfer the loan to the borrower's wallet address. This contract constantly checks whether a loan is still to be repaid or not. Again, a mapping structure is used to track how many loans the borrower has taken so far, which is utilized for Risk Assessment purpose described in the next subsection.

### 5.2. Risk Assessment

All of the system's transactions are recorded in the immutable ledger of Ethereum network. Any transaction regarding successful or unsuccessful payback is stored in the blockchain and thus can be used for risk factor assessment. Each user will have their own risk factor that indicates how much risky it is to provide them a certain amount of loan. Risk factor of a user can be calculated using the following formula:

$$1 - \frac{Total\ Number\ of\ Succesful\ Paybacks}{Total\ Number\ of\ Loans\ Taken} \tag{2}$$

Fig. 8 contains the smart contract snippet to assess the Risk Factor. The assessment procedure of is described below:

**Risk Assessment**

```
Solidity Segment

FUNCTION riskAssesment(address _borrower, address[] _blockLoanStatus): public unit
256 factor
    INITIALIZE VARIABLE unit256 i TO 0
    WHILE borrowerLoanStatus[_borrower][i] IS NOT EQUAL TO NULL:
        IF searchStr(block.data(borrowerLoanStatus[_borrower][i])) RETURN SUCCESS:
            INCREMET successCount BY 1
            INCREMENT i by 1
        END IF
    END WHILE
    RETURN (1 - (successCount/totalLoans[_borrower]))
END



JavaScript Segment

INITIALIZE assessingRisk=
ARROW FUNCTION(event): async
    event.preventDefault()
    INITIALIZE VARIABLE const riskScore TO loanManagement.methods.riskAssesment(th
is.state.borrower).send({from: adminAccount, gas: '1000000'})
    CALL FUNCTION setState ON THIS AND PASS ARGUMENT {riskScore}
END
```

**Fig. 8. Risk Factor Calculation Using Smart Contract**

Loan managing contract stores the block address in its memory against each borrower of the system. Each time before broadcasting a borrower's loan request, this contract assesses the block data using the address and calculates the risk factor. The contract utilizes borrower's address and the addresses of the block containing the loan status against each borrower. The system then fetches the information from the specific blocks. This smart contract searches for the transactions containing the term 'success' from the fetched data and once it finds all the blocks containing desired transaction status, it will count the number of blocks. Finally, the risk factor against a particular borrower is calculated by ***1 – (Number of Success Counts / Total Number of Loans Taken to Date)***. The risk factor status of a borrower is displayed when the system broadcasts his/her loan request. For example, if a borrower takes 10 loans from different lenders and successfully paid 5 of them, then the risk factor 50% will be displayed beside his/her loan request. The schematic diagram for understanding the system's risk factor assessment procedure is illustrated by Fig. 9.

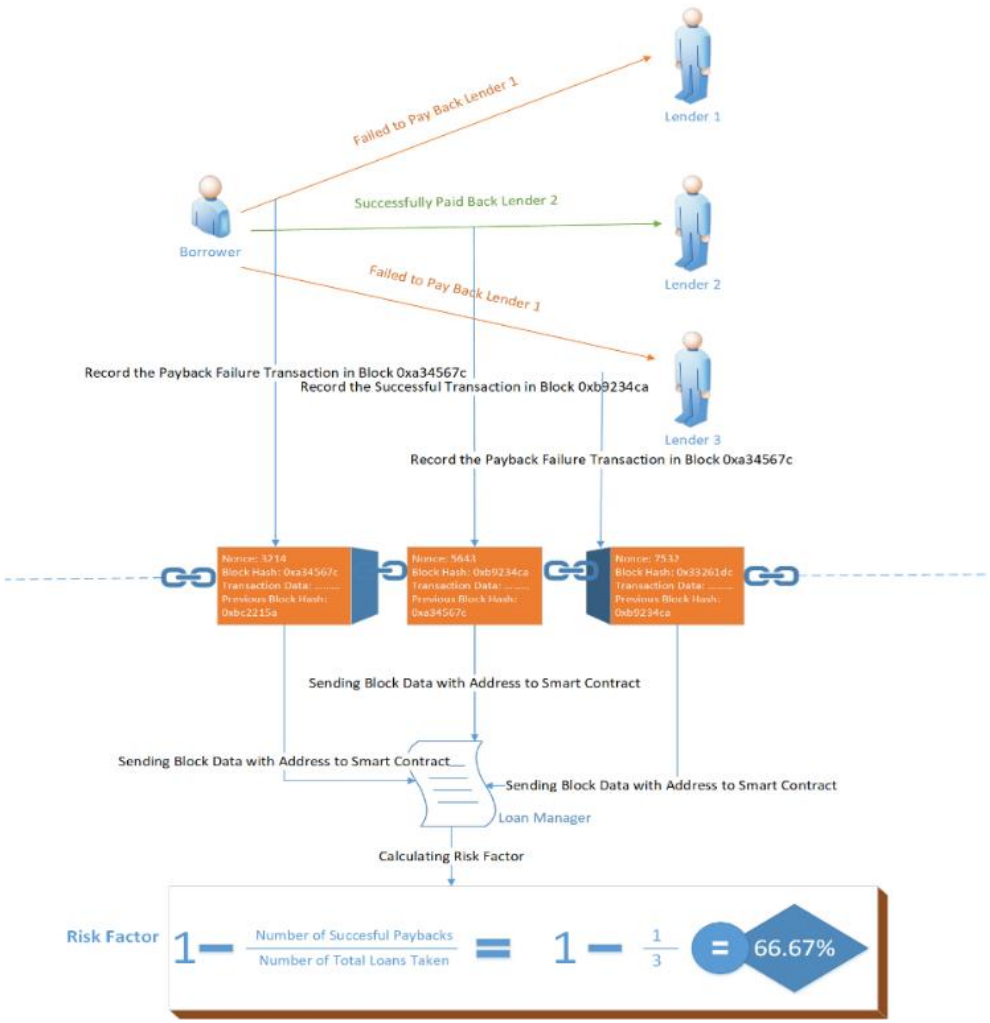


**Fig. 9. Accessing Block Data to Calculate Risk Assessment Factor**

### 5.3. Mitigating Financial Risk by Incrementing Token Price and Generating Interest

To mitigate the risk of financial loss of the lender and also to provide profit, the price of the tokens seized as collateral is increased periodically as follows: if the token price increases by the rate of 2% per day, the price of each token in Ether as per the exchange rate of loan issuance date is ***TP*** and the number of days between the date on which the loan was provided and the repayment date is ***R***, then the increment of per token price in each day will be:

$$\sum_{i=1}^{R} \mathrm{TP_i} \times 2\% \tag{3}$$

This increment is added to the actual cost of the token. The interest on the borrowed amount is be calculated as follows: If the interest is based on daily basis and the daily interest is 2%, the number of Ethers borrowed is ***E*** and ***M*** is the minimum interest to be paid (irrespective of the numbers of days passed since the loan issuance date), then the total amount of interest to be paid is:

$$\sum_{i=1}^{R} (E \times 2\%) \geq M \tag{4}$$

The steps mentioned above are implemented using Solidity and React.js by the following means: A Solidity mapping structure takes the loan ID and price of the tokens as its index values to keep track of different token pricing, as periodical price increment of specific token occurs continuously. Loan ID is used here to refer to the loans of which the collateral price is increased and pricing denotes all the pricing variants of the collateral provided by the borrower. From the front-end section, a Javascript segment invokes the smart contract to increment the token value once in a day, providing the loan ID and the chosen combination of different price variant tokens (which will be seized as collateral) as the arguments. Meanwhile, loan managing contracts also assess the expiration of deadline. If the loan is active and deadline is not crossed, then it increments each of price variants of the tokens by 2%, belonging to a specific loan ID. This increment continues until the case of the loan is closed or the deadline is expired. Upon the expiration of deadline, all the seized collateral whose price is incremented are then transferred from the contract's address to the lender's address. The contract also calculates the interest until the status of a loan ID is still active. Values of the incremented price variants under a particular user wallet are stored in the smart contract's memory, which will later be used to create any collateral combination for taking loans in the future. Javascript front-end segment again invokes the contract side, passing the status of loan, deadline and number of days elapsed as necessary arguments to calculate interest for a particular loan. If the loan is still active, deadline is not crossed and the number of passed days is 1, then system will calculate interest for 15 days (as per the rule of the system described below), the interest value will be stored against a particular loanID and the increment will stop for 15 days. If more than 15 days have passed, then again, the increment will be started on 2% daily basis. The formalization of the above techniques is provided in Fig. 10.

**Increment Token Price**

```
FUNCTION incrementTokenPrice(unit256 loanID, unit256[] pricing): public
    IF statusOfLoan[loanID] IS True AND deadline[loanID] IS False:
        THEN:
            WHILE prcing[i] IS NOT NULL:
                INCREMENT tokenPriceVariants[loanID][pricing[i]] BY tokenPriceVa
riants[loanID][pricing[i]] * 0.02
            END WHILE
    ELSE IF statusOfLoan[loanID] IS True AND deadline[loanID] IS True:
        THEN:
            WHILE pricing[i] IS NOT NULL:
                SET tokenContract.balanceOf[lender[loanID]][tokenPriceVariants[l
oanID][pricing][i]] TO tokenContract.balanceOf[this][tokenPriceVariants[loanID][
pricing[i]]]
                SET tokenContract.balanceOf[this][tokenPriceVariants[loanID][pri
cing[i]]] TO NULL
                CALL FUNCTION push ON userTokenPriceVariants[lender[loanID]] and
 PASS ARGUMENT: tokenPriceVariants[loanID][pricing[i]]
            END WHILE
    END IF
END
```

**Calculating Interest**

```
FUNCTION generateInterest(unit256 baseAmount, unit256 loanID): public
    IF statusOfLoan[loanID] IS True AND deadline[loanID] IS FALSE AND firstDay
 EQUAL TO daysPassed EQUAL TO 1:
        THEN:
            SET interest[loanID] TO amountBorrowed[loanID] * 0.02 * 15
            IF statusOfLoan[loanID] IS True AND deadline[loanID] IS False AND
daysPassed IS LESS THAN 15:
                THEN:
                    CONTINUE
            ELSE:
                INCREMENT interest[loanID] BY interest[loanID] * 0.02
            END IF
    END IF
END
```

**Fig. 10. Smart Contract Management for Mitigating Loan Risk**

Javascript front-end segment again invokes the contract side, passing the status of loan, deadline and number of days elapsed as necessary arguments to calculate interest for a particular loan. If the loan is still active, deadline is not crossed and the number of passed days is 1, then system will calculate interest for 15 days (as per the rule of the system described below), the interest value will be stored against a particular loanID and the increment will stop for 15 days. If more than 15 days have passed, then again, the increment will be started on 2% daily basis. The formalization of the above techniques is provided in Fig. 10.

## 5.4. Repaying the Borrowed Amount

The loan managing contract is to be triggered by the borrower to repay the loan. The increment of both the collateral price and interest continues until the payback date. While the borrower is willing to repay the money, the system prepares to check how much the exchange rate of Ether on the repayment date varies from the exchange rate on loan issuance date. If the exchange rate of Ether decreases, the system then calculates the extra amount Ether which the borrower needs to add to the original payback amount. On the other hand, if the exchange rate increases, then the borrower needs to pay the original amount. System's payback and liquidation management are graphically represented using Fig. 11.

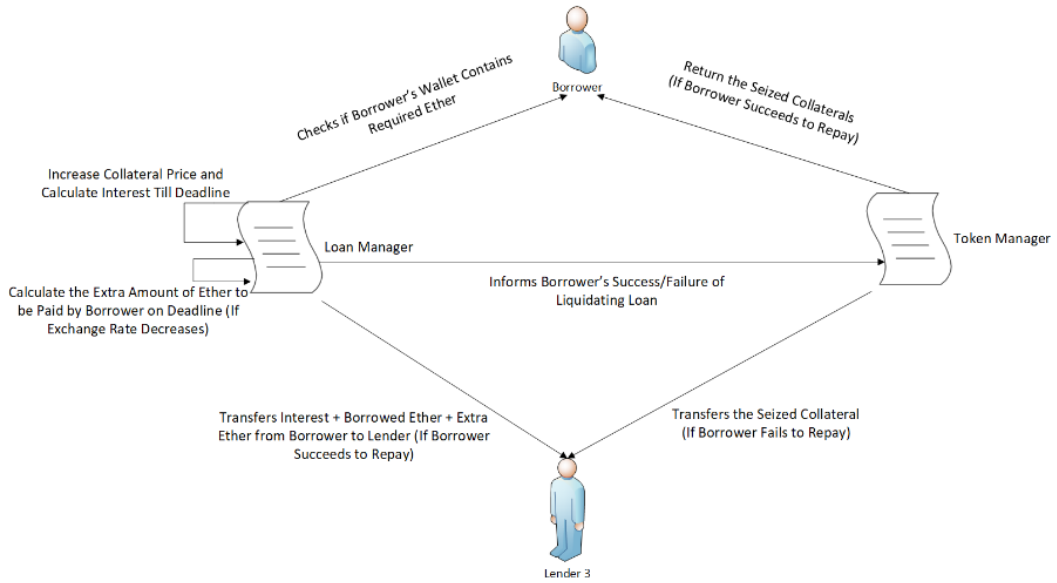


**Fig. 11. Payback and Liquidation Management Using Smart Contracts**

Suppose, at the time of borrowing, the exchange rate of 1 Ether was equal to ***D*** dollars and the borrower wanted ***B*** dollars from the lender. Then, the borrower will get ***(B/D)*** Ether. When repaying the amount, the exchange rate of 1 Ether decreases to ***D'*** dollars. Then the extra amount of Ether the borrower must provide to the lender will be according to the following equation:

$$\left({}^{D}/_{D'} - {}^{B}/_{D}\right) Ether \tag{5}$$

This is due to the fact that, the system refrains the borrower's opportunity to provide less Ether if exchange rate decreases as this phenomenon reduces the equivalent Ether of a certain amount of fiat money. According to the above discussion, the total payback amount a borrower must return by the deadline will follow the equation stated below:

$$E + \left({}^{D}/_{D'} - {}^{B}/_{D}\right) + (E \times 2\% \times N)\ Ether \tag{6}$$

where ***E***, ***[(D/D') - (B/D)]*** and ***(E × 2% × N)*** denote to the original borrowed amount, the extra Ether to be paid if exchange rate decreases and the amount of interest respectively (***N*** refers to the number of days between the loan issuance date and the payback date). If the borrower is able to provide the amount calculated using the above formula, only then the request to repay the borrowed amount is accepted and all the tokens are returned to his/her wallet. If the debtor does not repay the borrowed amount, all tokens whose prices were being increased on a regular basis to compensate for the unpaid amount are transferred from the smart contract's account to the lender's wallet. It is to be noted that, upon successful payback, the increment of the collateral price is reverted before being returned to the borrower's account to avoid the overflow of variances of token prices. The aforementioned techniques to mitigate is implemented in the loan managing smart contract by the following means: From the Javascript end, the system first fetches the loan status and deadline status of a particular loan ID to check the list of unpaid

amounts. If the loan status is active but the deadline is expired, then system will directly trigger the transfer to send all the seized collateral to the lender's account. In case of payment imitative taken by the borrower, the payback functionality of smart contact is triggered by the borrower to repay the money. This payback requires the current exchange rate to calculate the updated price of payback amount and also the loan ID. These parameters are passed by the React.js front-end code snippet.

**Borrower's Payback Procedure**

```
JavaScript Segment

INITIALIZE VARIABLE onPayment =
    ARROW FUNCTION(event): async
        event.preventDefault()

        INITIALIZE VARIABLE loanStatus AND STORE AWAIT
        moneyLending.methods.getLoanStatus(this.state.loanID).call()
        INITIALIZE VARIABLE deadlineStatus AND STORE AWAIT
        moneyLending.methods.getDeadlineStatus(this.state.loanID).call()
        IF loanStatus IS True AND deadlineStatus IS False:
            THEN:
                INITIALIZE VARIABLE lender AND STORE AWAIT
                moneyLending.methods.getLender(this.state.loanID).call()
                AWAIT tokenContract.methods.transfer(this.state.contractAddress,l
ender, this.state.priceVariants).send({
                    from: this.state.contractAddress, gas:'1000000'}
                })
        END IF
    END IF



Solidity Segment

FUNCTION payback(unit256 loanID, unit256 currentRate, unit256[] pricing): public
payable BOOLEAN
    IF msg.value IS EQUAL TO MULTIPLICATION OF dollarBorrowed[loanID] AND current
Rate , ether + interest[loanID] ether:
        THEN:
            CALL FUNCTION transfer ON tokenContract AND PASS ARGUMENTS: this, msg
.sender,pricing
            CALL FUNCTION lenders[loanID] AND PASS ARGUMENT: msg.value
            SET statusOfLoan[loanID] TO False
            deadline[loanID] TO NULL
            RETURN True
    ELSE:
        RETURN False
    END IF
END
```

**Fig. 12. Reimbursement Technique to Payback Lender**

To evaluate the current exchange rate, the code segment to fetch the required information using 'cheerio' and 'request' modules are described in Fig. 4. Also, it needs the amount of generated interest under a specific loan ID, which can be found in the contract memory. After calculating the returnable amount, smart contract checks if the payback amount equals the calculated amount plus the amount of interest generated. If it matches, the contract will execute the transfer to liquidate lender, returns all the seized collateral from the contract address to the borrower's one, and mark the status of loan as closed. If the borrower's wallet does not have the required amount of money, he/she will be warned about this issue by the front-end section. The overall lending management is depicted using the flowchart in Fig. 13.

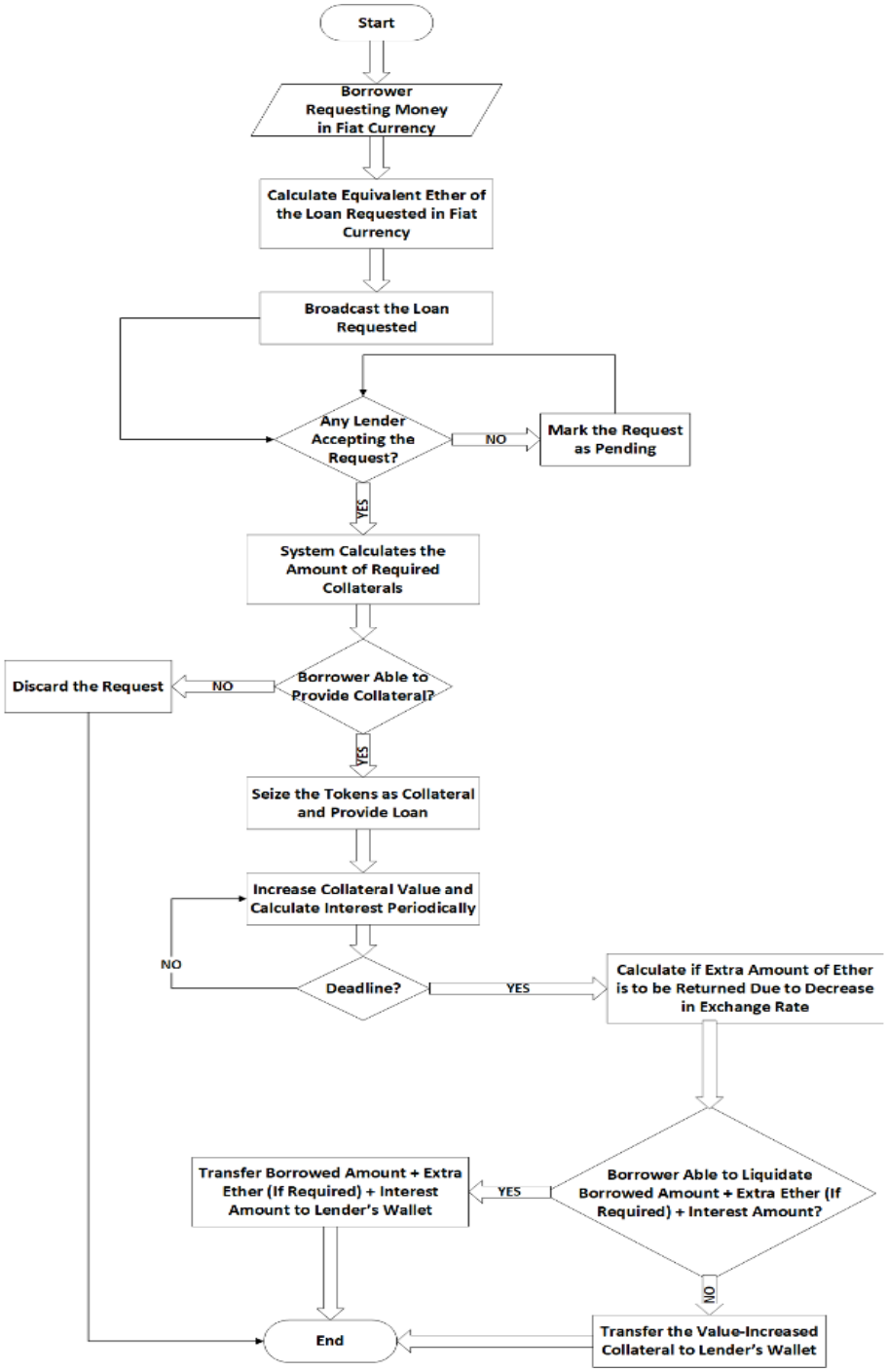


**Fig. 13. Flowchart of the Overall Lending Management System**

## 6. RESULT ANALYSIS

React, a JavaScript library is used to build the user interface for the proposed architecture by which the borrowers and lenders will interact with each other and the system. Infura is a back-end infrastructure where all the smart contracts are uploaded to connect this decentralized lending system app to the Ethereum network. The front-end communicates with these smart contracts via web3 and Metamask. Fig. 14 depicts the aforementioned decentralized lending system structure. To assess the effectiveness of our system, some test cases are evaluated using the system which can be found in the Table 1.

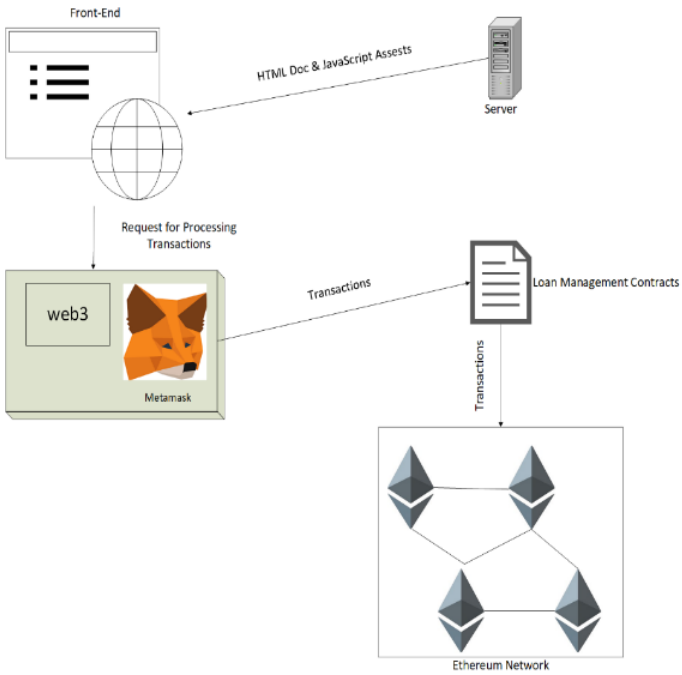


**Fig. 14. Architecture of the Decentralized Lending System**

From the instances of Table 1, it is noticeable that in case of Test 1, 2, 3, 4, 5 and 8; the exchange rates of Ether were decreased on the loan repayment date compared to loan issuance date. If the borrower would return the same base amount which the lender lent on the loan issuance date, lender would actually receive less fiat currency because of the downfall of the exchange rate. This can cause financial loss to the lender, in terms of fiat money. For example, in the first case, lender provided 500 USD to the borrower which was equivalent to 1.865 Ether according to the exchange rate of 17th Feb, 2020. After 39 days, when the borrower returned the money on 26th March, 2020, the exchange rate fell from 268.03 USD to 139.00 USD and according to the updated exchange rate, 1.865 Ether would actually be equivalent to 259.235 USD. So, if the borrower returned exactly 1.865 Ether, the lender would receive 240.765 USD less, but according to our system, the payback must be according to the fiat currency the borrower had taken (500 USD) and the exchange rate of the reimbursement date. For this reason, the borrower must provide 3.595 Ether which is equal to 500 USD on the loan repayment date.

For this reason, the borrower must provide 3.595 Ether which is equal to 500 USD on the loan repayment date. In cases of 6, 7 and 9; the exchange rate increases and it seems that the borrower may provide less Ether to the lenders, but to make the system profitable for its users, the protocol requires the borrower to pay the same base amount of Ether he/she borrowed.

**Tab. 1. Test Case Evaluation Using the Proposed System: Incrementing Token Price to Mitigate Risk (Source: www.coingecko.com, Author Generated Test Cases)**

| Test Case No. | Loan Issuance Date | Loan Repayment Date | Amount Borrowed (USD/Ether) | Exchange Rate of Ether on Loan Issuance Date | Exchange Rate of Ether on Loan Repayment Date | Amount to be Repaid (In Ether) | Extra Amount of Ether Paid |
|---|---|---|---|---|---|---|---|
| 01 | 17 February, 2020 | 26 March, 2020 | $500/1.865 ETH | 268.03 USD | 139.00 USD (-) | 3.595 ETH | + 1.73 ETH |
| 02 | 18 February, 2020 | 11 March, 2020 | $300/1.064 ETH | 281.95 USD | 194.22 USD (-) | 1.545 ETH | + 0.481 ETH |
| 03 | 23 February, 2020 | 18 March, 2020 | $350/1.274 ETH | 274.63 USD | 117.70 USD (-) | 2.974 ETH | + 1.699 ETH |
| 04 | 2 May, 2020 | 11 May, 2020 | $400/1.871 ETH | 213.82 USD | 184.85 USD (-) | 2.164 ETH | + 0.293 ETH |
| 05 | 10 March, 2020 | 16 March, 2020 | $700/3.487 ETH | 200.75 USD | 110.99 USD (-) | 6.307 ETH | + 2.82 ETH |
| 06 | 23 May, 2020 | 31 May, 2020 | $820/3.965 ETH | 206.80 USD | 231.54 USD (+) | 3.542 ETH | N/A |
| 07 | 13 May, 2020 | 30 May, 2020 | $960/4.799 ETH | 200.01 USD | 243.28 USD (+) | 3.946 ETH | N/A |
| 08 | 14 Feb, 2020 | 12 March, 2020 | $1100/3.870 ETH | 284.23 USD | 110.60 USD (-) | 9.945 ETH | + 6.075 ETH |
| 09 | 15 April, 2020 | 29 April, 2020 | $990/6.461 ETH | 153.22 USD | 217.32 USD (+) | 4.555 ETH | N/A |

For example, in the last case, the exchange rate decreased on 29$^{th}$ April and according to that borrower should have paid 4.555 Ether which is still equivalent to 900 USD. But, the protocol of our system forced the borrower to pay 6.461 Ether and, in that case, the lender received profit of extra 414 USD. The following chart compares our protocol with existing Blockchain based lending protocols (which require only the base borrowed amount to be repaid, besides the interest) corresponding to the extra payment made for the compensation of the loss that could occur due to the downfall of exchange rate. Here, from the chart represented below by Fig. 15, it is clearly visible that our system (orange colored line) forces the borrower to mitigate the financial loss of lender by providing extra Ether in 6 out of 9 cases as the exchange rate descended on the repayment date. Also, in case of the rest 3 cases (where exchange rate increased), the system performs the same as compared to other Blockchain based lending Protocol (e.g., Dharma). Table 2 demonstrates the history of the collateral seized at the time of taking loans in all the 9 test cases. It also illustrates how the periodic increment of collateral price can compensate the loss which could happen due to the borrower's failure to payback.

To understand how the increment of collateral price mitigates the financial risk of lender, we explain the scenario of the first test case in which the borrower took 500 USD as loan on 17 February, 2020; which is equivalent to 1.865 Ether according to the exchange rate of that loan issuance date. The borrower chose a suitable combination of tokens as collateral which

were seized temporarily by the system. Borrower provided 100 tokens of price 0.00373 Ether, 75 tokens of price 0.00799 Ether and 45 tokens of 0.01632 Ether, totaling 1.70260 Ether, which is about 90% of the borrowed amount. Until the repayment date arrived, the price of these tokens increased daily by 2%.

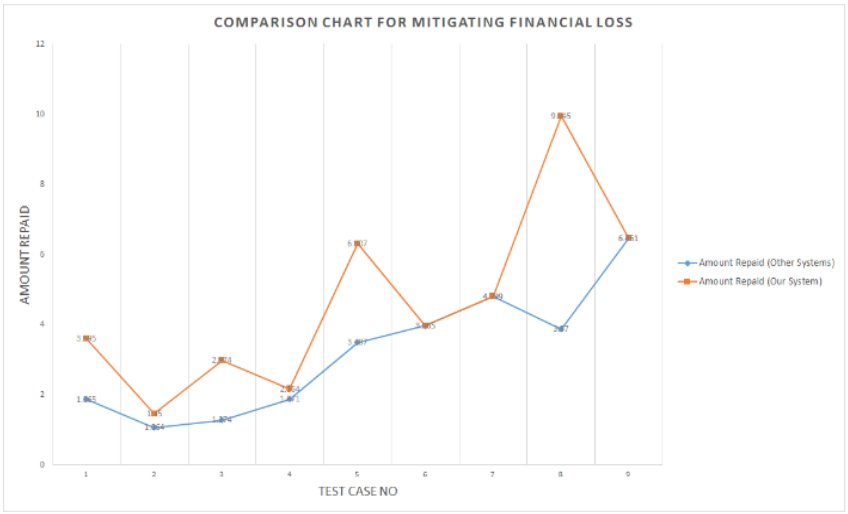


**Fig. 15. System's Efficiency to Tackle Low Exchange Rate Compared to the Basic Protocols**

Assuming the loan repayment date as deadline day, if the borrower failed to repay the loan, then all the seized tokens equivalent to 3.03055 Ether would be transferred to the lender's account, which is greater than the base amount 1.865 Ether. The column chart in Fig. 16 depicts how the periodic increment of the token price compensates the base amount upon failure of payback. From this chart, it is clearly reflected that in all of the 9 test cases, if the borrower failed to payback the borrowed amount, the lender would not face any loss as the total updated price of the seized collateral price is greater than the base amount.

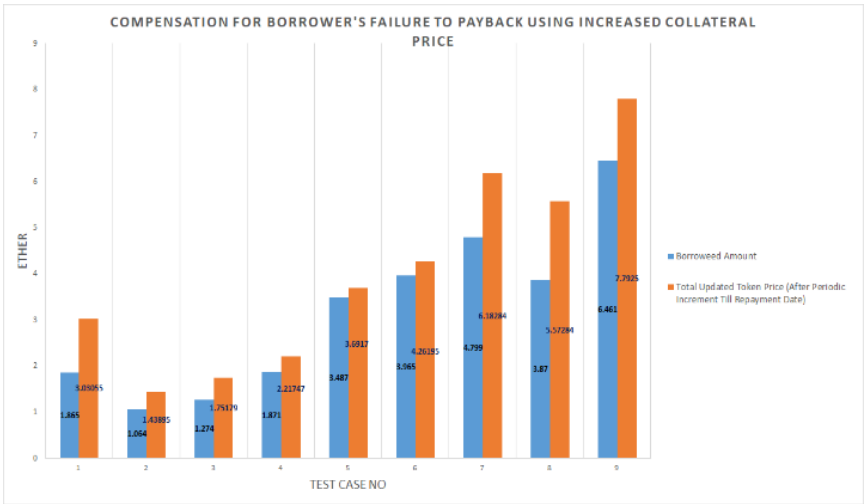


**Fig. 16. Visual Demonstration of Compensating Borrower's Payback-Failure with Increasing Collateral Price**

Finally, the summarization of the cases tested using the lending system is represented by Table 3 (includes the amount of interest and total repayable balance).

**Tab. 2. Test Case Evaluation Using the Proposed System: Incrementing Token Price to Mitigate Risk (Source: www.coingecko.com, Author Generated Test Cases)**

| Test Case No. | Loan Issuance Date | Loan Repayment Date | Amount Borrowed (USD/ Ether) | Tokens Combination with Price (In Ether) | Token Price Incremented (Incremented Periodically Till Repayment Date) | Total Price of Seized Collateral |
|---|---|---|---|---|---|---|
| 01 | 17 February, 2020 | 26 March, 2020 | $500/1.865 ETH | (i) 0.00373 ETH: 100 Tokens (ii) 0.00799 ETH: 75 Tokens (iii) 0.01623 ETH: 45 Tokens | (i) +0.00291 ETH: 100 Tokens (ii) +0.00623 ETH: 75 Tokens (iii) +0.01266 ETH: 45 Tokens | (i) 0.66400 ETH + (ii) 1.06650 ETH + (iii) 1.30005 ETH = 3.03055 ETH |
| 02 | 18 February, 2020 | 11 March, 2020 | $300/1.064 ETH | (i) 0.00354 ETH: 60 Tokens (ii) 0.00417 ETH: 45 Tokens (iii) 0.01953 ETH: 30 Tokens | (i) +0.00163 ETH: 60 Tokens (ii) +0.00192 ETH: 45 Tokens (iii) +0.00896 ETH: 30 Tokens | (i) 0.31020 ETH + (ii) 0.27405 ETH + (iii) 0.85470 ETH = 1.43895 ETH |
| 03 | 23 February, 2020 | 18 March, 2020 | $350/1.274 ETH | (i) 0.00364 ETH: 70 Tokens (ii) 0.00458 ETH: 35 Tokens (iii) 0.0511 ETH: 15 Tokens | (i) +0.00182 ETH: 70 Tokens (ii) +0.00229 ETH: 35 Tokens (iii) +0.02555 ETH: 15 Tokens | (i) 0.38220 ETH + (ii) 0.21984 ETH + (iii) 1.14975 ETH = 1.75179 ETH |
| 04 | 2 May, 2020 | 11 May, 2020 | $400/1.871 ETH | (i) 0.00468 ETH: 80 Tokens (ii) 0.00679 ETH: 45 Tokens (iii) 0.06487 ETH: 18 Tokens | (i) +0.00094 ETH: 80 Tokens (ii) +0.00136 ETH: 45 Tokens (iii) +0.01297 ETH: 18 Tokens | (i) 0.44960 ETH + (ii) 0.36675 ETH + (iii) 1.40112 ETH = 2.21747 ETH |
| 05 | 10 March, 2020 | 16 March, 2020 | $700/3.487 ETH | (i) 0.00498 ETH: 70 Tokens (ii) 0.00725 ETH: 50 Tokens (iii) 0.08423 ETH: 30 Tokens | (i) +0.00070 ETH: 70 Tokens (ii) +0.00102 ETH: 50 Tokens (iii) +0.01179 ETH: 30 Tokens | (i) 0.39760 ETH + (ii) 0.41350 ETH + (iii) 2.88060 ETH = 3.69170 ETH |
| 06 | 23 May, 2020 | 31 May, 2020 | $820/3.965 ETH | (i) 0.004835 ETH: 90 Tokens (ii) 0.04236 ETH: 75 Tokens | (i) +0.00087 ETH: 90 Tokens (ii) +0.00762 ETH: 75 Tokens | (i) 0.51345 ETH + (ii) 3.74850 ETH = 4.26195 ETH |
| 07 | 13 May, 2020 | 30 May, 2020 | $960/4.799 ETH | (i) 0.004999 ETH: 60 Tokens (ii) 0.09875 ETH: 43 Tokens | (i) +0.00180 ETH: 60 Tokens (ii) +0.03555 ETH: 43 Tokens | (i) 0.40794 ETH + (ii) 5.77490 ETH = 6.18284 ETH |
| 08 | 14 Feb, 2020 | 12 March, 2020 | $1100/ 3.870ETH | (i) 0.003518 ETH: 55 Tokens (ii) 0.08456 ETH: 40 Tokens | (i) +0.00197 ETH: 55 Tokens (ii) +0.04735 ETH: 40 Tokens | (i) 0.30184 ETH + (ii) 5.27640 ETH = 5.57284 ETH |
| 09 | 15 April, 2020 | 29 April, 2020 | $990/6.461 ETH | (i) 0.00652 ETH: 75 Tokens (ii) 0.08423 ETH: 65 Tokens | (i) +0.00196 ETH: 75 Tokens (ii) +0.02527 ETH: 65 Tokens | (i) 0.63600 ETH + (ii) 7.15650 ETH = 7.79250 ETH |

**Tab. 3. Test Case Evaluation Using the Proposed System: Providing Extra Ether for Exchange Rate Fall Down (Source: System's Evaluation Results)**

| Test Case No. | Loan Issuance Date | Loan Repayment Date | Amount Borrowed (USD/Ether) | Exchange Rate of Ether on Loan Issuance Date | Exchange Rate of Ether on Loan Repayment Date | Tokens Combination with Price (In Ether) | Total Price of Seized Collateral (Incremented Periodically Till Repayment Date) | Amount of Interest Generated (2% Daily Basis, Min. 15 Days) | Amount to be Repaid (In Ether) | Total Amount of Ether to be Paid (Interest + Base Amount) | Loss |
|---|---|---|---|---|---|---|---|---|---|---|---|
| 01 | 17 February, 2020 | 26 March, 2020 | $500/1.865 ETH | 268.03 USD | 139.00 USD (-) | (i) 0.00373 ETH: 100 Tokens<br>(ii) 0.00799 ETH: 75 Tokens<br>(iii) 0.01623 ETH: 45 Tokens | 3.03055 ETH | 1.4547 ETH | 3.595 ETH | 5.0494 ETH | NO |
| 02 | 18 February, 2020 | 11 March, 2020 | $300/1.064 ETH | 281.95 USD | 194.22 USD (-) | (i) +0.00163 ETH: 60 Tokens<br>(ii)+0.00192 ETH: 45 Tokens<br>(iii)+0.00896 ETH: 30 Tokens | 1.43895 ETH | 0.48944 ETH | 1.545 ETH | 2.03444 ETH | NO |
| 03 | 23 February, 2020 | 18 March, 2020 | $350/1.274 ETH | 274.63 USD | 117.70 USD (-) | (i) +0.00182 ETH: 70 Tokens<br>(ii) +0.00229 ETH: 35 Tokens<br>(iii) +0.02555 ETH: 15 Tokens | 1.75179 ETH | 0.63700 ETH | 2.974 ETH | 3.61100 ETH | NO |
| 04 | 2 May, 2020 | 11 May, 2020 | $400/1.871 ETH | 213.82 USD | 184.85 USD (-) | (i) +0.00094 ETH: 80 Tokens<br>(ii) +0.00136 ETH: 45 Tokens<br>(iii) +0.01297 ETH: 18 Tokens | 2.21747 ETH | 0.56130 ETH | 2.164 ETH | 2.53820 ETH | NO |
| 05 | 10 March, 2020 | 16 March, 2020 | $700/3.487 ETH | 200.75 USD | 110.99 USD (-) | (i) +0.00070 ETH: 70 Tokens<br>(ii) +0.00102 ETH: 50 Tokens<br>(iii) +0.01179 ETH: 30 Tokens | 3.69170 ETH | 1.04610 ETH | 6.307 ETH | 6.9518 ETH | NO |
| 06 | 23 May, 2020 | 31 May, 2020 | $820/3.965 ETH | 206.80 USD | 231.54 USD (+) | (i) +0.00087 ETH: 90 Tokens<br>(ii) +0.00762 ETH: 75 Tokens | 4.26195 ETH | 1.18950 ETH | 3.965 ETH | 4.67870 ETH | NO |
| 07 | 13 May, 2020 | 30 May, 2020 | $960/4.799 ETH | 200.01 USD | 243.28 USD (+) | (i) +0.00180 ETH: 60 Tokens<br>(ii) +0.03555 ETH: 43 Tokens | 6.18284 ETH | 1.72764 ETH | 4.799 ETH | 6.52664 ETH | NO |
| 08 | 14 Feb, 2020 | 12 March, 2020 | $1100/3.870ETH | 284.23 USD | 110.60 USD (-) | (i) +0.00197 ETH: 55 Tokens<br>(ii) +0.04735 ETH: 40 Tokens | 5.57284 ETH | 2.16720 ETH | 9.945 ETH | 12.11220 ETH | NO |
| 09 | 15 April, 2020 | 29 April, 2020 | $990/6.461 ETH | 153.22 USD | 217.32 USD (+) | (i) +0.00196 ETH: 75 Tokens<br>(ii) +0.02527 ETH: 65 Tokens | 7.79250 ETH | 1.93830 ETH | 6.461 ETH | 8.39930 ETH | NO |

## 7. CONCLUSION AND FUTURE RECOMMENDATION

Our proposed collateral-based lending system supports the periodical increment of collateral price, compensating the borrower's intentional or unintentional failure to pay back the debt. As token fare raises on a daily basis, the collateral price becomes almost the same as the lent amount or surpasses it, completely eliminating the lender's financial loss. Classical loan management systems are unable to calculate the accurate credit score of their clients, as it is easy to temper any financial/bank statement of a certain period of time. As a result, loan might be provided to the defaulters. In case of our proposed blockchain based lending system, the transactions are immutable, which means that they are unchangeable. For this reason, precise risk assessment is guaranteed in our system and transparency is maintained. Furthermore, the fall of exchange rate of Ether is tackled by considering the fiat amount while returning the money, instead of the cryptocurrency amount. In conclusion, we can say that the proper utilization of this suggested protocol can definitely lessen the loan defaulting as it compensates the lender using the escalating price of tokens and its exchange rate fluctuation tackling mechanism. Moreover, our system can prove to be a better substitution to the classical insecure lending system which is vulnerable to the loan defaulters.

However, the users will carry different price-variant tokens which may cause a disarray for the system as the collateral price needs to be increased to return lender's lent amount along with the interest. Hopefully, this issue will be solved by optimizing the principle of the system in near future and is surely an open challenge for the researchers.

### REFERENCES


Ali, M., Nelson, J., Shea, R., & Freedman, M.J. (2016). Blockstack: A global naming and storage system secured by blockchains. In *2016 {USENIX} annual technical conference ({USENIX}{ATC} 16* (pp. 181–194). USENIX Association.

Burns, L., & Moro, A. (2018). What makes an ico successful? an investigation of the role of ico characteristics, team quality and market sentiment. *An Investigation of the Role of ICO Characteristics, Team Quality and Market Sentiment (September 27, 2018)*. https://dx.doi.org/10.2139/ssrn.3256512

Buterin, V. (2014). *Ethereum: A next-generation smart contract and decentralized application platform*. https://blockchainlab.com/pdf/Ethereum_white_paper-a_next_generation_smart_contract_and_ decentralized_ application_platform-vitalik-buterin.pdf

Cao, D., Husbands, K., Zhang, E., Binns, B., Kassam, A., & Lan, A. (2018). *Oneledger: Public blockchain whitepaper*. www.oneledger.io/hubfs/Website/Whitepaper/oneledger-whitepaper.en.pdf

Christidis, K., & Devetsikiotis, M. (2016). Blockchains and smart con- tracts for the internet of things. *IEEE Access, 4*, 2292– 2303. https://doi.org/10.1109/ACCESS.2016.2566339

CoinGecko. (2021). *Cryptocurrency prices & market capitalization*. https://www.coingecko.com/en/ pricecharts/ethereum/usd.

Fenu, G., Marchesi, L., Marchesi, M., & Tonelli, R. (2018). The ico phenomenon and its relationships with ethereum smart contract environment. In *2018 International Workshop on Blockchain Oriented Software Engineering (IWBOSE)* (pp. 26–32). IEEE. https://doi.org/10.1109/IWBOSE.2018.8327568

Firdaus, A.H., & Nugraha, I.G.B.B. (2019). Saving and loan transaction system in cooperative using blockchain. In *2019 Inter- national Conference on ICT for Smart Society (ICISS)* (vol. 7, pp. 1–4). IEEE. https://doi.org/10.1109/ICISS48059.2019.8969847

Fröwis, M., Fuchs, A., & Böhme, R. (2019). Detecting token systems on ethereum. In *International conference on financial cryptography and data security* (pp. 93–112). Springer. https://doi.org/10.1007/978-3-030-32101-7_7

Gazali, H.M., Hassan, R., Nor, R.M., & Rahman, H.M. (2017). Re-inventing ptptn study loan with blockchain and smart contracts. In *2017 8th International Conference on Information Technology (ICIT)* (pp. 751–754). IEEE. https://doi.org/10.1109/ICITECH.2017.8079940

Guo, C., Ma, S., Wang, H., Cheng, S., & Wang, T. (2018). Loc: Poverty alleviation loan management system based on smart contracts. In *2018 IEEE International Conference on Internet of Things (iThings) and IEEE Green Computing and Communications (GreenCom) and IEEE Cyber, Physical and Social Computing (CPSCom) and IEEE Smart Data (SmartData)* (pp. 1527–1532). IEEE. https://doi.org/10.1109/Cybermatics_2018.2018.00257

Heilman, E., Alshenibr, L., Baldimtsi, F., Scafuro, A., & Goldberg, S. (2017). Tumblebit: An untrusted bitcoin-compatible anonymous payment hub. In *Network and Distributed System Security Symposium*. http://dx.doi.org/10.14722/NDSS.2017.23086

Hollander, N. (2017). *Dharma: A generic protocol for tokenized debt issuance*. http://whitepaper.dharma.io.

Hrga, A., Benčić, F.M., & Žarko, I.P. (2019). Technical analysis of an initial coin offering. In *2019 15th International Conference on Telecommunications (ConTEL)* (pp. 1–8). IEEE. https://doi.org/10.1109/ConTEL.2019.8848532

Juels, A., Kosba, A., & Shi, E. (2016). The ring of gyges: Investigating the future of criminal smart contracts. In *Proceedings of the 2016 ACM SIGSAC Conference on Computer and Communications Security* (pp. 283–295). ACM Digital Library. https://doi.org/10.1145/2976749.2978362

Li, D., Fung, C., Tang, J., & Song, C. (2018). *Mixin: A free and lightning-fast peer-to-peer transactional network for digital assets*. https://mixin.one/assets/Mixin-Draft-2018-07-01.pdf

Lleshaj, L., & Korbi, A. (2020). Portfolio selection and var estimation: Evidence from western balkan countries. *Universal Journal of Accounting and Finance*, *8*(4), 92–102. https://doi.org/10.13189/ujaf.2020.080402

Luu, L., Chu, D.-H., Olickel, H., Saxena, P., & Hobor, A. (2016). Making smart contracts smarter. In *Proceedings of the 2016 ACM SIGSAC conference on computer and communications security* (pp. 254–269). ACM Digital Library. https://doi.org/10.1145/2976749.2978309

Mohanta, B.K., Panda, S.S., & Jena, D. (2018). An overview of smart contract and use cases in blockchain technology. In *2018 9th International Conference on Computing, Communication and Networking Technologies (ICCCNT)* (p. 14). IEEE. https://doi.org/10.1109/ICCCNT.2018.8494045

Narayanan, A., Bonneau, J., Felten, E., Miller, A., & Goldfeder, S. (2016). *Bitcoin and cryptocurrency technologies: a comprehensive introduction*. Princeton University Press.

Okoye, M.C. & Clark, J. (2018). Toward cryptocurrency lending. In *International Conference on Financial Cryptography and Data Security* (pp. 367–380). Springer. https://doi.org/10.1007/978-3-662-58820-8_25

Rosic, A. (2017). What is an initial coin offering? raising millions in seconds. https://blockgeeks.com/guides/initial-coin-offering/

Sinaga, J.S., Muda, I., & Silalahi, A.S. (2020). The effect of bi rate, exchange rate, inflation and third party fund (dpk) on credit distribution and its impact on non performing loan (npl) on xyz commercial segment bank. *Universal Journal of Accounting and Finance*, *8*(3), 55–64. https://doi.org/10.13189/ujaf.2020.080301

Singh, S., & Singh, N. (2016). Blockchain: Future of financial and cyber security. In *2016 2nd international conference on contemporary computing and informatics (IC3I)* (pp. 463–467). IEEE. https://doi.org/10.1109/IC3I.2016.7918009

Somin, S., Gordon, G., Pentland, A., Shmueli, E., & Altshuler, Y. (2020). Erc20 transactions over ethereum blockchain: Network analysis and predictions. *arXiv preprint arXiv:2004.08201*. https://arxiv.org/abs/2004.08201

Swan, M. (2015). *Blockchain: Blueprint for a new economy*. O'Reilly Media, Inc.

Victor, F., & Lüders, B.K. (2019). Measuring ethereum-based erc20 token networks. In *International Conference on Financial Cryptography and Data Security* (pp. 113–129). Springer. https://doi.org/10.1007/978-3-030-32101-7_8

Watanabe, H., Fujimura, S., Nakadaira, A., Miyazaki, Y., Akutsu, A., & Kishigami, J.J. (2015). Blockchain contract: A complete consensus using blockchain. In *2015 IEEE 4th global conference on consumer electronics (GCCE)* (pp. 577–578). IEEE. https://doi.org/10.1109/GCCE.2015.7398721

Yang, X., Chen, Y., & Chen, X. (2019). Effective scheme against 51% attack on proof-of-work blockchain with history weighted information. In *2019 IEEE International Conference on Blockchain (Blockchain)* (pp. 261–265). IEEE. https://doi.org/10.1109/Blockchain.2019.00041

Yuan, Y., & Wang, F. (2016). Development status and prospect of blockchain technology. *Journal of automation*, *42*(4), 481–494.

Zetzsche, D.A., Buckley, R.P., Arner, D.W., & Föhr, L. (2017). The ico gold rush: It's a scam, it's a bubble, it's a super challenge for regulators. *University of Luxembourg Law Working Paper*, *11*, 17–83. https://dx.doi.org/10.2139/ssrn.3072298